On-chip micro-supercapacitors based on nano-structured carbon materials

Peihua Huang

THESE

En vue de l'obtention du

DOCTORAT DE L'UNIVERSITÉ DE TOULOUSE

Délivré par *l'Université Toulouse III - Paul Sabatier*
Discipline ou spécialité : *Génie Electrique*

Présentée et soutenue par *HUANG Peihua*
Le *8 Janvier, 2013*

Titre : *On-chip Micro-supercapacitors based on Nano-structured Carbon Materials/Micro-supercondensateurs sur puce à base de carbones nanostructurés*
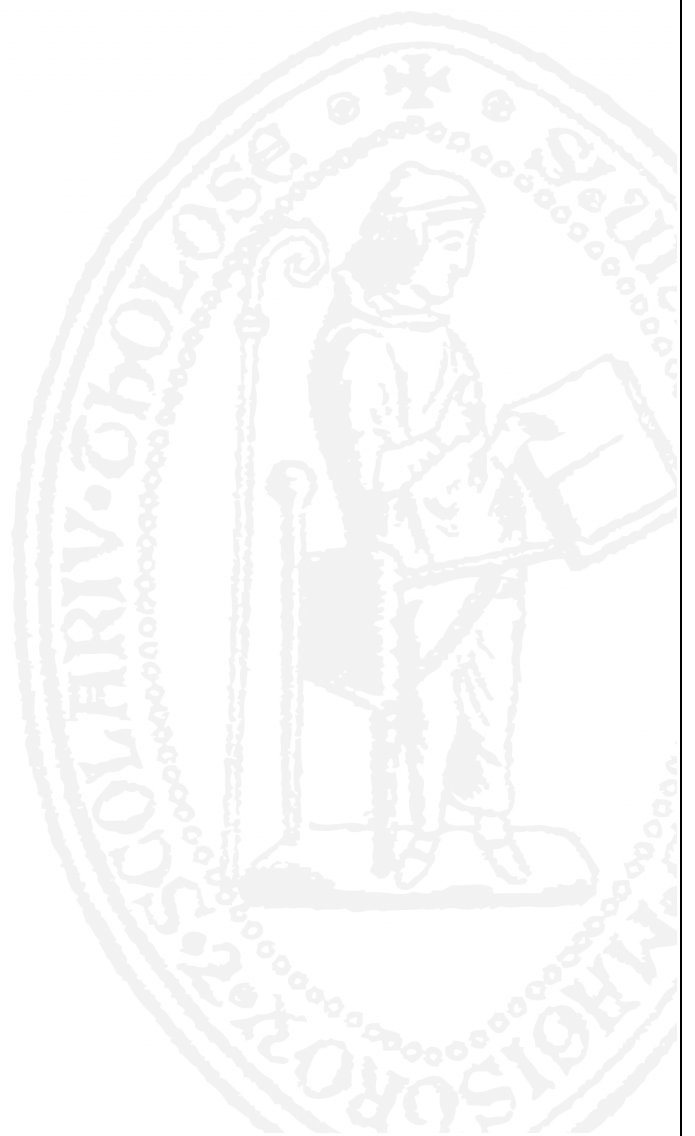

JURY
G. AMARATUNGA/Rapporteur
F. FAVIER/Rapporteur
M. BRUNET/Directeur de Thèse
P. SIMON/Directeur de Thèse
K. GUERIN/Examinateur
P.-L. Taberna/Invité
D. Pech/Invité

Ecole doctorale : *Génie Electrique, Electronique et Télécommunications (GEET)*
Unité de recherche : *LAAS & Institut Carnot CIRIMAT*
Directeur(s) de Thèse : *M. BRUNET & P.SIMON*
Rapporteurs :

Acknowledgement

First and foremost, I would like to thank my supervisors, Magali Brunet and Professor Patrice Simon. It has been an honor to be their PhD student. They have been good examples of researchers for me to follow. I am also grateful for all the ideas, time, and funding they offered both to establish and enrich my PhD experience. Their enthusiasm and passion for research are impressive and brought me through difficult periods during my PhD pursuit.

My PhD was much more difficult than I had imagined. There was always something not functioning or that could not be explained by commonsense. Fortunately, there were also Pierre-Louis Taberna and David Pech, who were always there to help me by analyzing experiments details and trying to find the key issues which stopped me from advancing in my research.

Our collaborator at Drexel University in Philadelphia (USA) Min Heon, prepared many CDC film samples for me and Professor Yury Gogotsi always participated in the discussion of the topic even with his extremely busy schedule. In addition, the warm reception I received during my stay at Drexel University was unforgettable. Members in the group were also source of friendship and allowed me to integrate quickly into the team and the community.

Working in the clean room, many of the operations were carried out by the technicians. I was thankful to them for my samples as soon as possible, sometimes even after hours. I would like to particularly mention Monique Benoit for her organization of affaires in the clean room; Pascal Dubreuil for his work in reactive ion etching; Laurent Bouscayrol for the use of the ovens; Pierre-Francois Calmon for his fabrication of masks; David Colin and Samuel Charlot for wire-bonding process; Franck Carcenac for the great training of SEM; Laurent Mazenq for

the training and help of photolithography process; and Ludovic Salvagnac and Sébastien Pinaud for the deposition of metal.

The time during my PhD was made enjoyable in large part thanks to the many friends that became a part of my life, Barbara, Emilie, Julie, Jérémy, Wanyu, Lorie, Etsuro and Rongying from the lab and Valerie, Chantal, Zhongda, Yijun, Hong and Tong, etc. Thank you for accompanying me and listening.

For this PhD thesis, I would like to thank the rapporteurs: Professor Gehan Amaratunga and Professor Frederic Favier, for their time, interest and helpful comments as well as another member of my defense committee, Katia Guerin, for her time and insightful questions.

Lastly, I would like to acknowledge the contribution of my family. They have been supportive of my work since my decision to come abroad. It has not been easy for them, especially since I had been with them in the same city for 23 years. During my Masters and my PhD studies, despite the physical distance of almost 10,000 km, our hearts became much closer than when I was physically there with them. And without their support, I could never have made it through this PhD. In the summer of 2010, the trip I took with my mother in Europe is probably the best memory of my life, and it was satisfying to be able to repay some of their support.

Unfortunately, my uncle Gao passed away because of lung cancer at the very end of my thesis writing. I was planning to go back China to visit him after finishing the thesis draft, as he was already very sick at that time. It was such a pity I could not be there in time. He had treated me like his own daughter since childhood and was always very proud of me no matter what I was doing. I hope he is still here to be able to hear my gratitude to him… Thank you.

<div align="right">

Peihua HUANG

Université Paul Sabatier

January 2013

</div>

Abstract

The increasing number of functions in portable electronic devices requires more and more energy and power within a limited space. Li-ion thin film or so-called micro-batteries are the current solution for power supply. Drawbacks of these storage elements are poor power performance with limited life-span and temperature range. Carbon-based micro-supercapacitors, on the other hand, are able to deliver energy in short time, thus offering high power capability, to work at low temperature and they present an unlimited life-span. This thesis proposes several carbon-based micro-supercapacitors, to be integrated on a silicon substrate together with other electronics components or sensors. They are foreseen as a potential replacement or complement of Li-ion micro-batteries to enhance the total performance of the whole power source system. The thesis work is mainly focused on adapted materials and technologies for enabling micro-supercapacitors realization.

Two types of on-chip micro-supercapacitors with planar interdigitated electrodes configuration were developed: one prepared from Electrophoretic deposition (EPD) and its combination of different carbon materials and different types of electrolytes, the other from patterned titanium or silicon carbide derived carbon film (TiC-CDC or SiC-CDC) on Si chip with different microfabrication techniques. Onion like carbon-based micro-supercapacitor by EPD shows high power delivery (scan rate up to 100V/s) in organic electrolyte, and high temperature range (-50 °C – 80 °C) in a eutectic mixture of ionic liquids. Different techniques for patterning carbide films have been developed to fabricate a CDC based micro-supercapacitor: reactive ion etching (RIE) or focused ion beam (FIB). TiC-CDC film based micro-supercapacitors show promising preliminary results. The developed technologies pave the way to a full and effective integration of micro-size energy storage devices on-chip.

Table of Contents

General Introduction

Portable electronic devices (PEDs), such as laptop computers, smart phones, tablet computers, referring to any non-stationary electronic apparatus with singular or multiple capabilities, have been widely developed in the last decades. Faster processing is always one of the most important objectives to achieve for PEDs; it requires more electronic components to process and transmit data, thus demanding higher power. On the other hand, multifunction in PEDs, for instance cameras, motion detection, lights, calls for additional MEMS (Microelectromechanical systems) such as sensors or actuators resulting in even higher power demands. However, high power – i.e. high rate discharge – reduces batteries run time (the time PED will run before it must be recharged), which is the major power source in PEDs. In contrast, from point of view of customers, longer battery run time is desired. To solve this contradiction, supercapacitors can offer a complementary solution for power sources, thanks to their high discharge rates. Placed in parallel of a battery, a supercapacitor helps increasing the run time of the power source and helps extending the battery's lifetime [1]. Better portability, featuring smaller volume of PED, is also required by customers. While the size of active circuits diminishes quickly according to Moore's Law [2], while at the same time numerous microsystems are introduced, the remaining issue is the size of power sources [3]. Thus batteries and supercapacitors, which could be integrated on-chip in millimeter or even micrometer size, are strongly required.

In some particular cases such as wireless sensor networks, the sensing node which contains MEMS (accelerometer, temperature sensors…etc) coupled with RF emitter and transceiver and micro-controller are expected to function independently, i.e. to be autonomous in energy. These sensors network can be implemented in structures permanently (for structure health monitoring) or spread around in the environment [4]: batteries with their limited lifetime

should be thus avoided. A way to obtain energy autonomy is to power MEMS through energy harvesting and storage units on the same chip. Current energy harvesting systems collect energy from environment such as vibration (mechanical energy), thermal gradient, photovoltaics (solar thermal energy), etc [5]. However, energy from environment is not always available, posing the problem of intermittence. Energy storage is unavoidable in this context: a solution could be carbon-based supercapacitors, since they present longer lifespan thanks to electrochemically stable carbon electrode [6]. For implementing supercapacitors on these applications, miniaturization (small foot prints, low profiles) is required together with resistance to harsh environment. In this context, miniaturization of an energy storage element such as a supercapacitor is a real challenge, especially if it is intended to be on-chip.

On-chip energy storage micro-devices allows size reduction but other advantages are foreseen: monolithic integration indeed with collective fabrication of the energy storage micro-device along with the MEMS and/or the power management active circuit could bring benefits such as: reduction of losses thanks to optimized and short connections, lower manufacturing costs and enhanced reliability.

Following the major advances in harvesting micro-devices for wireless sensors networks, research on micro-scale energy storage and in particular supercapacitors, has increased significantly in the last ten years. The first published micro-supercapacitors in the early 2000s were based on pseudo-capacitive electrode material (RuO_2) in a sandwich configuration [7]. Later-on (from 2006), carbon-based micro-supercapacitors started to appear [8]. This emerging interest can be explained by the fact that carbon is the most widely used electrode material for macroscopic supercapacitors, since it is more stable electrochemically than any other electrode materials for supercapacitors. Furthermore, combined with organic electrolytes, large voltage window and large temperature ranges could be obtained. Carbon-based on-chip micro-supercapacitors have not been well developed, since there are still

2

several unsettled issues concerning technology. Most reported carbon-based micro-supercapacitors were either fabricated by non-widely used microfabrication techniques or their performance could not match the performance with the same electrode material in macroscopic supercapacitors, or neither.

Therefore, in this thesis, there are two principal objectives: first, establishing routine processes with widely used micro-fabrication techniques to process carbon materials into on-chip micro-supercapacitors; second, improving performance including power and energy density to offer an enabling solution of energy storage on-chip.

The first chapter is a bibliographic summary. Macroscopic supercapacitors are firstly discussed. Principles and mechanisms of carbon-based supercapacitors are introduced with discussion of carbon electrodes materials and electrolytes, which are the most important components for carbon-based supercapacitors. Principles of electrochemical characterization including Electrochemical Impedance Spectroscopy (EIS) and Cyclic Voltammetry (CV) are explained to link the test results with performance. Micro-supercapacitors are then introduced with a description of common microfabrication techniques that are used to prepare the micro-devices. The state-of-the-art of micro-supercapacitors is discussed, especially carbon-based micro-supercapacitors, both in sandwich configuration and on-chip interdigitated configuration.

The second chapter describes all the carbon-based on-chip micro-supercapacitors prepared by electrophoretic deposition (EPD) technique. This collective deposition technique consists in processing carbon powder onto patterned current collectors. Pretreatment and EPD parameters were adjusted to achieve a homogeneous and adhesive carbon layer. Activated carbon (AC) was used in a three-electrode configuration to study the influence of thickness of the active film. Then the carbon was deposited on interdigitated current collectors to set up a routine processes. With AC, an improved power performance was found compared with

macroscopic AC-based supercapacitors in the same organic electrolyte. Onion-like carbon (OLC) was then used to further improve power density, although capacitance was compromised. Later, OLC-based on-chip micro-supercapacitors were tested in an ionic liquids mixture (ILM). Compared to organic electrolytes, an enlarged temperature range (-50 °C – 80 °C) was achieved with enlarged voltage window (3.7 V) and enhanced capacitance, hereby improved energy density.

The third chapter presents all the micro-supercapacitors fabricated from carbide-derived carbon (CDC) films which are binder-free films and proved to show large volumetric capacitance. Different processing strategies were developed to produce micro-supercapacitors: either by reactive ion etching (RIE) of CDC films, both SiC-CDC and TiC-CDC films or by reactive ion etching of carbide films (SiC or TiC) transformed later on into carbon films. Other than this, focused ion beam (FIB) was also used to fabricate micro-supercapacitors in micrometer range. Produced micro-supercapacitors with interdigitated current collectors were tested electrochemically and their performance compared with macroscopic supercapacitors and with stat-of-the-art micro-supercapacitors.

Reference

1. Huggins, R.A., *Supercapacitors and electrochemical pulse sources*. Solid State Ionics, 2000. **134**(1, 2): p. 179-195.

2. Moore, G.E., *Lithography and the future of Moore's law*. Proc. SPIE, 1995. **2437**: p. 2-17.

3. Schmidt, M.A. *Portable MEMS power sources*. in *Solid-State Circuits Conference, 2003. Digest of Technical Papers. ISSCC. 2003 IEEE International*. 2003.

4. Srivastava, N., *Challenges of Next-Generation Wireless Sensor Networks and its impact on Society*. Journal of Telecommunications, 2010. **1**(1): p. 128-133.

5. Seah, W.K.G., E. Zhi Ang, and T. Hwee-Pink. *Wireless sensor networks powered by ambient energy harvesting (WSN-HEAP) - Survey and challenges*. in *Wireless Communication, Vehicular Technology, Information Theory and Aerospace & Electronic Systems Technology, 2009. Wireless VITAE 2009. 1st International Conference on*. 2009.

6. Pandolfo, A.G. and A.F. Hollenkamp, *Carbon properties and their role in supercapacitors*. Journal of Power Sources, 2006. **157**(1): p. 11-27.

7. Yoon, Y.S., et al., *Solid-state thin-film supercapacitor with ruthenium oxide and solid electrolyte thin films*. Journal of Power Sources, 2001. **101**(1): p. 126-129.

8. Ho, C., et al. *Dispenser Printed Electrochemical Capacitors for Power Management of Millimeter Scale Lithium Ion Polymer Microbatteries for Wireless Sensors*. in *Power MEMS Conference*. 2006.

Chapter I Bibliographic Summary

I   Macroscopic Supercapacitors

Although in different sizes, carbon-based micro-supercapacitors share the same charge storage mechanism, the same electrode materials and the same electrolytes with macroscopic supercapacitors.

While the first EDLC was described in 1957 [1], carbon-based supercapacitors have only been widely studied and developed since the 1990s [2].

Referring to the Ragone plot in Figure I.1 [3] which shows the specific power versus the specific energy of different energy storage devices, Li batteries, including Li primary batteries and Li-ion secondary batteries, show the best energy performance. Because batteries store energy in the bulk of electrode material via electrochemical reactions, the lighter the redox couple is, the higher the energy density is (per e⁻ exchanged). However, concerning power density, because of the restriction from diffusion of electrolyte ions throughout the active materials (solid diffusion coefficient within the 10^{-10} to 10^{-14} $cm^2.s^{-1}$ range) as well as kinetics of electrochemical reactions, energy delivery can not be achieved in short times: power density is thus limited. Compared to batteries, electrochemical double layer capacitors have lower energy density but much higher power density, thanks to their mechanism of charge storage based on adsorption of ions on the surface of porous structured electrodes.
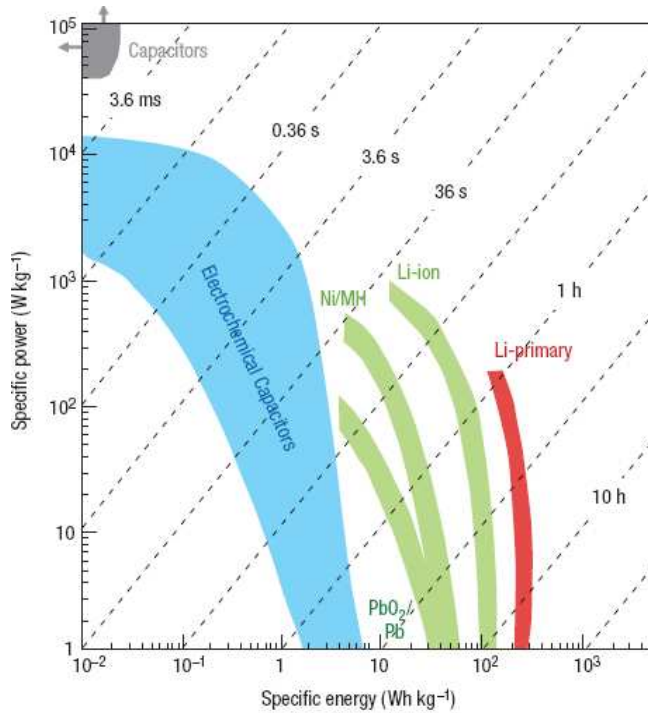
Figure I.1 Ragone Plot for various electrical energy storage devices [3].

I.1   Theory of Electric Double Layer Capacitors (EDLCs)

I.1.1   Conventional Capacitors

Conventional dielectric capacitors contain two parallel metallic plates with a dielectric material in between as shown in Figure I.2.
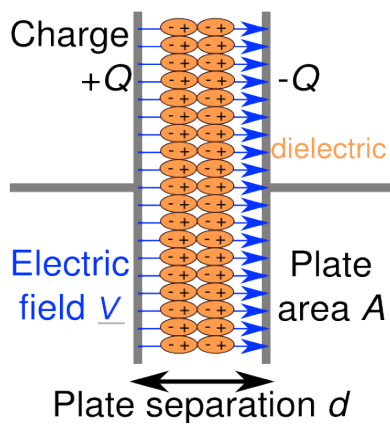
Figure I.2 Schematically representative of a conventional capacitor.

When there is a potential difference across the conductive plates, a static electric field develops across the dielectric layer, leading to charge accumulation on each plate. Energy is thus stored in the electrostatic field.

The quantity of charge stored is proportional to the potential applied according to Eq. 1.

Eq. 1

$$Q = CV$$

where Q (*A.s or Coulomb, C*) is the charge stored in the capacitor. V (*V*) is the potential applied which is limited by the dielectric breakdown between the two plates and C (*F*) is the capacitance defined by Eq. 2.

Eq. 2

$$\frac{C}{A} = \frac{\varepsilon_r \varepsilon_0}{d}$$

where A (*m^2*) is the electrode surface area, d (*m*) is the distance between the layers of opposite charges, ε_0 is the dielectric constant of the vacuum (8.85×10^{-12} F.m^{-1}) and ε_r is the relative dielectric constant of the materials introduced between the two plates. The dielectric materials adopted can neither be too thick or too thin. If it is too thick, the capacitance is largely reduced and more defects might be introduced. Then since a dielectric has a breakdown voltage MV/cm proportional to thickness, the minimum thickness is thus limited to ensure a certain operation voltage.

I.1.2   Supercapacitors

Electrochemical capacitors, also called Electrical Double Layer Capacitors (EDLCs) or Supercapacitors, are composed of two electrodes separated by an ionic conductive but electronic insulated separator soaked in an electrolyte (see Figure I.3).
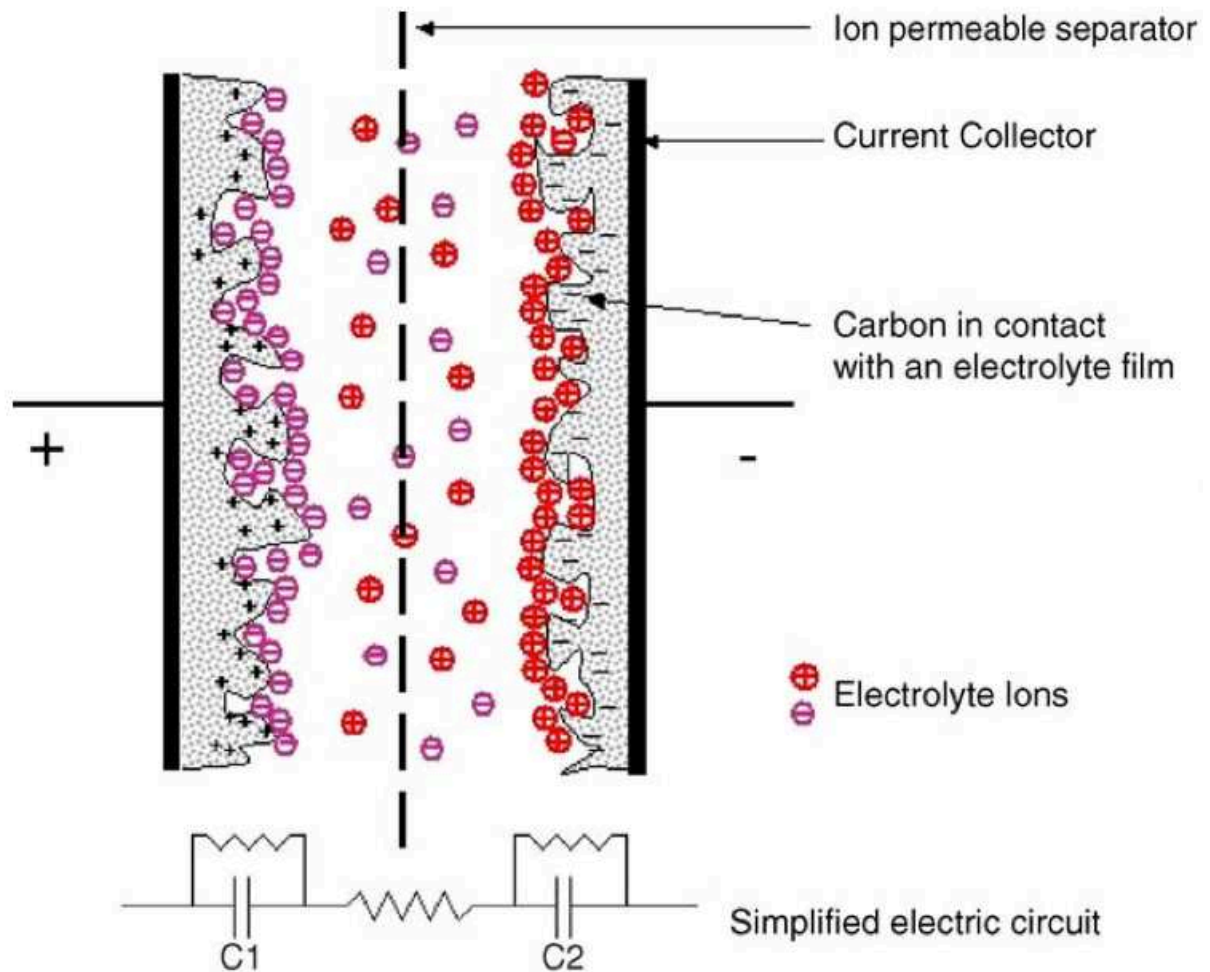
Figure I.3 Representation of an EDLC with carbon as active materials (in the charged state) [4].

Charge storage is achieved through charge separation on a large surface area: the ions from the electrolyte are adsorbed onto a high specific surface area conducting active material. The extended high surface area is due to the porous structure of the active material, the carbon, which can reach up to 3000 m^2/g, thus offering extremely high number of available sites to accommodate cations and anions in the electrolyte. The extremely thin layer (few nanometers or so in organic electrolytes) of charge separation corresponding to electrochemical double layer (EDL), compared with the "d" of Eq. 2, substantially enlarges the capacitance.

The EDL theory was firstly proposed by Helmholtz to describe the charge distribution at the interface of colloidal particles [5]. The EDL was then simply described as two layers of

opposite charge accumulated at the electrolyte/electrode interface (Figure I.4a). The separation between the layers of opposite charge was within the solvated radius of electrolyte ions, limited to the electrode surface. This model was later modified by Gouy and Chapman by introducing a diffuse model of the EDL, in which the potential at a surface decreases exponentially due to distribution of counter-ions from the electrolyte solution in the vicinity of electrode driven by thermal motion (Figure I.4b) [6, 7]. After, Stern combined the former two theories by dividing the area in the vicinity of the electrode into two parts, the compact layer right next to the electrolyte/electrode interface, also called Stern layer, and Diffuse layer [8] (Figure I.4c).
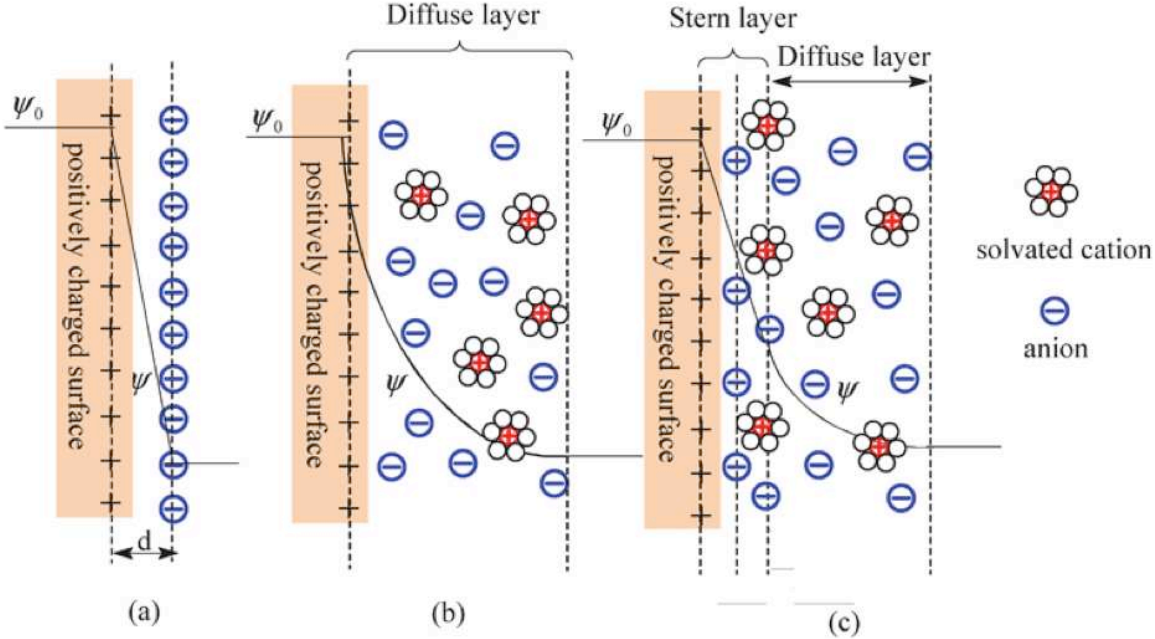
Figure I.4 Models of the electrochemical double layer at a positively charged surface: (a) the Helmholtz model, (b) the Gouy-Chapman model, and (c) the Stern model [9].

The Gouy-Chapman-Stern model shows that the interface behaves like the combination of the two capacitors in series:

Eq. 3

$$\frac{1}{C_{dl}} = \frac{1}{C_{Helmholtz}} + \frac{1}{C_{GouyChapman}} = \frac{d}{\varepsilon_r \varepsilon_0 A} + \frac{1}{\varepsilon_r \varepsilon_0 \kappa_D A}$$

where κ_D is the Debye length or $1/\kappa_D$ is diffusion length of Gouy-Chapman layer.

For highly concentrated electrolyte like in our case, $1/\kappa_D$ tends to 0 and then the double layer capacitance can be defined as the Helmholtz capacitance:

Eq. 4

$$\frac{1}{C_{dl}} = \frac{1}{C_{Helmholtz}}$$

As defined by the modern EDL theory, an increase of the surface area (A) and a decrease of the ion and charged surface distance (d) in Eq. 2 respectively, both lead to the increase of capacitance. The energy stored in EDLCs is therefore several orders of magnitudes higher than conventional capacitors according to Ragone plot shown in Figure I.1 as the prefix "super-" indicates.

Since there is one double layer on each electrode of a supercapacitor, the total capacitance (cell capacitance) is thus written as:

Eq. 5

$$\frac{1}{C_{total}} = \frac{1}{C_+} + \frac{1}{C_-}$$

Hereby, the stored energy W (J) and the maximum power P_{max} (W) are calculated according to Eq. 6 and Eq. 7 respectively.

Eq. 6

$$W = \frac{1}{2} C V_0^2$$

Eq. 7

$$P_{max} = \frac{V_0^2}{4R}$$

where R (Ω) is equivalent series resistance (ESR), the resistance of internal components of the supercapacitor such as current collectors, electrodes materials, electrolytes in supercapacitors. The voltage window is an important parameter in terms of both energy density and power density. However, the P_{max} calculated here in Eq. 7 is the theoretical power

density that the device could reach according only to the voltage window and ESR; it is thus different from the useable power. P_{max} is the power density where energy density close to 0 in the Ragone Plot. For real supercapacitor applications, there are several other factors that could take effect on the useable power density, like the thickness and porosity of electrodes, the voltage window, the series resistance, etc.

Since for supercapacitors the charge storage is achieved at the surface of the active materials, as opposed to batteries where electrochemical reactions occur in the bulk thus reducing the stability of electrodes, the cyclability of supercapacitors is much longer than batteries. In addition, this also leads to a better power performance for supercapacitors thanks to the absence of restriction of kinetics from electrochemical reactions.

To assess the efficiency of charging and discharging for EDL, the minimum time needed to reach a stable capacitance, named time constant, $\tau(s)$, is introduced and defined by Eq.8 as follow.

Eq. 8

$$\tau = RC$$

Resistance of the capacitor, with its capacitance, defines time constant. High capacitance of supercapacitors, even with very low resistance, introduces several seconds of time constant.

Other than EDL capacitors, some other electrochemical devices have a "pseudo"-capacitive behavior but are based on kinetically fast faradaic reactions [10]. Typical materials are oxides (RuO_2, MnO_2, etc.) and electronically conducting polymers (polypyrrole, polyaniline, etc.). Although the restriction from kinetics of reactions is alleviated, the limitations in power delivery and cyclability are still issues compared to EDL capacitors, whose electrode material is usually porous carbon.

I.2   Carbon Materials for Supercapacitors

Among all the carbon materials, activated carbons (ACs) are the most widely used active materials for EDLCs because of its high conductivity, high electrochemical stability, high surface area and relatively low cost. They can be obtained from various carbon rich organic precursors such as wood, pitch, coal, coke or fruit shell such as coconut or even synthetic polymer precursors [4]. The activation is carried out through either physical activation by high temperature treatment in oxidizing atmosphere or/and chemical activation by hot acidic or alkaline oxidation. Activation could be controlled by adjusting the reaction parameters, i.e. activation time, activation temperature etc... to create a porous network within the carbon grains leading to high specific surface area.

The activation treatments lead to the porous structure including all kinds of pores, as shown in Figure I.5, according to IUPAC [11], micropores with pore size smaller than 2 nm, mesopores with pore size between 2 nm and 50 nm, macropores with pore size larger than 50nm.
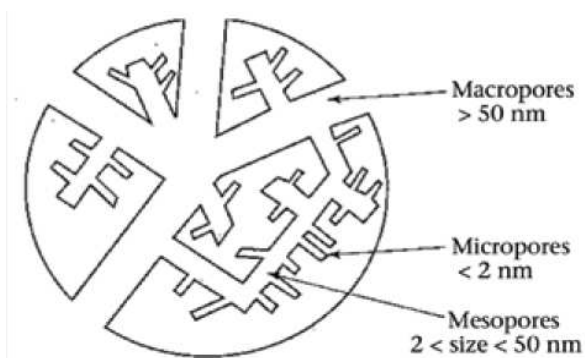
Figure I.5 Schematic diagram of the pore size network of an activated carbon grain.

The ratio between different types of pore size, i.e. the pore size distribution (for example Figure I.6), could be controlled by parameters of the activation process such as activation temperature and activation time or with different precursor. The specific surface area is

generally from 500 to 2500 m^2/g, corresponding to the high specific capacitance around 100 – 150 F/g in organic electrolyte with operating voltage up to 3 V or in aqueous electrolyte around 200 F/g but only 1 V, since the electrolyte voltage window limits the cell voltage [3].
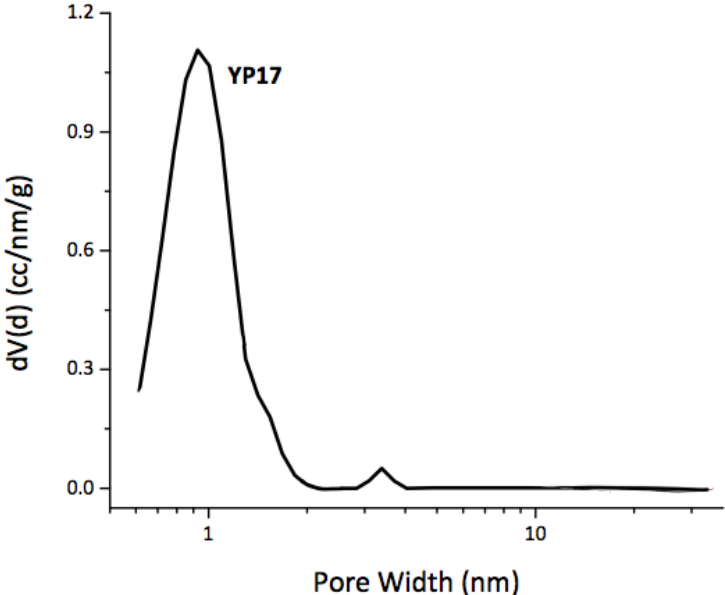
Figure I.6 Pore size distribution of an activated carbon YP-17 [12].

In spite of the high specific surface area of ACs, not all of the materials give high capacitance as expected [13, 14]. It was attributed to the inaccessibility of the solvated ions to the micropores as shown in Figure I.7 [15].

Figure I.7 Schematics of the traditional view of mechanism of the solvated ion adsorption in activated carbons (ACs).

Micropores (< 2 nm) were considered too small for ions to enter, since they are smaller than the size of the solvated ion, especially in organic electrolyte [15]. Consequently, they were thought to have no contribution to the charge storage, i.e., the capacitance. Macropores (> 50 nm) were too large to be fully occupied, thus wasting the pore spaces inside the active materials (dead volume), i.e., not efficient for maximizing t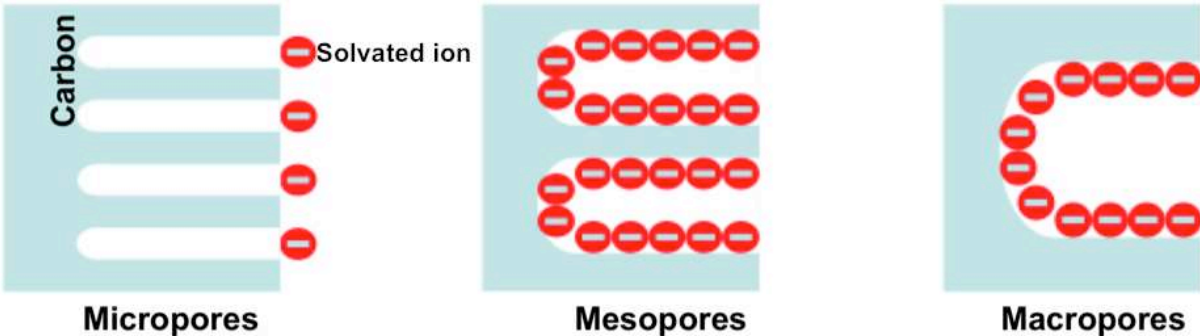he capacitance. Mesopores, as the compromise of the former two situations, were considered as the most ideal one to produce capacitance.

Therefore, plenty of efforts were made on adjusting most of the pores inside the carbon grain into the size around two times of the solvated ions sizes, i.e., (2 − 5 nm in organic electrolyte) which in the range of mesopores, to maximize the capacitance [16]. However, the improvement was not as distinct as expected. In contrary, several studies showed increased capacitance in mesoporous ACs with large amount of micropores [17-19]. The same phenomena were observed with microporous ACs [20]. A possible mechanism as the partial desolvation of the ions to enter into micropores was suggested [17-19, 21]. However, since the pore size cannot be finely controlled using activation treatments, ACs show a large pore size distribution, ranging between ~ 0.5 nm to ~ 5 nm. This large pore size distribution of ACs, involving still certain amount of mesopores and macropores even in microporous ACs, made the proposed mechanism quite suspicious. For example, a typical AC called YP17 shows a range of pore size around 1 nm, around microporous range (Figure I.6). However, there are still mesopores and macropores existing in YP17.

Finally, the effect of micropores was firstly observed using carbide derived carbons (CDCs) obtained through extraction of metals from carbides (TiC, SiC and other) by etching in halogens at high temperatures [22-24].

Eq. 9

$$TiC + 2Cl_2 \xrightarrow{HT} TiCl_4 + C$$
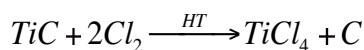
As shown in Eq. 9, the withdrawal of metals from crystalline structures of the carbides keeps the structures and leads to a controlled and narrow pore size distribution in CDCs. An anomalous increase in carbon capacitance was achieved with different temperature treated TiC-CDCs, i.e., with different sub-nanometer pore sizes ranging from 0.6 to 1.1 nm (Figure I.8) [24].
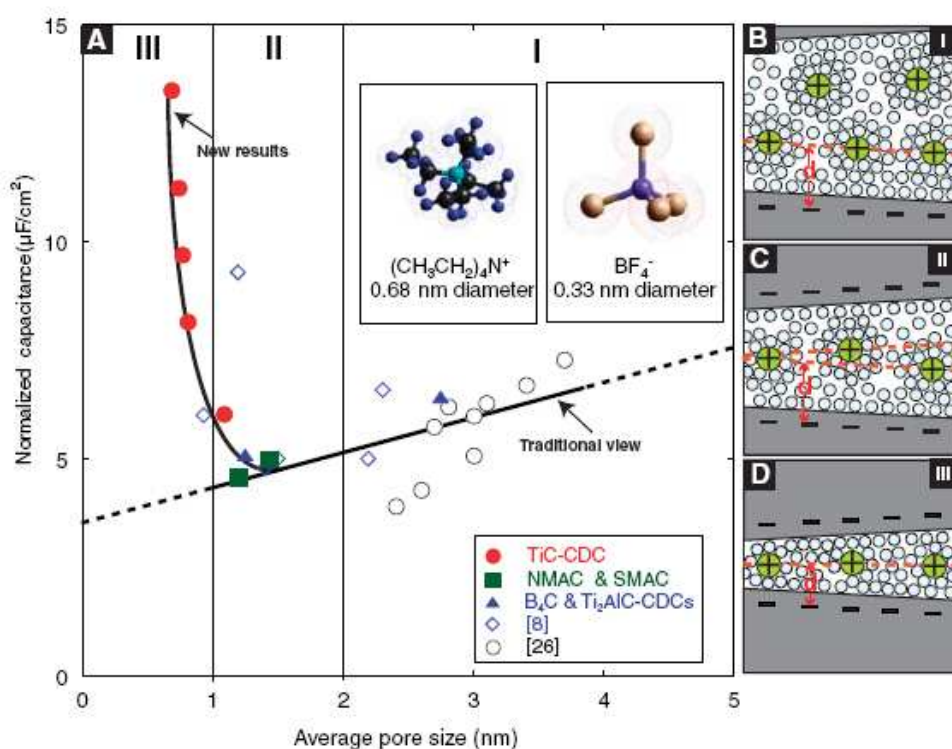
Figure I.8 (A) Plot of specific capacitance vs. average pore size and (B to D) schematic drawing of ions inside the pores with sizes (B) larger than 2 nm, (C) between 1 and 2 nm, (D) smaller than 1 nm [24].

The results were achieved in 1.5M NEt4BF4 acetonitrile (AN), in a 2-electrode configuration, and the solvated ions diameter in this solvent are 1.3 and 1.2 nm respectively for cation and anion. The normalized capacitance decreases with the decrease of pore size and unexpectedly increased at around the solvated ion size. The gravimetric and volumetric capacitances obtained by CDCs are around 50% and 100% respectively higher than that of

ACs. Thanks to the very narrow pore size distribution, the increase of the normalized capacitance could be attributed to diminishing pore sizes, hence making the partial desolvation mechanism [24] proposed earlier for the microporous ACs, more consistent.

Carbide derived carbon structure was analyzed by Raman spectroscopy [25], which is a standard non-destructive analysis tool widely used for characterization of carbon materials. In Raman spectra recorded in the near-infrared and visible light regimes, carbon materials typically exhibit two broad bands, called D (disordered) and G (graphitic). The presence and position of D- and G-peaks, their intensity ratio (I_D/I_G) and full width at half maximum (FWHM) can be used to extract the structural information of the materials. Appearance of both peaks in visible Raman spectra depends fundamentally on the ordering of sp^2 sites and only indirectly on the fraction of sp^3 sites. The G-peak appears due to the in-plane bond-stretching motion of pairs of C sp^2 bonded atoms. This mode does not require the presence of six-fold benzene rings, it occurs at all sp^2 sites. The D-peak is symmetry forbidden in perfect graphite and is activated only in the presence of disorder (sp^3 structure). The spectra of CDC show two main features: the D- and G-peaks situated around $1350 \, cm^{-1}$ and $1600 \, cm^{-1}$, respectively (Figure I.9). The peak positions, their intensities (I_D/I_G) and full width at half maximum (FWHM), as well as their wavelength dependent dispersion, were used to obtain information about the degree of disorder in CDCs.
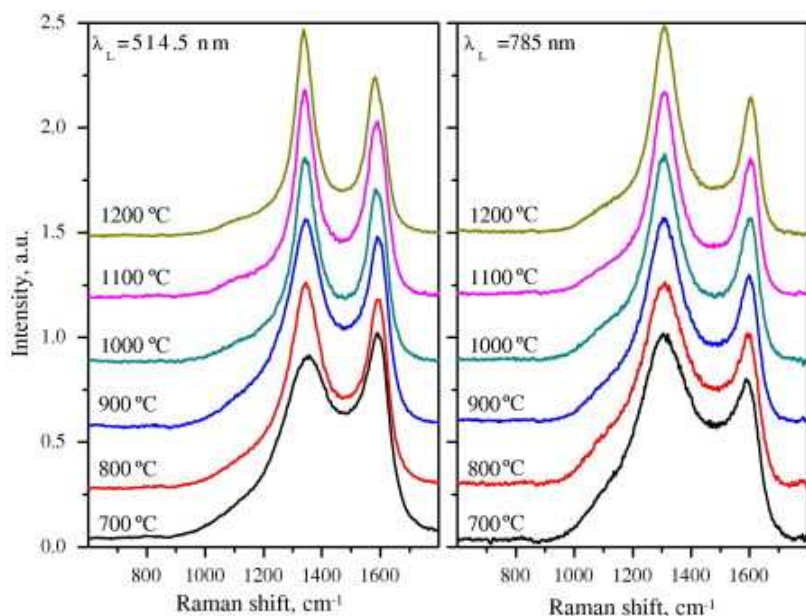
Figure I.9 Raman spectra of TiC-CDCs made at different temperatures recorded using wavelengths indicated in the figure [25].

Chlorination at different temperatures leads to different carbon structures. Corresponding to the sharper peaks at higher temperature in Raman spectra, TiC-CDC is better organized at higher temperature with more graphitic structures in TEM pictures (Figure I.10), thus more conductive.
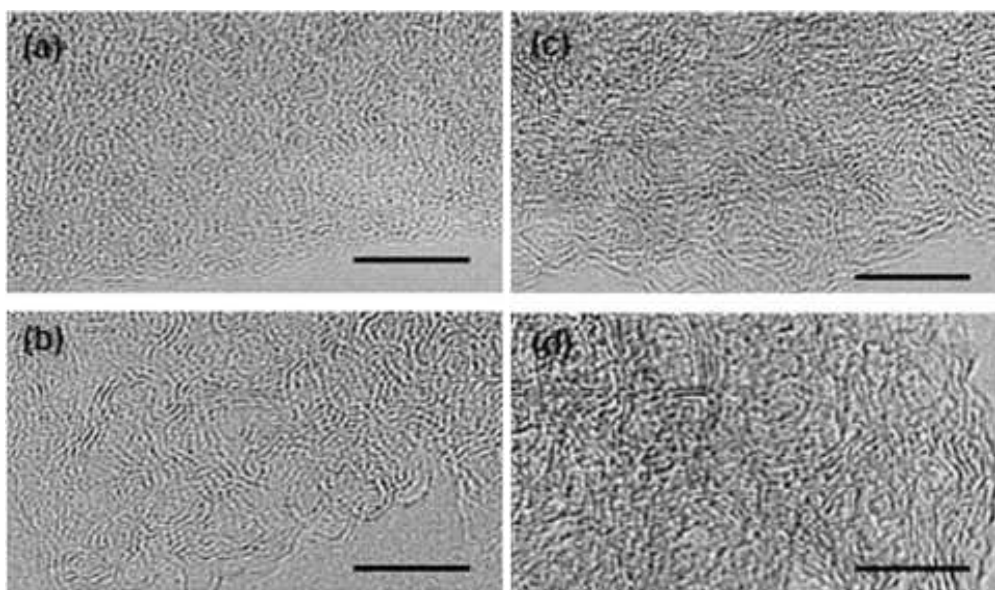
Figure I.10 TEM pictures of TiC-CDCs produced by chlorination of TiC at a) 400 °C, b) 800 °C, c) 1000 °C and d) 1200 °C with a scale bar at 5 nm [26].

Other carbon materials, especially carbon nanomaterials such as carbon nanotubes (CNTs) [27, 28] and onion like carbon (OLC) [29-31] can be used as active materials in EDLC electrodes. Despite a specific surface area much lower than activated carbons (1300 $m^2.g^{-1}$ for CNTs and 500 $m^2.g^{-1}$ for OLC), these exohedral carbons have a non-porous fully accessible surface area helps fast charging and discharging of supercapacitors and show high conductivities that facilitate the polarization of the device.

OLC is synthesized through annealing of nanodiamond powder at high temperatures [32] to graphitize the nanodiamond into OLC. A spherical particle of OLC is shown in Figure I.11. The bent graphitic layers in the onion were observed. Thanks to the highly graphitized structure, the conductivity of OLC is very high, similar to carbon black (around 4 $S.cm^{-1}$) [33]. Specific surface area is around 500 $m^2.g^{-1}$, in a moderate range.
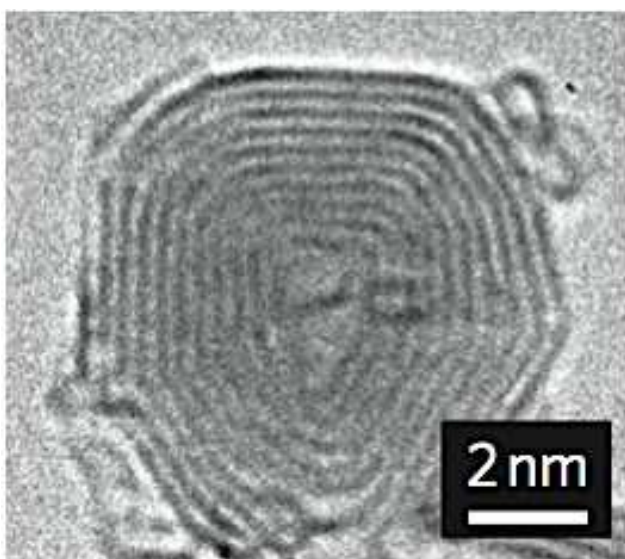
Figure I.11 TEM picture of an OLC particle.

Lack of porous structure obviously sacrifices the capacitance without enough surface area to accommodate electrolyte ions. However, these spherical particles allow ultrafast adsorption

and desorption of electrolyte ions, since there is no need to diffuse or even squeeze into pores. In spite of the high cost, high power supercapacitors have been prepared with OLC [29, 30].

I.3 Electrolytes

According to Eq. 6 ($W=CV^2/2$) and Eq. 7 ($P_{max}=V^2/4R$), the voltage is a key factor for increasing both the energy and power performance of supercapacitors. The voltage window is usually limited by electrolyte. Being able to apply into all kinds of electrochemical devices, four types of electrolytes widely used in carbon-based symmetric supercapacitors are introduced here: aqueous electrolytes, organic electrolytes, gel polymer electrolytes and ionic liquids.

I.3.1 Aqueous Electrolytes

Aqueous electrolytes, i.e. water-based electrolyte, are widely used in electrochemical devices because of their high ionic conductivity (1 S.cm^{-1}) and high capacitance when used in supercapacitors, but the water electrolysis beyond 1 V limits the operating voltage, as well as both the energy and power densities, and thus their applications. However, using aqueous electrolytes is more convenient for assembly of supercapacitors with no particular caution, while electrolytes with voltage window > 1 V are usually assembled in dry room with H_2O content lower than 1 ppm. Aqueous electrolytes are thus widely used in supercapacitors, since they are easier to handle. Acid and basic aqueous solutions such as H_2SO_4, H_3PO_4 or KOH are the most widely used aqueous electrolytes thanks to their high conductivity.

I.3.2 Organic Electrolytes

Organic electrolytes show larger voltage window stability (up to about 5 V) instead of 1 V in aqueous electrolytes. As a result, supercapacitors using organic electrolytes show higher cell voltage. Although the conductivity of organic electrolytes is at least one order of

magnitude lower than aqueous ones, they are still preferred as the energy density is largely improved. The most widely used organic solvents are acetonitrile (AN) and propylene carbonate (PC). AN has a lower boiling point (bp 82 °C) and a higher melting point (mp -45 °C), compared to PC (bp 241 °C and mp -55 °C). Despite a low flash point (5 °C), AN still prevails over PC thanks to a lower viscosity that reduces the internal resistance of the devices.

Table I.1 Comparison of organic solvents acetonitrile vs propylene carbonate.

Solvent	m.p. /°C	b.p./°C	Flash point/°C	Viscosity (25 °C)/mPa.s	Dielectric constant (20°C)
Acetonitrile (AN)	-48	81 - 82	5.5	0.369	36.64
Propylene carbonate (PC)	-55	241.7	132	2.8	64.9

However, AN is starting to be substituted by PC, because it is flammable and harmful. Choice of salts for supercapacitor mainly depends on decomposing potentials of the solute ionic species. The preferred solutes are tetraalkylammonium salts of anions that are electrochemically stable, such as PF_6^-, BF_4^- and AsF_6^-. The most widely applied salt for organic electrolyte is tetraethylammonium tetrafluoroborate (NEt_4BF_4). The concentration of electrolyte is usually determined by final conductivity of electrolytes and the operating temperature range. If the carbon pore size of the electrode material could be adapted to the electrolyte ion size, the capacitance and the energy density would increase significantly.

I.3.3   Gel Polymer Electrolytes

The gel polymer electrolytes started drawing attention since their introduction by M. Armand into the battery field [34]. Since then, gel polymer electrolytes have been widely developed as the conductivity of electrolyte was ensured to be used in electrochemical systems. For instance, KOH-PEO (potassium hydroxide – polyethylene oxide) gel polymer electrolyte was used in carbon aerogel based supercapacitor [35]. Compared with KOH aqueous electrolyte, resistance was comparable, but capacitance was decreased in half.

There are several advantages with gel polymer electrolytes: no volatile organic solvent and lightweight of electrolyte films. Nowadays, besides supercapacitors [36, 37], it could be also applied in other electrochemical systems such as electrochromic windows [38, 39] and sensors [40, 41]. This is the first type of solid-state electrolyte that could be applied to build an all-solid-state power source.

The gel polymer electrolyte is a two-phase system composed of ionically conducting medium (liquid electrolyte) entrapped in host polymer matrix.

The polymer matrix, based on poly(propylene), poly(vinylidene difluoride), poly(tetrafluoroethylene), poly(ethylene oxide) (PEO), polyaniline (PANI), poly(methyl methacrylate) (PMMA), is regarded as the supporting structure of the solid-state electrolyte to offer mechanical strength, but it has no influence on electrochemical processes in the device.

However, gel polymer electrolyte suffers from poor mechanical strength. On-going researches has already suggested several solutions, such as composite gel polymer electrolytes and porous polymer electrolytes.

I.3.4   Ionic Liquid

The advantage of organic electrolytes over inorganic electrolytes is the high voltage window, leading to high energy density. To further enlarge the voltage window, ionic liquids (ILs), with voltage window up to 6 V, were studied as electrolyte for supercapacitors applications [42].

ILs are solvent-free electrolytes (molten salt like sodium chloride at 800 °C), that are liquid at low temperature. Such ILs are called Room Temperature Ionic Liquids (RTILs). Basically, in ILs, there are organic anions and cations with asymmetric size and aspect ratio, which greatly reduces lattice energy and thus lower the melting point. A second key feature is the low vapor pressure even at an elevated temperature, which reduces the risk of flammability.

Although higher voltage window unquestionably increases the energy of the devices, the high viscosity and low conductivity of ILs drastically reduce the power performance at temperature lower than room temperature. To settle this issue, operation temperature of supercapacitors using ILs is usually at temperature higher than room temperature.

Supercapacitors rarely operate at high temperature except when used near electronic components generating heat, but this is not controllable source of heat. There is thus the need to extend the temperature window of such devices so they can operate at lower temperatures, while at the same time keeping the high temperature range.

In the case of aerospace or aircraft industry, the temperatures requirements are even more drastic with operation below 0 °C down to -50 °C. Work has been done by Brandon et al to design electrolytes for operation down to -60 °C based on AN/NEt$_4$BF$_4$ mixture. However, these mixtures were limited at 50 °C at high temperature [43]. In order to use supercapacitors at low temperature as well as high temperature, temperature tolerance should also be developed. Recently, a eutectic mixture of ionic liquids (ILM) N-methyl-N-propylpiperidinium bis(fluorosulfonyl)imide (PIP$_{13}$FSI) and N-butyl-N-methylpyrrolidinium bis(fluorosulfonyl)imide (PYR$_{14}$FSI) with a temperature range from -50 to 100°C during electrochemical characterization of supercapacitors based on carbon nanotubes (CNTs) and onion like carbon (OLC) [31] was reported. This electrolyte could be of great interest as well for micro-supercapacitors, enlarging the temperature operation range.

I.4   Electrochemical Characterization

In this thesis, two electrochemical characterization techniques were mainly used to measure the electrochemical performance of the micro-supercapacitors fabricated: Electrochemical Impedance Spectroscopy (EIS) and Cyclic voltammetry (CV).

I.4.1 Eletrochemical Impedance Spectroscopy (EIS)

Electrochemical impedance spectroscopy is a steady state technique used to distinguish individual contributions of various phenomena. A sinusoidal voltage punctuation of small amplitude (typically ± 5 mV) and frequency f ($\omega=2\pi f$) is superimposed to a bias voltage (stationary-state). Electrochemical impedance spectroscopy is obtained by scanning different frequencies, typically from 50 kHz to 10 mHz. The applied voltage is varied according to Eq. 10.

Eq. 10

$$V = V_0 + \Delta V \sin(\omega t)$$

where V_0 is initial steady state potential of supercapacitor (V), in all study in this thesis, V_0 is the open circuit potential of the cell, 0 V; ΔV is amplitude of the signal (V); ω the pulsation; $\omega = 2\pi f$, where f is the signal frequency.

The response of this applied potential is a sinusoidal current, with amplitude of ΔI and a shifted angle φ of phase indicated in Eq. 11.

Eq. 11

$$I(t) = I_0 + \Delta I \sin(\omega t - \varphi)$$

where I_0 is the initial steady state current of the supercapacitor (A), in all study in this thesis, I_0 is 0;

The potential applied and the current response could also be transformed to facilitate the mathematical treatment (Eq. 12 and Eq. 13):

Eq. 12

$$V(\omega) = V_m \exp(j\omega t)$$

Eq. 13

$$I(\omega) = I_m \exp\left[j\left(\omega t - \varphi\right)\right]$$

The complex impedance is defined by the ratio between the applied voltage and current response (Eq. 14)

Eq. 14

$$Z_\omega = \frac{V(\omega)}{I(\omega)} = \frac{V_m}{I_m}\exp\left(-j\varphi\right)$$

The complex impedance is composed of a real part, corresponding to the resistance, and an imaginary part, corresponding to the capacitance.

The variation of impedance is usually represented in terms of Nyquist plot: the imaginary part of the impedance -Im(Z) is plotted versus the real part Re(Z) at different frequencies (Figure I.12c). The RC circuit models proposed in Figure I.14 fails to simulate Nyquist plot of real supercapacitors with three-dimensional porous electrodes. This porous electrode could be described as a succession of series/parallel RC components, according to De Levie model [44], with electrolyte ions reaching the outer surface area, which is in contact with the bulk electrolyte solution, then entering into the inner surface of the pore channels. This model (Figure I.12a) was proposed by De Levie in 1963 [45] with its equivalent circuit (Figure I.12b), called the Transmission Line Model.
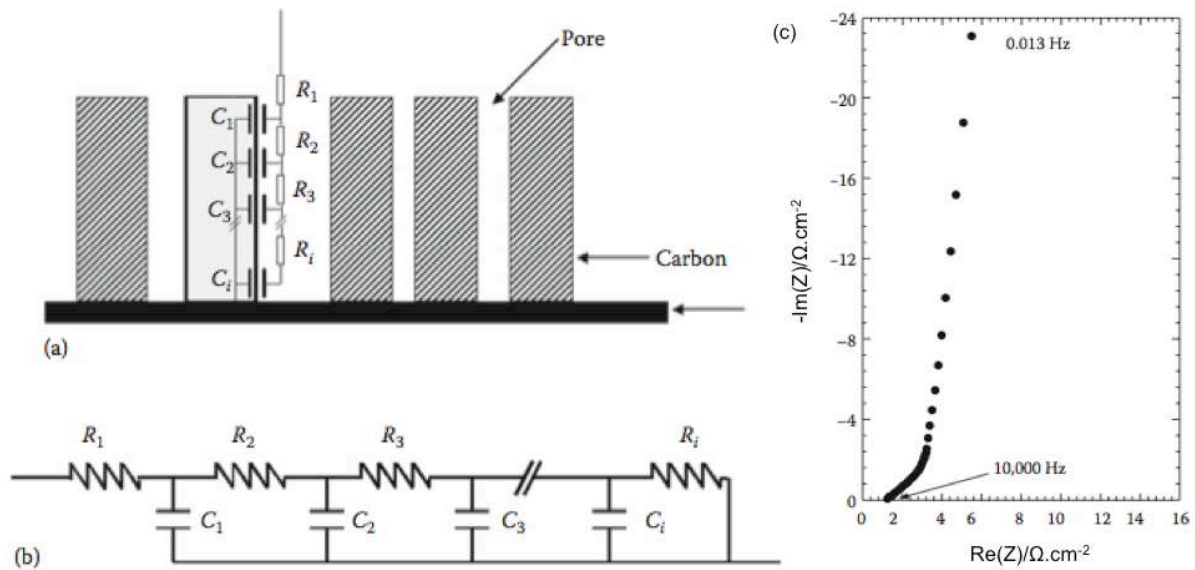
Figure I.12 a) A schematic plot of Transmission Line Model proposed by De Levie and b) its equivalent circuit; c) an example of Nyquist plot of supercapacitors with activated carbon as electrodes in organic electrolyte [46].

The electrode shown in Figure I.12a has pores with cylindrical shape in uniform size. Upon potential polarization, electrolyte ions adsorption takes place at the outer surface of the electrodes. The transportation of electrolyte ions from bulk electrolyte onto the surface of the electrode causes a resistance corresponding to equivalent series resistance (ESR). Ions go deeper into the pore depth to charge C_1, C_2, C_3,…C_i (as double layer capacitance along the pore) with resistance R_1, R_2, R_3,…R_i (as electrolyte resistance inside the pore). At high frequency, the ions can only reach the outer surface of the electrolyte, with the real resistance as ESR. When frequency decreases, at mid-frequency, the ions can move deeper into the pores, thus showing higher resistance at lower frequency. At low frequency, both capacitance and resistance reach the maximum with no change theoretically, showing an almost vertical line. The cross point of the low frequency vertical line and the mid-frequency line is "the knee frequency".

With Nyquist plot, the complex impedance could be written as $Z = Re(Z) - jIm(Z)$. A supercapacitor could also be described as a combination of a resistor and a capacitor as

function of frequency *f* in series: the real part of impedance is the impedance of the resistor R and the imaginary part is the impedance of the ideal supercapacitor $1/(jC\omega)$. Hereby the complex impedance of this combined circuit could be also written in Eq. 15.

Eq. 15

$$Z = R(\omega) + \frac{1}{jC(\omega)\omega} = \frac{1}{jC_{complex}\omega} = \mathrm{Re}(Z) - j\,\mathrm{Im}(Z)$$

Complex capacitance $C_{complex}$ could be represented as follow in Eq. 16 [46].

Eq. 16

$$C_{complex} = \frac{1}{\omega(j\,\mathrm{Re}(Z) - \mathrm{Im}(Z))} = \frac{j\,\mathrm{Re}(Z) - \mathrm{Im}(Z)}{\omega(\mathrm{Re}^2(Z) + \mathrm{Im}^2(Z))} = \frac{j\,\mathrm{Re}(Z) - \mathrm{Im}(Z)}{2\pi f\,(\mathrm{Re}^2(Z) + \mathrm{Im}^2(Z))}$$

Thus, real part and imaginary part of the complex capacitance noted as C' and C" respectively could be drawn out in Eq. 17.

Eq. 17

$$C' = \frac{-\mathrm{Im}(Z)}{2\pi f\,[\mathrm{Re}(Z)^2 + \mathrm{Im}(Z)^2]}$$

$$C'' = \frac{\mathrm{Re}(Z)}{2\pi f\,[\mathrm{Re}(Z)^2 + \mathrm{Im}(Z)^2]}$$

where *C'* is the capacitance of the supercapacitor; *f* is the frequency, Im(Z) is the imaginary part of the impedance and *C"* the loss.

An example of real part and imaginary part of capacitance versus frequency is shown in Figure I.13.
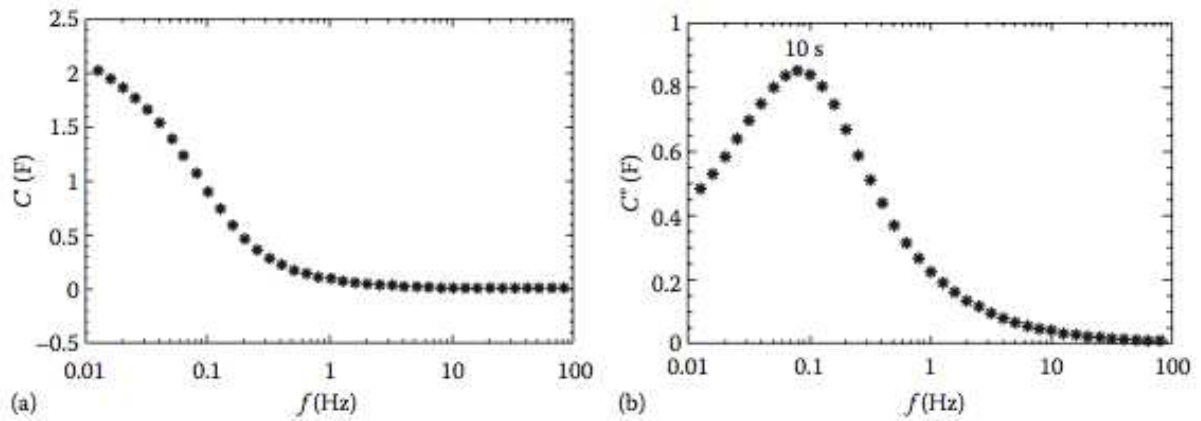
Figure I.13 a) Real part and b) imaginary part of the complex capacitance versus frequency.

The capacitance of supercapacitors is defined by the plateau at low frequency (Figure I.13s). Specific capacitances of the devices have been normalized in this thesis by the footprint area of the device and the volume of a single electrode, respectively. With C'' vs f (Figure I.13b), time constant τ could be extracted as the frequency f_{max} where C'' reaches the maximum and $\tau = 1/f_{max}$. The smaller the time constant τ is, the faster the supercapacitor could be fully discharged with an energy efficiency ≥ 50 %, and the higher the real power delivery is.

I.4.2 Cyclic Voltammetry (CV)

Cyclic voltammetry has been used to investigate the capacitive behavior and the stability of supercapacitors with different active materials and different electrolytes within different voltage range.

A scan with potential changing linearly with the time at a constant rate is applied on the cell:

Eq. 18

$$E = E_0 + vt$$

where E_0 is the initial potential of the scan, generally the rest potential of the cell (*V*), *v* is the scan rate (*V/s*), *t* is time (*s*).

To perform Cyclic Voltammetry experiment, the linear potential sweep is reversed when it reaches a set potential. The current response as a function of potential is recorded during the charge/discharge cycle.

Using the RC model proposed by De Levie [44], with an ideal supercapacitor of an identical capacitance at all voltage, when the scan rate *dV/dt* is constant, current *I=dQ/dt=CdV/dt* is thus also constant. The cyclic voltammogram, as a perfect rectangular, is shown in Figure I.14a. However, in reality, there are several factors can cause deviation from ideal CV plot. Equivalent Series Resistance (ESR) is introduced to be in series with the ideal capacitance and mainly defined by resistance of the electrolyte and electrode, leading to a period of time to reach a stable capacitive current, called time constant τ = RC. Before reaching the stable capacitive current, current slowly increases at the beginning of the positive scan and reverse scan, as shown in Figure I.14b. Another type of resistance is called leakage resistance, concerning undesired redox reaction or self-discharge inside the supercapacitor, thus in parallel to the capacitance. If the leakage resistance tends to ∞, it remains as an ideal supercapacitor. The smaller the leakage resistance is, the higher the leakage current is, as shown in Figure I.14c. The leakage resistance could be calculated from reciprocal of slope of the positive scan or negative scan. The combination of these two factors is shown in Figure I.14d, close to the real supercapacitor electrochemical signature. Despite this model, there are still several other factors affecting the shape of CV plots such as pore size distribution, especially for electrodes made of porous materials.
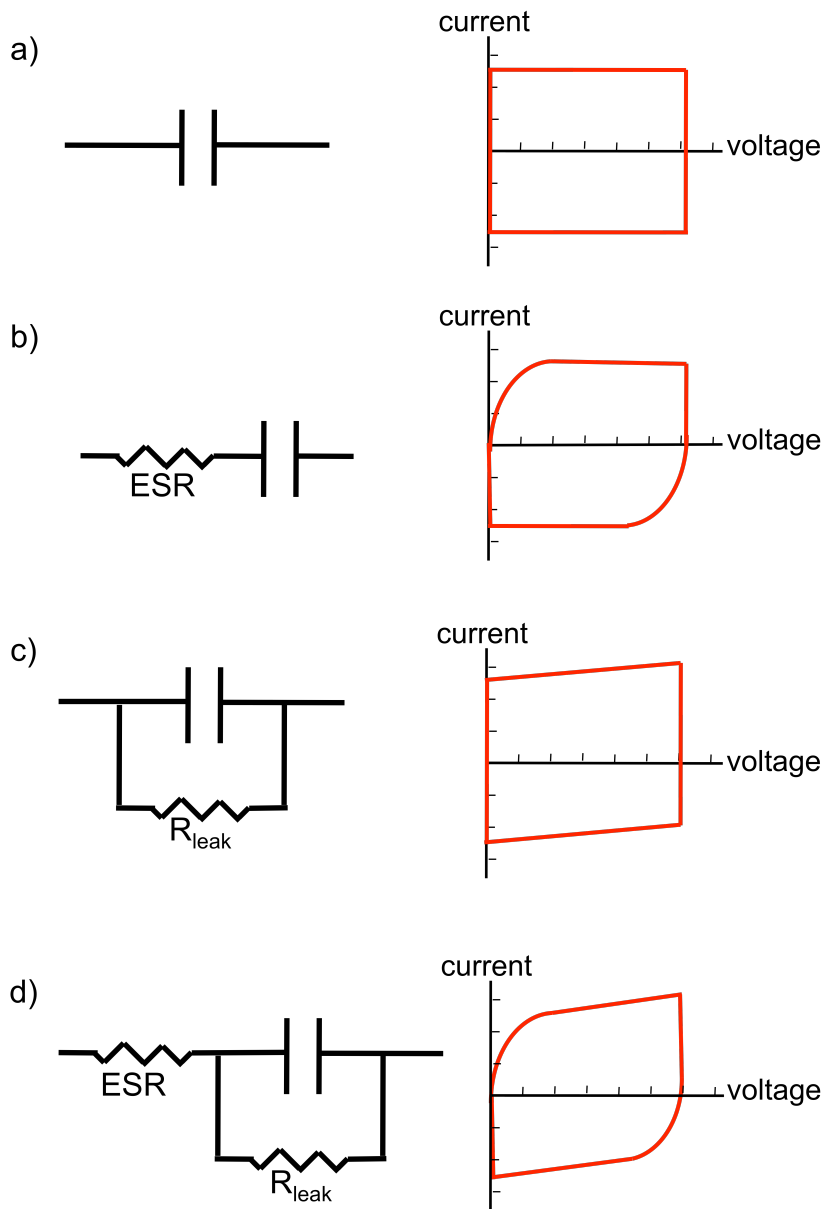
Figure I.14 Cyclic Voltammogram of a) an ideal supercapacitor, b) combination of a supercapacitor and a resistor in series or c) in parallel, d) a supercapacitor with resistors in series and in parallel at the same time.

From cyclic voltammetry technique, the capacitance of supercapacitor can be calculated from the integration of the current (by plotting current vs time using the potential scan rate) and dividing by voltage window, according to Eq. 1 $Q=CV$. The specific capacitance of the device will be then recalculated in terms of the footprint area of the micro-supercapacitors in this thesis.

II   Micro-supercapacitors

Micro-supercapacitors, in this thesis, are defined as supercapacitors able to be integrated onto chip, where electrodes are not assembled with the help of clips or Swagelok cell but realized layer by layer. Micro-scale dimension is another characteristic of these devices. To operate at this scale, microfabrication is necessary to produce micro-supercapacitors.

Microfabrication includes the processes for fabrication of miniature structures, usually in micrometer size or even smaller in a collective way on or within a single substrate such as silicon. In the microelectronics industry, miniaturization of integrated circuits (IC), which are composed of silicon-based electronic components, is possible thanks to the permanent improvement of microfabrication technologies. The integration of new functions, i.e. sensors, actuators or other MEMS (Micro Electro Mechanical Systems), forced the industry to develop technologies allowing surface and bulk micromachining of silicon substrate.

Hereafter, we introduce microfabrication techniques for depositing materials in thin film form and patterning them. Then, state-of-the-art micro-supercapacitors will be overviewed with a particular focus on the different strategies adopted to integrate non-conventional active materials (such as carbon) in a planar configuration and achieve at the same time high performance.

II.1   Microfabrication Techniques

Devices prepared by microfabrication are generally not self-supported but formed on a support substrate with thickness in micro-scale. Silicon, largely used in microelectronics and MEMS is the most logical solution (available, well-known). The substrate offers an easy handling platform for the device during several steps of different fabrication processes. Except for semi-conductors components, the substrate is usually only for supporting purpose. Materials in thin-film form [47], i.e. conductors, insulators, or semiconductors (for

microelectronics) are then deposited on the substrate to create the microdevices. For optical applications, deposited thin films could be reflective, transparent, light guiding or scattering. Films could also have chemical or mechanical properties according to the application. Deposition techniques could be divided into two categories: growth and deposition. Growth includes thermal oxidation for very thin oxide layers and epitaxy [48]. Deposition includes chemical vapor deposition and physical vapor deposition which comprises sputtering and evaporation, electrodeposition and printing techniques [49]. It will be shown later in this chapter that the most commonly used deposition techniques in micro-supercapacitors are sputtering and electrodeposition for pseudo-capacitive materials (RuO$_2$) [50] and printing techniques for carbon powders [51, 52].

The deposited layers in most cases should be patterned in order to realize different functions. The patterning is generally from millimeter scale to nanometer scale, which is the feature of micro-fabrication. The most widely applied patterning technique is photolithography: the use of a chromic mask to transfer the desired pattern onto the thin-film followed by etching [53]. Etching is the process of removing unwanted part from a thin film in order to form the pattern in micrometer scale. The part of unprotected film is exposed to etchant that can physically or chemically attack the target materials until they are totally removed. Etching techniques include dry etching and wet etching. Dry etching, or plasma etching, includes ion beam etching and Reactive Ion Etching (RIE) [54]. In RIE, the thin film is attacked by ionized chemically active plasma where high speed is generated by an electric field. Thus, both chemical etching and physical etching are involved in RIE. The etch rate and selectivity of chemical etching and physical could be adjusted by source power and bias power, respectively, according to the properties of thin film etched and the protecting layer. Wet etching involves usually chemical agent to dissolve part of the unprotected thin film.

Another possible technique, to pattern a thin film, is to grow it through a mask: for instance electrodeposition through a photoresist mask. Alternatively, a physical mask (called shadow mask or stencil) can be placed directly on the substrate during deposition. The deposition technique can be sputtering or evaporation or even screen-printing.

Direct writing [55] such as inkjet printing [52] could be applied automatically to the substrate to transfer the material by contact, offering other possibilities for patterning. The material is deposited only on the necessary areas, thanks to a head. Alternatively nanoimprint where a stamp (made of nano or micro features) inked with the desired material, can be used.

Focus ion beam (FIB) can also be used to physically etch away undesired part to pattern with heavy ions without any protection as the ion beam is focused.

To fabricate on-chip micro-supercapacitors that are able not only to be integrated into Microsystems, but also be of good performance, fabrication techniques should be chosen carefully.

II.2 State-of-the-art of micro-supercapacitors

Micro-supercapacitors were firstly reported in 2001 [50]. Since then, there have been several models developed. However, it is early stage of technology and many microfabrication techniques combined with the synthesis of active materials are under test.

Electrode materials of micro-supercapacitors evolve from easy fabricated but expensive ruthenium oxide [50, 56-58] to widely used carbon materials with advanced microfabrication techniques [52, 59-62].

There have been already several trials on fabricating thin-film electrodes with different materials deposited with different techniques such as RuO_2-SnO_2 electrode via reactive sputtering [58], carbon nanotubes/graphenes via layer by layer (LBL) [63], cone-shaped polypyrrole/RuO_2 via anodic deposition [64] and carbide derived carbon film via chlorination

[59, 65], etc. Thin films of carbon nanotubes and chemically reduced graphenes were synthesized by layer-by-layer assembling [63]. A volumetric capacitance of 160 F.cm^{-3} for the 350 nm thick hybrid carbon layer was achieved in 0.5 M H$_2$SO$_4$ aqueous electrolytes, higher than its macroscopic supercapacitors in the same electrolyte (130 F.cm^3), thanks to the thin layer of electrode.

Although not ready for integrating on-chip, these electrodes could be potentially used to fabricate on-chip micro-supercapacitors in the future.

In ready-to-integrate micro-supercapacitors, there are two configurations reported: stack configuration and interdigitated configuration shown in Figure I.15.
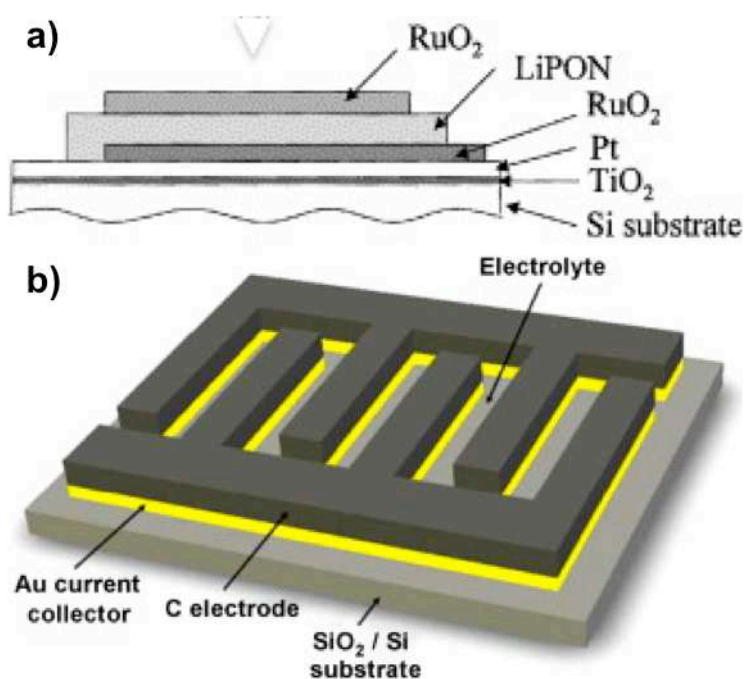
Figure I.15 Schematic pictures of a) a stack micro-supercapacitor and b) an interdigitated micro-supercapacitor.

Stack configuration forms a sandwich-like stacking with electrodes face to face and electrolyte in between. A separation between the electrodes is necessary: it can either be an insulating layer soaked with the electrolyte or the solid electrolyte itself. It is similar to macroscopic supercapacitors, but the different layers (electrodes and electrolyte) are

deposited by microfabrication techniques one after another to form the stack. The layers are then patterned and contacts are created to achieve the final integrated micro-device. Interdigitated configuration generally involves microfabrication on a substrate (in most cases silicon, but it can also be a polymer) with electrodes patterned in interdigitated form. The separation in this case is the lateral spacing between the interdigitated fingers.

For the purpose of making a summary, in this section, we divide reported micro-supercapacitors into two categories: stack micro-supercapacitors and interdigitated micro-supercapacitors. They have small footprint area ($\sim$ or < 1 cm^2) and small thickness (< 100 μm) and easy to be integrated into Microsystems. In addition, as microfabrication is involved during the process of realizing micro-supercapacitors, at the early stage of development, groups specialized in microfabrication took lead showing proofs of concepts with electrochemical data sometimes incomplete. Moreover, as different groups have different way of calculating the capacitance and/or energy density, it is difficult to compare directly by reported figures. Thus, in order to compare performance, capacitance, energy density and power density were recalculated according to the footprint area of the micro-scale device in this section.

II.2.1   Stack micro-supercapacitors

II.2.1.1   On a substrate

Most of the early works done as micro-supercapacitors were using metal oxides as active materials thanks to the large variety of deposition techniques (sputtering, atomic layer deposition – ALD, electrodeposition) available, despite poor conductivities ($\sim 10^{-6}$ S.cm^{-1}). A stack RuO$_2$-based micro-supercapacitor with Li$_{2.94}$PO$_{2.37}$N$_{0.75}$ (LiPON) as electrolyte was firstly reported in 2001 by simple sputtering deposition [50]. This system was selected because thin film of LiPON electrolyte had been successfully applied for thin film batteries

[66]. Despite LiPON was used instead of conventionally used proton H^+ for RuO_2 electrode, a capacitance of 47.5 mF.cm^{-2} was obtained within 2.5 V.

Later on, the same research group published on LiPON-based stack micro-supercapacitor modified by co-sputtering of RuO_2 with tungsten (W) to enlarge the interspace of atoms in RuO_2 to facilitate the mobility of Li^+ [57]. The modified stack micro-supercapacitor achieved 200 mF.cm^{-2} per footprint area capacitance under 2.5 V.

Electronically Conducting Polymers (ECPs), another electrode material for pseudo supercapacitors, have also been studied for stack micro-supercapacitors. Example of a polymer-based stack micro-supercapacitor was composed of polypyrrole (PPy)-decorated nanoporous gold (NPG) as electrode material and an aqueous $HClO_4$-poly(vinyl alcohol) (PVA) gel as electrolyte. 1.8 mF.cm^{-2} and 0.65 mJ.cm^{-2} were achieved as specific capacitance and specific energy, respectively, within 0.85 V [67].

One of the first carbon-based stack micro-supercapacitor was reported in 2006 [68] with 99 wt% Super P carbon black (with specific surface area of 62 m^2.g^{-1}) and 1 wt% polyvinylidene fluoride binder in N-Methyl-2-pyrrolidone as electrode material using not widely used microfabrication technique: Origami fabrication as shown in Figure I.16.
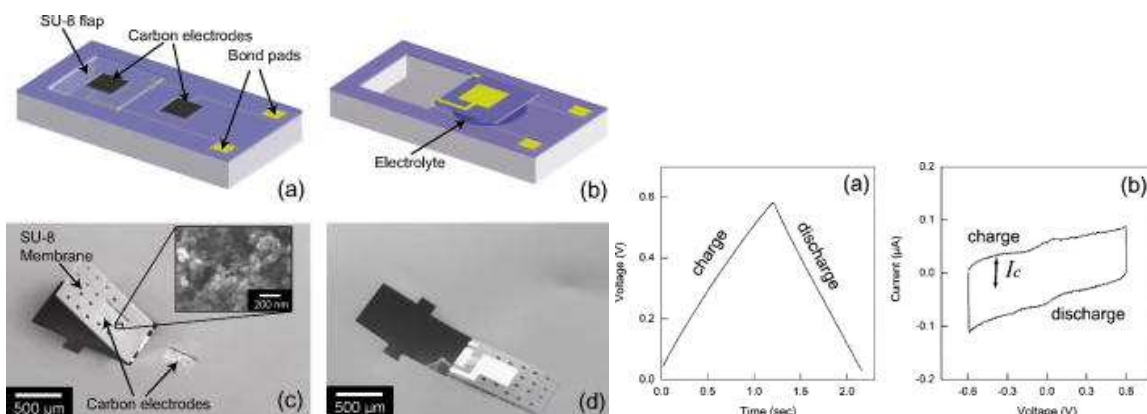

Figure I.16 A schematic illustration of carbon-based stack micro-supercapacitor fabricated via origami (left) and its electrochemical performance (right) in 1.5 M H_2SO_4 [68].

The device was electrochemically characterized in 1.5 M H_2SO_4 aqueous solution. Only 0.6 V was reached and poor capacitive behavior was presented by cyclic voltammogram at a scan rate of 50 mV/s. Specific capacitance of 0.8 $mF.cm^{-2}$ per footprint area and specific energy of 0.2 $mJ.cm^{-2}$ was achieved in this micro-supercapacitor.

During the same year, another stack micro-supercapacitor fabricated by dispenser printing of electrodes of mesocarbon microbead (with specific surface area of 10 $m^2.g^{-1}$) in a PVDF polymer binder and $BMIM^+BF_4^-$ ionic liquid in PVDF gel electrolyte was realized [51]. Poor capacitive behavior with a severely distorted CV plot was presented within 2 V voltage window. Electrochemical performance of this micro-supercapacitor was measured with specific capacitance of 0.3 $mF.cm^{-2}$ per footprint area and specific energy density of 0.5 $mJ.cm^{-2}$.

These two examples were only proof of concept of carbon-based stack micro-supercapacitors. The low specific surface area materials (62 $m^2.g^{-1}$ for the Origami fabricated device and 10 $m^2.g^{-1}$ for dispenser printed device) also explain the low capacitance.

Moving from low specific surface area carbon to carbon nanotubes (CNTs) as active material, higher energy and power densities could be obtained for flexible printable stack micro-supercapacitors [69]. An ideal capacitive behavior marked by quasi-rectangular shape of CV plot (at 10 mV/s within 3 V) was presented in organic electrolyte (1 M $LiPF_6$ in 1:1 ethylene carbonate/diethylcarbonate by weight). A specific capacitance of 1.2 $mF.cm^{-2}$ per footprint area could be achieved in aqueous-based gel eletrolyte PVA/H_3PO_4. The capacitance was not high, because single-walled carbon nanotubes (SWCNTs) thin-films (0.6 μm) were sprayed onto the current collector surface. Despite the low capacitance, at least better capacitive behavior was achieved (Figure I.17).
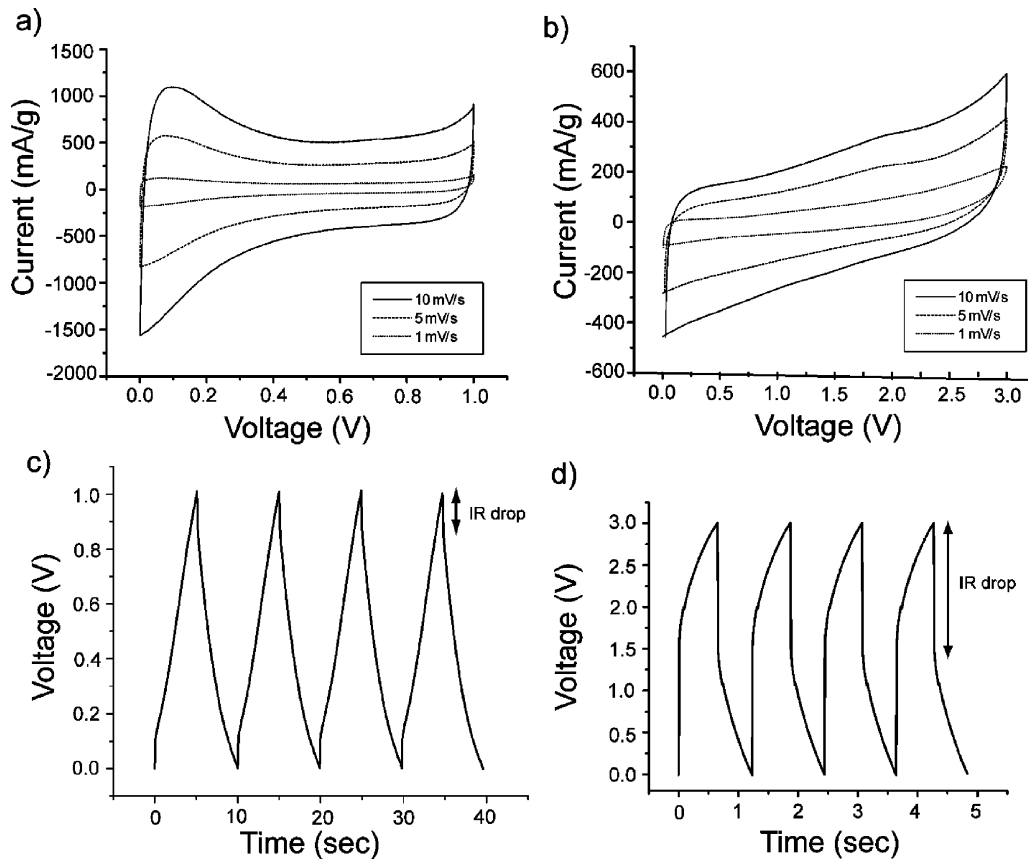
Figure I.17 Cyclic voltammetry of SWCNT supercapacitor in (a) PVA/H₃PO₄ polymer electrolyte and (b) LiPF₆/EC:DEC. Galvanostatic charge/discharge curves measured with a 1 mA/cm₂ (30 mA/mg) current density for a thin film SWCNT supercapacitor using (c) PVA/ H₃PO₄ polymer electrolyte and (d) LiPF₆/EC:DEC. [69]

II.2.1.2   Flexible stack micro-supercapacitors

As opposed to thin films deposited on a hard substrate (silicon), there are cases of micro-supercapacitors with stack configuration where the substrate is flexible (paper, polymer) or where one of the electrodes itself is flexible. A possible application field is the emerging printable electronics. For those flexible devices, several techniques can be applied to build the stack. Examples found in literature are mainly based on carbon nanotubes, such as Meyer rod coating method of CNT ink [70], layer-by-layer (LBL) assembling [63, 71], laser writing of graphenes [72] and CVD of CNTs [73]. Flexible micro-supercapacitors were fabricated from CVD of CNTs. The CNTs were vertically aligned on the current collectors as shown in Figure I.18 along with nanoporous cellulose paper soaked with various electrolytes. High specific

capacitance of 330 mF.cm^{-2} was achieved with 50 μm thick CNTs layer in ionic liquid electrolyte [73].
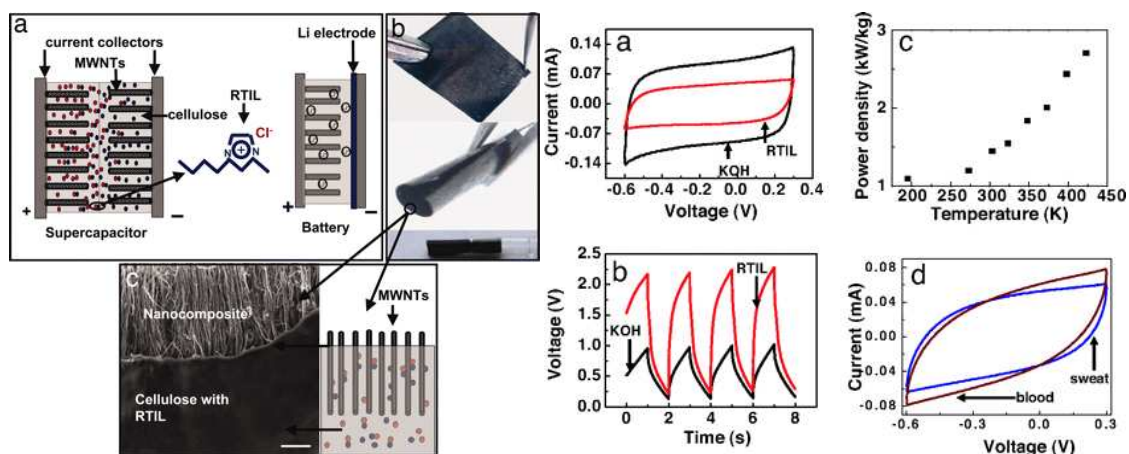

Figure I.18 Schematic pictures of the flexible micro-supercapacitors with electrochemical characterization results. [73]

Stack micro-supercapacitors, despite the large footprint areas, present still one dimension in micrometer scale. Theoretically, micro-scale device should be able to offer better performance than macroscopic supercapacitors regarding the size effect. The thinner the electrode layer is, the better the electrolyte ions could reach the full carbon layer. With this idea, several ultra-thin carbon-based supercapacitors were realized with the thickness less than 10 nm. In this scale, there should be no problem of adhesion between electrode materials, as there is little amount of powder to load on the electrodes.

A stack micro-supercapacitor was fabricated with only 10 nm of pristine graphene and multilayer reduced graphene oxide by "in-plane" fabrication approach as shown in Figure I.19 [74].
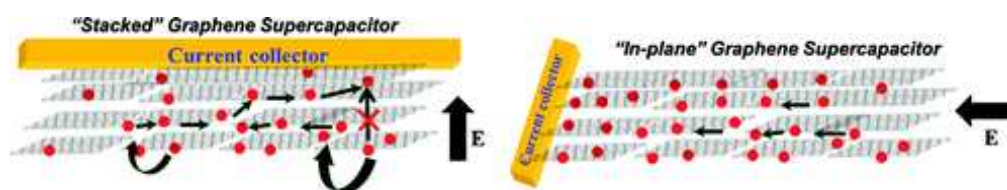

Figure I.19 Mechanism of "in-plane" carbon-based stack micro-supercapacitors [74].

By this difference in the orientation of graphene layers, 5 times higher specific capacitance per footprint area was achieved in a polymer-gel (PVA-H_3PO_4) electrolyte within 1 V. However, as a stack micro-supercapacitor itself, 0.4 mF.cm^{-2} per footprint area was not competitive enough among these already reported stack micro-supercapacitors.

Even though volumetric capacitance of the carbon materials does improve at this nanometer scale thickness, the performance of the whole device had no advantage in term of specific energy (J.cm^{-2}), despite high power capability. Similar comments could be made on stack micro-supercapacitors with 2-3 nm MnO_2 nanoflakes [75], 5 nm porous metal-oxide sheets [76], 7.4 nm nickel hydroxide nanoflakes [77] and <10 nm nickel hydroxidenitrate nanoflake–ZnO nanowire hybrid array [78]. In all these reported ultrathin stack micro-supercapacitors, thicknesses of electrodes are less than 10 nm; however, none of footprint capacitance was reported. As a conclusion, the advantage of ultrathin micro-supercapacitors is not really promising for matching the needs of the energy demand.

Besides stack micro-supercapacitors, interdigitated on-chip micro-supercapacitors, where the deposition of a separator is no longer necessary, were also developed.

II.2.2 Interdigitated on-chip micro-supercapacitors

Interdigitated on-chip micro-supercapacitors were firstly reported with Electronically Conducting Polymers (ECPs) as electrode materials [79]. Because ECPs can be synthesized accurately to a micron scale by polymerization of monomers onto current collectors in solution under an applied potential, conducting polymer based on-chip micro-supercapacitors could be easily fabricated.

Polypyrrole (PPy) being easy to synthesize, as well as exhibiting a high capacitance (200 F/g) in PC-based electrolyte [80], has been used as electrode materials for micro-

supercapacitors. Two-dimensional interdigitated patterns [79] were first designed in order to effectively use the electrode materials for micro-supercapacitors. However, the same issue for ECP-based supercapacitors – poor cyclability – limits their applications. Apart from pure electronically conducting polymers, combination with carbon materials [81] for electrodes was also tried out.

Although several devices based on ECPs have been reported, their poor cyclability due to the irreversible charge trapping and electrochemical degradation on cycling makes them difficult to be widely used. On contrary, carbon is an electrochemically stable material able to offer better cyclability.

The first on-chip carbon-based micro-supercapacitor with interdigited electrodes was fabricated by CVD growth of carbon nanotubes (Figure I.20) [82].
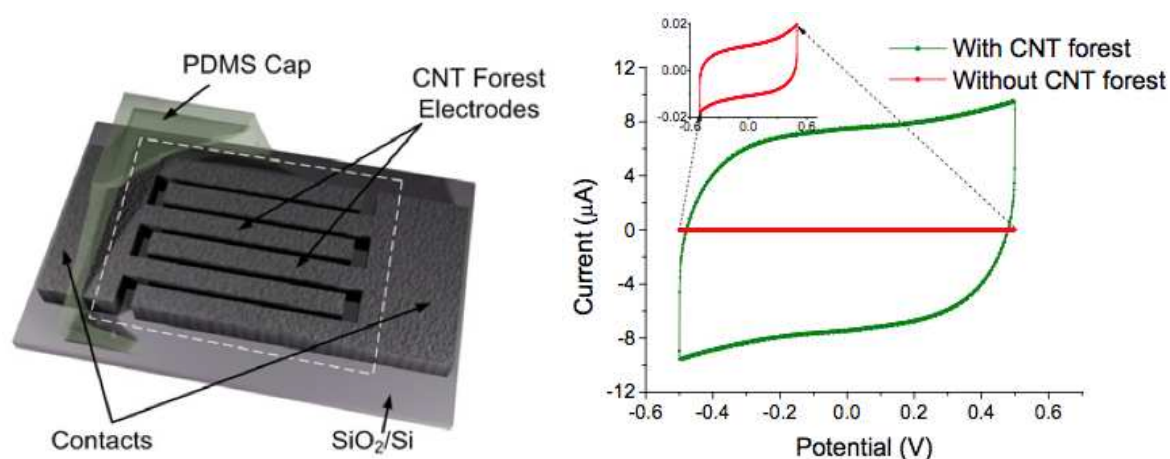

Figure I.20 Schematic illustration of on-chip micro-supercapacitors based on CNTs and its electrochemical performance in BMIM$^+$BF$_4^-$ ionic liquid [82].

In BMIM$^+$BF$_4^-$ ionic liquid, an ideal capacitive behavior was observed with a rectangular CV plot. 0.4 mF.cm^{-2} per footprint area capacitance and 0.05 mJ.cm^{-2} of specific energy was obtained, respectively. The low specific energy is due to the low specific capacitance of CNTs and the low voltage window of 0.5 V, as the device was assembled and electrochemically characterized in open air rather than in a low H$_2$O content glove box. Although this specific

capacitance and energy remained modest, ideal capacitive behavior was firstly achieved in carbon-based micro-supercapacitors. Direct growth of CNTs on pre-patterned interdigitated current collectors thus offers a first solution for processing carbon materials into a micro-scale device by using microfabrication techniques.

Another carbon-based micro-supercapacitor was fabricated by our group based on the same concept. On pre-patterned current collectors – fabricated by photolithography and etching – a carbon ink was deposited using inkjet-printing [52] as shown in Figure III.20.
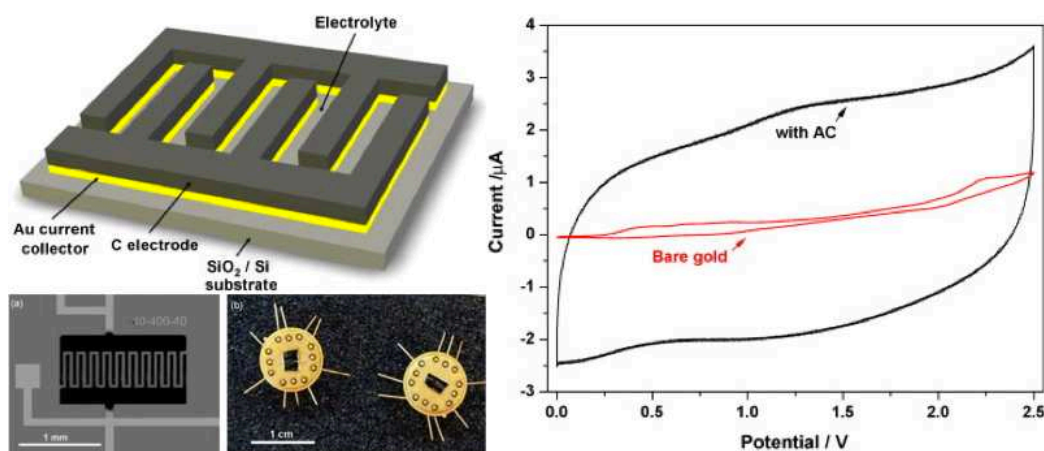

Figure I.21 Schematic picture of on-chip micro-supercapacitor prepared by ink-jet printing and the optical image of the micro-device with CV results [52].

The ink is composed of 3wt.% activated carbon of high surface area with 5wt.% polytetrafluoroethylene (PTFE) polymer binder in an ethylene glycol solvent. A Triton X100 (p-(1,3,3,-tetramethylbutyl) phenoxy-poly(ethylene glycol)) surfactant was added in order to stabilize the emulsion. The ink was then selectively ejected onto pre-patterned Au current collectors. Although the composition contained high portion of organic binder (5:3 by weight to carbon material), quasi-capacitive behavior was achieved by the rectangular shape of CV plot in 1M NEt_4BF_4/PC electrolyte within 2.5 V of voltage window. Decent performance (1.3 $mF.cm^{-2}$ footprint area specific capacitance and 4.2 $mJ.cm^{-2}$ specific energy density) was obtained for this micro-supercapacitor.

II.2.3   Patterned binder-free carbon films: an alternative strategy

Besides processing carbon powders with organic powders to form a film, direct transformation of a bulk film containing carbon precursor into a bulk porous carbon film is another strategy. In that case, self-supported, binder-free, bulk carbon films, having higher carbon density in the electrode and thus higher capacitance, can be obtained, increasing the energy density.

Carbon derived carbon (CDC) bulk films are interesting possible active material in micro-supercapacitors. A comparison between carbon films prepared from the chlorination of a 500 nm layer of sputtered TiC-film and TiC-CDC powder was published recently [83]. Raman spectroscopy and TEM for CDC film and CDC power are shown in Figure I.22.
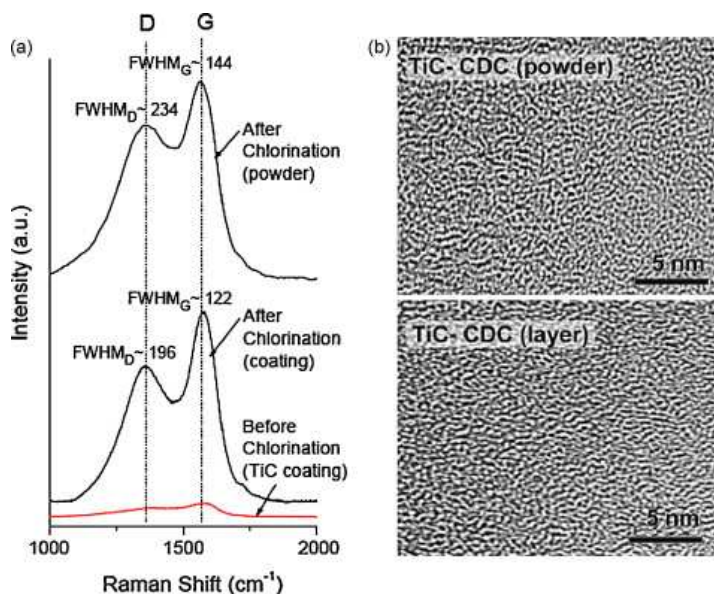

Figure I.22 The Raman spectroscopy of CDC films and comparison with that of CDC powders [83].

Like for CDC powders prepared from chlorination of carbide powders, carbide bulky ceramic pellet were tried for chlorination of surface layer of TiC [59]. A thin-film

supercapacitor was prepared with the surface chlorinated carbide ceramic. Later, TiC-CDC thin films were produced from the chlorination of TiC film sputtered on glassy carbon [65]. For both thin-film supercapacitors based on TiC-CDC films, high volumetric capacitance of 180 $F.cm^{-3}$ was found for TiC-CDC film, in 1.5M NEt_4BF_4/AN electrolyte, thus evidencing the potential interest for applications of these TiC-CDC films in carbon-based on-chip micro-supercapacitors. Specific capacitance of 9 $mF.cm^{-2}$ and specific energy of 18 $mJ.cm^{-2}$ per footprint area were found in this thin-film supercapacitor, much higher than most of the reported thin-film devices. These results indicate that CDC film could be potential electrode material for fabricating on-chip micro-supercapacitors.

In 2011, an on-chip micro-supercapacitor was realized by widely used microfabrication process via graphitization of patterned silicon carbide (Figure I.23) by Liu et al [60]. A specific capacitance of 0.7 $mF.cm^{-2}$ was achieved in 1M H_2SO_4 aqueous electrolyte within 0.5 V voltage window. Thus the specific energy was only 0.09 $mJ.cm^{-2}$, which is too small because of the limited voltage window. This micro-supercapacitor still remains as a proof of concept to show that it is possible to realize carbon-based micro-supercapacitors by widely used microfabrication techniques.
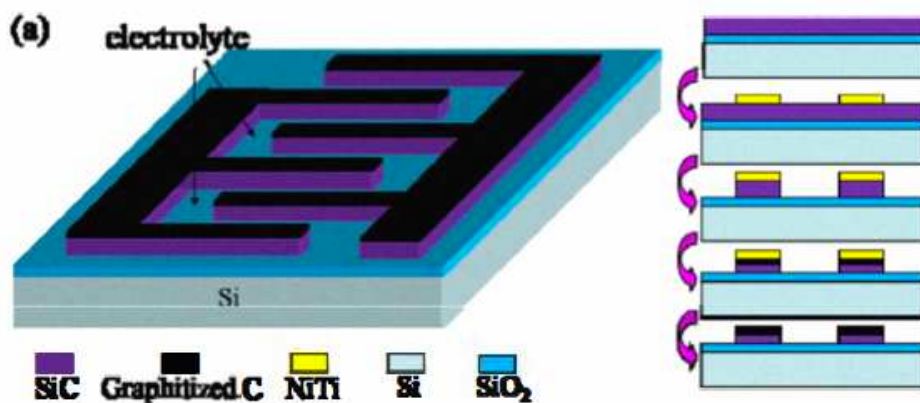

Figure I.23 Schematic picture of on-chip micro-supercapacitors and its fabrication processes [60].

At the same time, another micro-supercapacitor was fabricated by pyrolysis of patterned SU-8 post via widely used micro-fabrication process (Figure I.24) [62]. Specific capacitance of 18.8 mF.cm^{-2} and specific energy of 9.4 mJ.cm^{-2} was achieved in this micro-supercapacitor within 1 V in 0.5M H_2SO_4. Here the performance is good thanks to the height of the carbonized SU-8 (2 ± 0.08 μm).
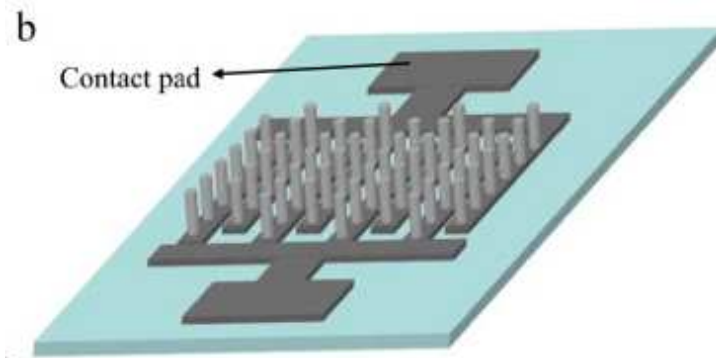

Figure I.24 Schematic illustration of the micro-supercapacitor prepared by pyrolysis [62].

Both micro-supercapacitors, either by graphitization or by pyrolysis, were fabricated via widely used micro-fabrication techniques. Carbon materials were produced by transformation of C-contained precursors.

These demonstrations of carbon layers with enhanced properties such as TiC-CDC and the already reported patterned micro-supercapacitors with in-situ transformation of a layer into carbon, show promises for the field.

Table I.2 shows a summary of some carbon-based on-chip micro-supercapacitors described in this section. Various carbon materials were processed to fabricate micro-supercapacitors with capacitance generally around 1 mF.cm^{-2}, except the one fabricated from C-MEMS arrays. Aqueous electrolytes were still widely used in micro-supercapacitors thank to its easy handling. Energy and power performances were thus not satisfying, although maximum power instead of real power was calculated.

Table I.2 A summary of information of several carbon-based micro-supercapacitors described in bibliography section.

Reference	Technique	Electrode Material	Electrolyte	Footprint area/mm^2
[67]	Origami	TIMCAL carbon	1.5M H_2SO_4	0.12
[50]	Dispenser printing	mesocarbon microbead	$BMIM^+BF_4^-$ PVDF	25
[81]	CVD	CNTs	$BMIM^+BF_4^-$	35
[51]	Inkjet	AC	NEt_4BF_4/PC	3.6
[59]	Micro-fabrication	graphitized SiC	1M H_2SO_4	no info
[61]	Micro-fabrication	carbonated 3D SU8	0.5M H_2SO_4	81

Reference	Thick-ness/µm	Voltage window/V	C/mF.cm^{-2}	Energy/mJ.cm^{-2}	P_{max}/mW.cm^{-2}
[67]	no info	0.6	0.8	0.2	1363
[50]	30	2	0.3	0.5	no info
[81]	80	0.5	0.4	0.05	0.3
[51]	1~2	2.5	1.3	4.2	28.8
[59]	~0.4	0.7	0.8	0.1	1.5
[61]	2	1	18.8	9.4	0.09

II.2.4 Other challenges

In most reported cases, except microsupercapacitors using gel electrolytes [51, 69, 74] or solid electrolytes [2, 50, 57, 67], the others are using liquid electrolytes. In order to integrate onto the same chip with other Microsystems, encapsulation of micro-supercapacitor is necessary i) to restrict liquid electrolyte in the region of micro-supercapacitors and ii) to isolate organic or ionic liquid electrolytes from moisture in the air. Attempts have been made in our group [61] on encapsulation of organic electrolytes at wafer-level for carbon-based micro-supercapacitors. However, intensive research is required to settle several issues such as hermeticity and persistence.

III Conclusion

There have been several prototypes of carbon-based on-chip micro-supercapacitors described in section II.2.2, basically proof of concept either without ideal capacitive behavior

or without expected performance, because of difficulties in carbon processing using a micro-fabrication process or the use of organic additives in the electrodes. Currently, the strategies for fabrication of micro-supercapacitors lies on i) processing carbon powers onto micro-sized current collectors or ii) processing carbon-containing films into the target pattern and then transforming the patterned films into carbon film.

IV   Objectives

Hereby, the objective of this thesis is to develop a method for fabricating high specific energy carbon-based on-chip micro-supercapacitors via microfabrication techniques with different strategies. The challenge of this thesis is: 1) to process powders of different carbon materials onto a patterned chip; 2) to process binder-free carbon films into an interdigitated patterns and create a solid connection for electrochemical characterization; and 3) to improve the performance of fabricated micro-supercapacitors as much as possible.

In Chapter II, activated carbon – the most widely used carbon material in supercapacitors – was used to set up a method according to the strategy of processing carbon powers via electrophoretic deposition (EPD) onto patterned gold micro-sized current collectors. A nanostructured non-porous carbon material onion-like carbon (OLC) was then used to build a micro-supercapacitor with high rate capability.

In Chapter III, carbide derived carbon (CDC) based on-chip micro-supercapacitors were fabricated by patterning of carbon films. On-chip micro-supercapacitors based on CDC were also prepared from chlorination of already patterned carbide. Carbide is ceramic thus could afford patterning with photolithography. The strategy is to transform the patterned carbide directly into carbon by chlorination.

Reference

1. Becker, H.I., *Low voltage electrolytic capacitor*. 1957, GEN ELECTRIC: United States.

2. Kanbara, T., M. Inami, and T. Yamamoto, *New solid-state electric double-layer capacitor using poly(vinyl alcohol)-based polymer solid electrolyte.* Journal of Power Sources, 1991. **36**(1): p. 87-93.

3. Simon, P. and Y. Gogotsi, *Materials for electrochemical capacitors.* Nature Materials, 2008. **7**(11): p. 845-854.

4. Pandolfo, A.G. and A.F. Hollenkamp, *Carbon properties and their role in supercapacitors.* Journal of Power Sources, 2006. **157**(1): p. 11-27.

5. Helmholtz, H., *Theory of Electrical Double Layer.* Wied. Ann., 1879. **7**: p. 337.

6. Gouy, G.J., J. Phys., 1910. **4**.

7. Chapman, D.L., *LI. A contribution to the theory of electrocapillarity.* Philosophical Magazine Series 6, 1913. **25**(148): p. 475 - 481.

8. Stern, O., *The theory of the electric double layer.* Z. Electrochem, 1924. **30**: p. 508.

9. Zhang, L.L. and X.S. Zhao, *Carbon-based materials as supercapacitor electrodes.* Chemical Society Reviews, 2009. **38**(9): p. 2520-2531.

10. Conway, B.E., V. Birss, and J. Wojtowicz, *The role and utilization of pseudocapacitance for energy storage by supercapacitors.* Journal of Power Sources, 1997. **66**(1-2): p. 1-14.

11. SING, et al., *Reporting physisorption data for gas/solid systems, with special reference to the determination of surface area and porosity (recommendations 1984).* Vol. 57. 1985, Research Triangle Park, NC, ETATS-UNIS: Pure and applied chemistry.

12. Jost, K., et al., *Carbon coated textiles for flexible energy storage.* Energy & Environmental Science, 2011. **4**(12): p. 5060-5067.

13. Gamby, J., et al., *Studies and characterisations of various activated carbons used for carbon/carbon supercapacitors.* Journal of Power Sources, 2001. **101**(1): p. 109-116.

14. Qu, D.Y., *Studies of the activated carbons used in double-layer supercapacitors.* Journal of Power Sources, 2002. **109**(2): p. 403-411.

15. Kim, Y.J., et al., *Correlation between the pore and solvated ion size on capacitance uptake of PVDC-based carbons.* Carbon, 2004. **42**(8-9): p. 1491-1500.

16. Jurewicz, K., et al., *Capacitance properties of ordered porous carbon materials prepared by a templating procedure.* Journal of Physics and Chemistry of Solids, 2004. **65**(2-3): p. 287-293.

17. Vix-Guterl, C., et al., *Electrochemical energy storage in ordered porous carbon materials.* Carbon, 2005. **43**(6): p. 1293-1302.

18. Eliad, L., et al., *On the mechanism of selective electroadsorption of protons in the pores of carbon molecular sieves.* Langmuir, 2005. **21**(7): p. 3198-3202.

19. Eliad, L., et al., *Assessing optimal pore-to-ion size relations in the design of porous poly(vinylidene chloride) carbons for EDL capacitors.* Applied Physics a-Materials Science & Processing, 2006. **82**(4): p. 607-613.

20. Raymundo-Pinero, E., et al., *Relationship between the nanoporous texture of activated carbons and their capacitance properties in different electrolytes.* Carbon, 2006. **44**(12): p. 2498-2507.

21. Salitra, G., et al., *Carbon electrodes for double-layer capacitors - I. Relations between ion and pore dimensions.* Journal of the Electrochemical Society, 2000. **147**(7): p. 2486-2493.

22. Janes, A. and E. Lust, *Electrochemical characteristics of nanoporous carbide-derived carbon materials in various nonaqueous electrolyte solutions.* Journal of the Electrochemical Society, 2006. **153**(1): p. A113-A116.

23. Shanina, B.D., et al., *A study of nanoporous carbon obtained from ZC powders (Z = Si, Ti, and B).* Carbon, 2003. **41**(15): p. 3027-3036.

24. Chmiola, J., et al., *Anomalous increase in carbon capacitance at pore sizes less than 1 nanometer.* Science, 2006. **313**(5794): p. 1760-1763.

25. Urbonaite, S., L. Halldahl, and G. Svensson, *Raman spectroscopy studies of carbide derived carbons.* Carbon, 2008. **46**(14): p. 1942-1947.

26. Dash, R., et al., *Titanium carbide derived nanoporous carbon for energy-related applications.* Carbon, 2006. **44**(12): p. 2489-2497.

27. An, K.H., et al., *High-capacitance supercapacitor using a nanocomposite electrode of single-walled carbon nanotube and polypyrrole.* Journal of the Electrochemical Society, 2002. **149**(8): p. A1058-A1062.

28. An, K.H., et al., *Electrochemical properties of high-power supercapacitors using single-walled carbon nanotube electrodes.* Advanced Functional Materials, 2001. **11**(5): p. 387-392.

29. Portet, C., G. Yushin, and Y. Gogotsi, *Electrochemical performance of carbon onions, nanodiamonds, carbon black and multiwalled nanotubes in electrical double layer capacitors.* Carbon, 2007. **45**(13): p. 2511-2518.

30. Pech, D., et al., *Ultrahigh-power micrometre-sized supercapacitors based on onion-like carbon.* Nature Nanotechnology, 2010. **5**(9): p. 651-654.

31. Lin, R.Y., et al., *Capacitive Energy Storage from -50 to 100 degrees C Using an Ionic Liquid Electrolyte.* Journal of Physical Chemistry Letters, 2011. **2**(19): p. 2396-2401.

32.   Kuznetsov, V.L., et al., *Onion-like carbon from ultra-disperse diamond.* Chemical Physics Letters, 1994. **222**(4): p. 343-348.

33.   McDonough, J.K., et al., *Influence of the structure of carbon onions on their electrochemical performance in supercapacitor electrodes.* Carbon, 2012. **50**(9): p. 3298-3309.

34.   Vashishta, P., J.N. Mundy, and G.K. Shenoy, *Fast ion transport in solids: electrodes, and electrolytes : proceedings of the International Conference on Fast Ion Transport in Solids, Electrodes, and Electrolytes, Lake Geneva, Wisconsin, U.S.A., May 21-25, 1979.* 1979: North Holland.

35.   Kalpana, D., N.G. Renganathan, and S. Pitchumani, *A new class of alkaline polymer gel electrolyte for carbon aerogel supercapacitors.* Journal of Power Sources, 2006. **157**(1): p. 621-623.

36.   Pandey, G.P., Y. Kumar, and S.A. Hashmi, *Ionic liquid incorporated polymer electrolytes for supercapacitor application.* Indian Journal of Chemistry Section a-Inorganic Bio-Inorganic Physical Theoretical & Analytical Chemistry, 2010. **49**(5-6): p. 743-751.

37.   Sun, S.J., et al., *Electrochemical properties of a low molecular weight gel electrolyte for supercapacitor.* Journal of Electroanalytical Chemistry, 2012. **676**: p. 1-5.

38.   Thakur, V.K., et al., *Hybrid Materials and Polymer Electrolytes for Electrochromic Device Applications.* Advanced Materials, 2012. **24**(30): p. 4071-4096.

39.   Wu, C.H., et al., *A photoelectrochromic device based on gel electrolyte with a fast switching rate.* Solar Energy Materials and Solar Cells, 2012. **99**: p. 148-153.

40.   Nadherna, M., F. Opekar, and J. Reiter, *Ionic liquid-polymer electrolyte for amperometric solid-state NO2 sensor.* Electrochimica Acta, 2011. **56**(16): p. 5650-5655.

41.   Faisal, S.N., et al., *Amperometric proton selective sensors utilizing ion transfer reactions across a microhole liquid/gel interface.* Physical Chemistry Chemical Physics, 2010. **12**(46): p. 15184-15189.

42.   Armand, M., et al., *Ionic-liquid materials for the electrochemical challenges of the future.* Nature Materials, 2009. **8**(8): p. 621-629.

43.   Brandon, E., M. Smart, and W. West, *Low-Temperature Supercapacitors.* NASA Tech Briefs, 2008. **32**: p. 32.

44.   De Levie, R., *Electrochemical Response of Porous Rough Electrodes.* Advances in Electrochemistry and Electrochemical Engineering, 1967. **6**: p. 329.

45.   de Levie, R., *On porous electrodes in electrolyte solutions: I. Capacitance effects.* Electrochimica Acta, 1963. **8**(10): p. 751-780.

46.   Fauvarque, J. and P. Simon, *Principles of Electrochemistry and Electrochemical Methods*, in *Carbon Materials for Electrochemical Energy Storage Systems*. 2009, Taylor & Francis.

47.   Maissel, L.I. and R. Glang, *Handbook of thin film technology*. 1970: McGraw-Hill.

48.   Ohring, M., *Materials Science of Thin Films*. 2001: Elsevier Science.

49.   Madou, M.J., *Manufacturing Techniques for Microfabrication and Nanotechnology*. 2009: Taylor & Francis.

50.   Yoon, Y.S., et al., *Solid-state thin-film supercapacitor with ruthenium oxide and solid electrolyte thin films.* Journal of Power Sources, 2001. **101**(1): p. 126-129.

51.   Ho, C., et al. *Dispenser Printed Electrochemical Capacitors for Power Management of Millimeter Scale Lithium Ion Polymer Microbatteries for Wireless Sensors*. in *Power MEMS Conference*. 2006.

52.   Pech, D., et al., *Elaboration of a microstructured inkjet-printed carbon electrochemical capacitor.* Journal of Power Sources, 2010. **195**(4): p. 1266-1269.

53. Lin, B.J., *Optical Lithography: Here Is Why*. 2009: SPIE.

54. Rossnagel, S.M., J.J. Cuomo, and W.D. Westwood, *Handbook of Plasma Processing Technology: Fundamentals, Etching, Deposition, and Surface Interactions*. 1990: Noyes Publications.

55. Hon, K.K.B., L. Li, and I.M. Hutchings, *Direct writing technology-Advances and developments*. Cirp Annals-Manufacturing Technology, 2008. **57**(2): p. 601-620.

56. Kim, H.K., et al., *Correlation between the microstructures and the cycling performance of RuO2 electrodes for thin-film microsupercapacitors*. Journal of Vacuum Science & Technology B, 2002. **20**(5): p. 1827-1832.

57. Kim, H., et al., *All solid-state rechargeable thin-film microsupercapacitor fabricated with tungsten cosputtered ruthenium oxide electrodes*. Journal of Vacuum Science & Technology B: Microelectronics and Nanometer Structures, 2003. **21**: p. 949-952.

58. Kim, H.-K., et al., *Characteristics of RuO2-SnO2 nanocrystalline-embedded amorphous electrode for thin film microsupercapacitors*. Thin Solid Films, 2005. **475**(1-2): p. 54-57.

59. Chmiola, J., et al., *Monolithic Carbide-Derived Carbon Films for Micro-Supercapacitors*. Science, 2010. **328**(5977): p. 480-483.

60. Liu, F., et al. *Graphitization of n-type polycrystalline silicon carbide and its application for micro- supercapacitors*. in *Solid-State Sensors, Actuators and Microsystems Conference (TRANSDUCERS), 2011 16th International*. 2011.

61. Durou, H., et al., *Wafer-level fabrication process for fully encapsulated micro-supercapacitors with high specific energy*. Microsystem Technologies-Micro-and Nanosystems-Information Storage and Processing Systems, 2012. **18**(4): p. 467-473.

62. Beidaghi, M., W. Chen, and C. Wang, *Electrochemically activated carbon micro-electrode arrays for electrochemical micro-capacitors.* Journal of Power Sources, 2011. **196**(4): p. 2403-2409.

63. Byon, H.R., et al., *Thin films of carbon nanotubes and chemically reduced graphenes for electrochemical micro-capacitors.* Carbon, 2011. **49**(2): p. 457-467.

64. Zang, J.F., et al., *Well-aligned cone-shaped nanostructure of polypyrrole/RuO2 and its electrochemical supercapacitor.* Journal of Physical Chemistry C, 2008. **112**(38): p. 14843-14847.

65. Heon, M., et al., *Continuous carbide-derived carbon films with high volumetric capacitance.* Energy & Environmental Science, 2011. **4**(1): p. 135-138.

66. Bates, J.B., et al., *Electrical-Properties of Amorphous Lithium Electrolyte Thin-Films.* Solid State Ionics, 1992. **53**: p. 647-654.

67. Meng, F. and Y. Ding, *Sub-Micrometer-Thick All-Solid-State Supercapacitors with High Power and Energy Densities.* Advanced Materials, 2011. **23**(35): p. 4098-4102.

68. In, H.J., et al., *Origami fabrication of nanostructured, three-dimensional devices: Electrochemical capacitors with carbon electrodes.* Applied Physics Letters, 2006. **88**(8): p. 083104.

69. Kaempgen, M., et al., *Printable Thin Film Supercapacitors Using Single-Walled Carbon Nanotubes.* Nano Letters, 2009. **9**(5): p. 1872-1876.

70. Hu, L.B., et al., *Highly conductive paper for energy-storage devices.* Proceedings of the National Academy of Sciences of the United States of America, 2009. **106**(51): p. 21490-21494.

71. Lee, S.W., et al., *Nanostructured carbon-based electrodes: bridging the gap between thin-film lithium-ion batteries and electrochemical capacitors.* Energy & Environmental Science, 2011. **4**(6): p. 1972-1985.

72.	Gao, W., et al., *Direct laser writing of micro-supercapacitors on hydrated graphite oxide films.* Nature Nanotechnology, 2011. **6**(8): p. 496-500.

73.	Pushparaj, V.L., et al., *Flexible energy storage devices based on nanocomposite paper.* Proceedings of the National Academy of Sciences of the United States of America, 2007. **104**(34): p. 13574-13577.

74.	Yoo, J.J., et al., *Ultrathin Planar Graphene Supercapacitors.* Nano Letters, 2011. **11**(4): p. 1423-1427.

75.	Jiang, H., et al., *Hierarchical porous nanostructures assembled from ultrathin MnO2 nanoflakes with enhanced supercapacitive performances.* Journal of Materials Chemistry, 2012. **22**(6): p. 2751-2756.

76.	Zhu, J., et al., *Bottom-Up Preparation of Porous Metal-Oxide Ultrathin Sheets with Adjustable Composition/Phases and Their Applications.* Small, 2011. **7**(24): p. 3458-3464.

77.	Jiang, H., et al., *Hierarchical self-assembly of ultrathin nickel hydroxide nanoflakes for high-performance supercapacitors.* Journal of Materials Chemistry, 2011. **21**(11): p. 3818-3823.

78.	Liu, J., et al., *Ultrathin nickel hydroxidenitrate nanoflakes branched on nanowire arrays for high-rate pseudocapacitive energy storage.* Chemical Communications, 2011. **47**(12): p. 3436-3438.

79.	Sung, J.H., S.J. Kim, and K.H. Lee, *Fabrication of microcapacitors using conducting polymer microelectrodes.* Journal of Power Sources, 2003. **124**(1): p. 343-350.

80.	Hannecart, E., et al., in *European Patent Application*, E.P. Application, Editor. 1991.

81.	Sarac, A.S., et al., *Electrochemically polymerized 2,2-dimethyl-3,4-propylenedioxythiophene on carbon fiber for microsupercapacitor.* Progress in Organic Coatings, 2007. **60**(4): p. 281-286.

82.   Jiang, Y., Q. Zhou, and L. Lin. *Planar MEMS Supercapacitor using Carbon Nanotube Forests*. in *22nd International Conference on MEMS*. 2009.

83.   Hoffman, E.N., et al., *Carbide-derived carbon membrane.* Materials Chemistry and Physics, 2008. **112**(2): p. 587-591.

Chapter II: On-chip Micro-supercapacitors by Electrophoretic Deposition (EPD)

I Introduction

As mentioned previously in the bibliographic part, most of the micro-supercapacitors reported employ sandwich configuration, which is in accordance with the macroscopic supercapacitors and thus easy to be fabricated. However, our aim is to develop a microdevice that could be incorporated on-chip with MEMS devices or electronics circuits. A planar configuration with electrodes patterned on a substrate is thus necessary. When starting the PhD, the team [1] had already elaborated an on-chip inkjet printed carbon-based micro-supercapacitor and a capacitance of 0.3 $mF.cm^{-2}$ per footprint area was achieved within 2.5 V. Here we present an original technique – electrophoretic deposition (EPD) [2, 3], for the deposition of more homogeneous layers of carbon materials without organic binder to achieve better performance, with larger voltage window and higher capacitance.

Two types of carbon materials were deposited by EPD to produce carbon-based interdigitated micro-supercapacitors. Porous activated carbon was first tried to establish a routine process for fabrication of micro-supercapacitors. Then onion like carbon (OLC) was deposited to produce high-power carbon-based micro-supercapacitors with different electrolytes.

II Materials & Electrolyte

The carbon materials used in this chapter include activated carbon (AC) YP-17 and onion like carbon (OLC). OLC is highly conductive spherical carbon particles with no porous structure. OLC with specific surface area of 500 $cm^2.g^{-1}$ was synthesized in Drexel University, Philadelphia, US.

MgCl$_2$ was used as charge carrier for EPD, as has already been used for deposition of various materials [4, 5].

Propylene carbonate (PC) is a safe choice as organic electrolyte with a high flash point (132 °C) and low toxicity, compared to acetonitrile (AN) whose flash point is only 5 °C and defined as "harmful".

Finally a new electrolyte – an ionic liquid mixture (ILM) [6], eutectic mixture of N-methyl-N-propylpiperidinium bis(fluorosulfonyl)imide (PIP$_{13}$FSI) and N-butyl-N-methylpyrrolidinium bis(fluorosulfonyl)imide (PYR$_{14}$FSI) was also used to explore the performance at a wider temperature range from -50 °C to 80 °C with a larger voltage window to achieve higher specific energy.

III Experimental

All micro-supercapacitors described in this chapter were prepared by the same technique – electrophoretic deposition (EPD), with different carbon materials – activated carbon (AC) and onion-like carbon (OLC). The same formula of carbon slurry was used in all experiments introduced below.

III.1 Design of the active area

The two designs of the interdigitated electrodes are shown here in Figure II.1.
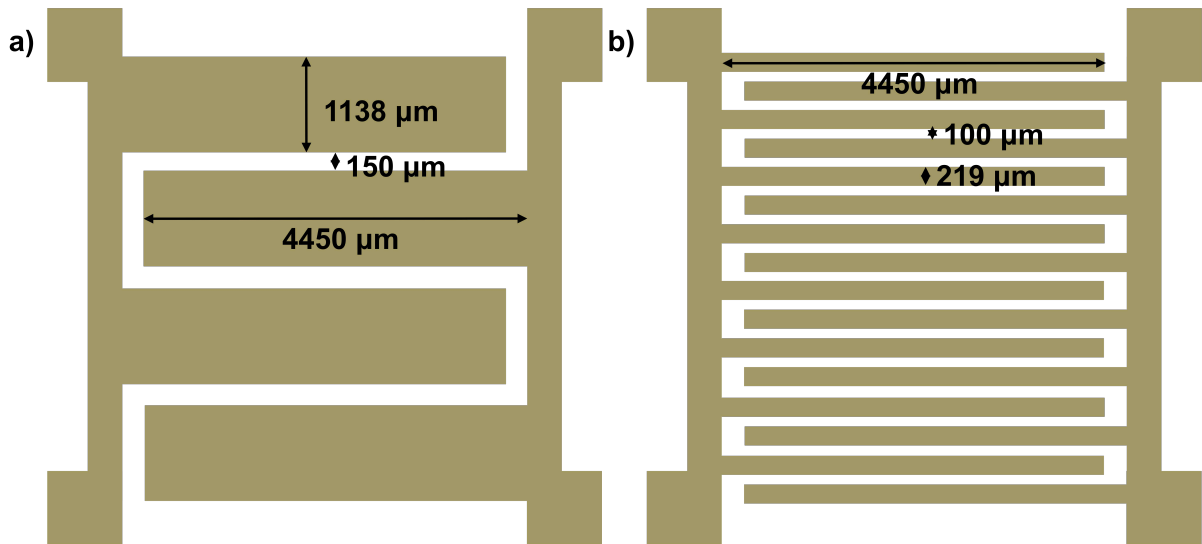
Figure II.1 The schematic illustration of the configuration of micro-supercapacitors used for EPD of carbon materials a) 4 fingers and b) 16 fingers.

The four relatively large pads at the four corners are the pads for wire bonding on a support in order to achieve electrochemical characterizations. And the center area makes an interdigitated pattern with an interspace of 100 μm for 16 fingers configuration and 150 μm for 4 fingers. The 4 fingers pattern shows a finger length of 4450 μm and a finger width of 1138 μm; while a 16 fingers pattern shows the same finger length but a finger width of 219 μm. This makes a footprint area (surface area that occupied by the micro-supercapacitor including the area of the active electrodes and interspace) of 0.25 cm^2 for both configurations shown in Figure II.1a and Figure II.1b and a single electrode area (the area of one electrode with active material loaded) of 0.11 cm^2 for 4 fingers configuration and 0.088 cm^2 for 16 fingers pattern, respectively, as shown in Table II.1.

Table II.1 Configurations of the micro-supercapacitors with details

Configuration	4 fingers	16 fingers
Finger length/μm	4450	4450
Finger width/μm	1138	219
Interspace/μm	150	100
Footprint area/cm^2	0.25	0.25

Single electrode area/cm^2	0.11	0.088

These patterns were drawn on a 5-inch photomask in order to transfer it to the 4-inch Si wafer.

III.2   Micro-fabrication

A layer of 800 nm SiO$_2$ was grown on a 4-inch wafer by thermal oxidation under 800 °C via the reaction Si + 2H$_2$O $\rightarrow$ SiO$_2$ + 2H$_{2(g)}$ and Si + O$_2$ $\rightarrow$ SiO$_2$. Afterwards, a layer of 100 nm Ti and a layer of 800 nm Au were deposited by evaporation on the wafer successively. Au is the material of current collectors of the targeted micro-supercapacitors and Ti is an intermediate layer in order to enhance the adherence between the SiO$_2$ layer and deposited Au layer. The wafer was annealed later in N$_2$ atmosphere at 250 °C for 20 minutes to reduce structural defects created during deposition within the Au layer: this way, the electrical conductivity is optimized and the mechanical stress is reduced [7]. The anneal step insures optimum conditions for the wire-bonding steps afterwards.

A standard photolithography process was applied on the Au deposited 4-inch wafer with the mask described above. It consists in the following steps: the Au coated wafer was cleaned in chromo sulfuric acid, rinsed and dehydrated at 200 °C for 20 min. A layer of positive photoresist was spin-coated on the wafer and then exposed to the UV light through a designed photomask with patterns shown in Figure II.1 to allow this part of the photoresist to be soluble in a developer. After development, the pattern was then transferred to Ti/Au layer by immersing the wafer first in a KI + I$_2$ solution to etch away the gold layer and then in 5 % hydrofluoric acid (HF) buffer solution to remove the titanium layer. At the end of the etching step, the photoresist was dissolved by acetone. The wafer was then cut into pieces for EPD.

III.3 EPD conditions

Electrophoretic deposition (EPD) aims at depositing a uniform layer of materials onto conductive electrode surfaces using suspensions with colloidal particles as electrolytes under migration by applying an electric field. Unlike electroplating, i.e. electro deposition, producing metallic coating, a wider range of materials, such as metals, ceramics, polymers, etc. could be deposited by EPD upon a better design of the suspensions. Thus it could be one of suitable choices for deposition of carbon materials for processing powders into thin film.

EPD is composed of two processes: i) electrophoresis – the motion of charged particles in a suspension under an electric field; and ii) deposition – the coagulation of particles to a dense mass.

The key issue of electrophoresis is the stability of suspensions. In organic media, without dissociation or ionization of surface groups, adsorption of ionized species onto carbon powders is required to form a suspension. The stability of suspensions is determined by interaction between charged particles, mainly repulsion between particles to avoid coagulation when they collide. The repulsion could be evaluated by zeta potential, which the potential between particle surface and the shear layer plane that could be experimentally measured. [8]

The amount of electrophoretically deposited powder depends on a number of parameters of the deposition process, summarized in an empirical relation known as Hamaker's Law:

$$w = \int_{t_1}^{t_2} \mu EAC dt$$

The representation of Hamaker's law has changed over the years, but it relates deposited powder mass (w) to the electric field strength (E), electrophoretic mobility (μ), surface area of the electrode (A) and the particle mass concentration (C) in the suspension. [9]

In the work of this chapter, the electrolyte bath which developed by Pech et al for EPD was a suspension which is based on a mixed solvent with 95 vol% of ethanol and 5 vol% of water. 0.3 wt% of carbon material as active material and 0.03 wt% of $MgCl_2$ were added together to form as the charge carrier during EPD in the finally formed carbon film on the electrode [10].

EPD was performed with the setup shown in Figure II.2, under a voltage of 50 V at room temperature under constant agitation by a magnetic stirring bar; carbon was then deposited only onto the current collector area with different thickness according to different deposition time.
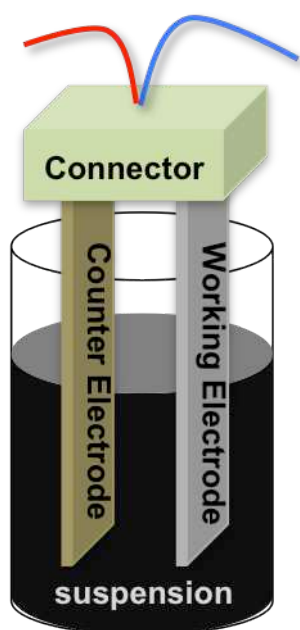
Figure II.2 A schematic illustration of EPD setup.

As the carbon is conductive, the grains deposit on top of each others. It is inevitable that some carbon grain might occupy the interspace between the interdigitated fingers and cause short circuit if the deposition time is too long. Thus, samples are washed in an organic solvent (ethanol or acetone) between each 10s of EPD to wash away those carbon grains at the

interspace as much as possible. In addition, no thick carbon layer (thickness > 20 µm) could be deposited onto interdigitated patterned current collectors without short circuit.

The deposited sample was then annealed at 250 °C in order to ensure a water content as low as possible. The thickness of the carbon material deposited was measured by confocal microscope.

III.4 Electrochemical Characterization

The chip was glued on a 16-pin TO-8 support, and wire bonding was performed between the contact pads of the micro-device and the support's pads as shown in Figure II.3, thus facilitating the electrochemical characterization.
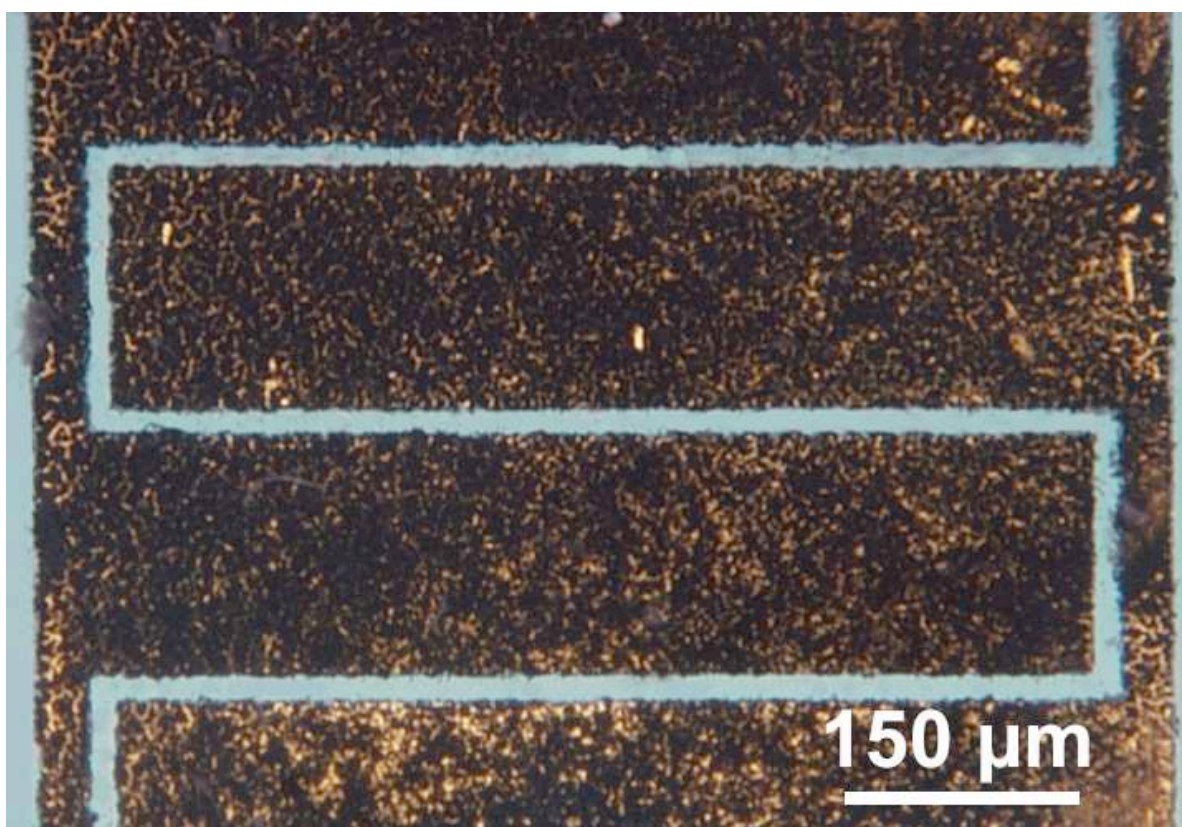
Figure II.3 A microscopic photo of a micro-supercapacitor prepared by EPD for electrochemical characterization.

After wire bonding, the micro-supercapacitor was kept under vacuum at 130 °C to remove water trace which would cause electrolysis of water at >1 V during the EC test, hereby reduce the voltage window.

The samples were characterized in 1M tetraethylammonium tetrafluoroborate (NEt_4BF_4) in propylene carbonate (PC) electrolyte or eutectic ionic liquid mixture (ILM) in a glove box under Ar atmosphere (H_2O and O_2 level lower than 0.1 ppm). The electrochemical test was carried out using a Biologic VMP2 potentiostat. Cyclic Voltamogram with different scan rates were conducted using the same equipment. EIS (Electrochemical Impedance Spectroscopy) measurements were done at the rest potential by applying a sinusoidal potential signal. Then the response within a proper frequency range (usually from 50 KHz to 10 mHz) was collected.

IV   Results & Discussion

First, the pretreatment of Au current collectors, which are also the substrate of EPD, were studied to improve the adherence between current collectors and deposited carbon powders. In order to get a homogeneous carbon layer with clear interspace between two electrodes, deposition conditions were examined afterwards. Then, with activated carbon, thickness of active films was varied by varying deposition time on a non-patterned Au-coated Si/SiO_2 chip in 3-electrodes configuration with Au surface as counter electrode and silver wire as the quasi-reference electrode. The relationship between thickness of the active material and capacitance was studied. On-chip micro-supercapacitors were prepared via EPD technique with AC and OLC, then tested electrochemically in 1M NEt_4BF_4/PC electrolyte. OLC based micro-supercapacitor was also characterized in a eutectic ionic liquid mixture (ILM) for temperature range study.

IV.1   Preparation of the substrate

The deposited Au current collectors were prepared as the electrode of EPD. The surface treatment of Au by chromo sulfuric acid allows removal of the organic residues from photolithography processes and organic contamination from gold deposition [11]. However, with sample dried and exposed to the air even shortly (around 20 min) after the surface treatment, adherence of EPD deposited sample was not satisfactory. Carbon powders were easily falling off from the substrate by a slight shock.

Hereby the evolution of the contact angle upon exposure to the air after cleaning with chromo sulfuric acid is presented in Figure II.4.
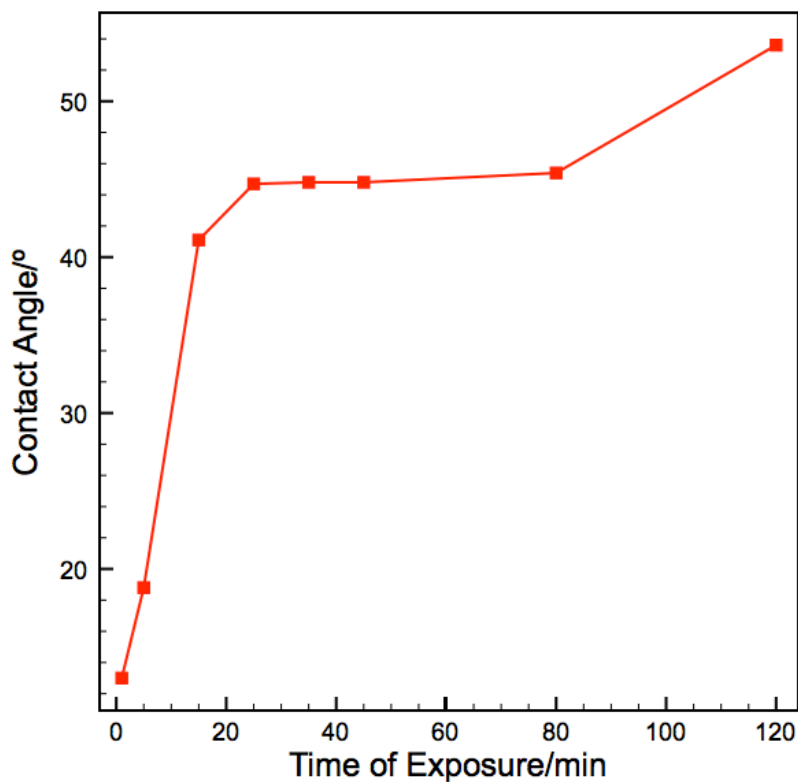
Figure II.4 The evolution of the contact angle upon exposure to air after cleaning with chromo sulfuric acid

From Figure II.4, it is very clear that the contact angle is getting larger upon exposure to the air. 15 minutes is enough to increase the contact angle from 18°C to 42°. Since gold surface

exposes to the air, the contact angle increases with the time of exposure. This might be from the adsorption of CO_2 molecules in the air which increases the hydrophobicity and decreases the adherence as well [12]. To maximize adherence of deposited carbon layer on the Au layer, the Si chips with Au current collectors were thus kept in distilled water between the surface treatment and EPD procedure.

IV.2 Deposition conditions

During EPD, the Si chips should be washed in the solvent to remove the adsorbed carbon on the interspace to avoid short circuit every 10 seconds. Two solvents, ethanol and acetone, were tried to see the effect of removal, as shown in Figure II.5.
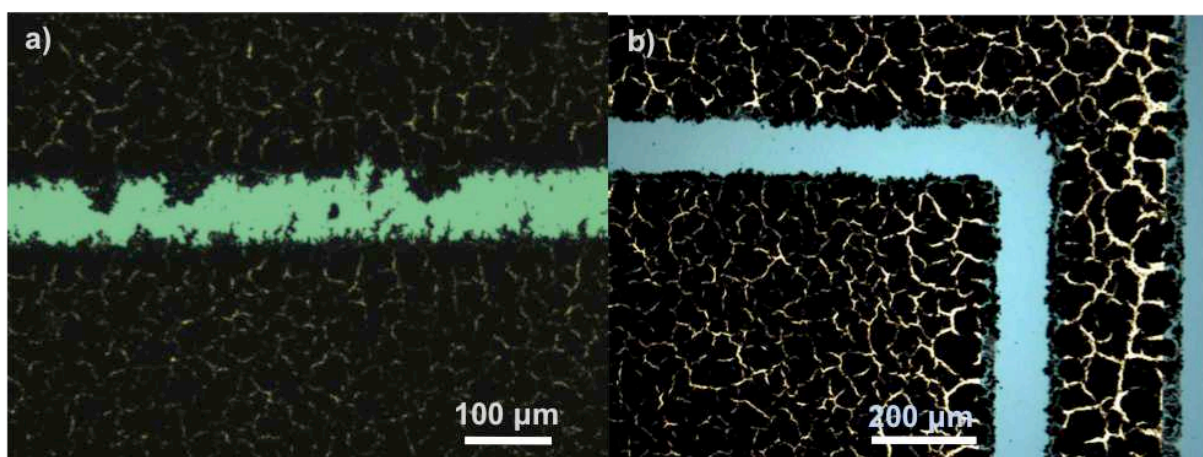
Figure II.5 Microscope pictures of samples deposited with Onion Like Carbon (OLC) in 5s washed by a) ethanol and b) acetone.

Both depositions exceed the area of the gold electrode and have carbon at the border of the interspace. This was due to the edges of gold current collectors which also attract charged carbon grains in the suspension. The sample washed by ethanol still has carbon left at the interspace, which bridged the two electrodes and will cause short circuit during the electrochemical test. Another washing in acetone seems more effective and could be a better choice to clean the interspace after EPD. In addition, the cracks of the deposited carbon are

68

more obvious in the sample with acetone as wash solvent, due to the faster drying rate of acetone than that of ethanol.

However, in the cases where the pretreatment of the substrate in chromo sulfuric acid were not applied before EPD, the carbon material deposited would not adhere enough to the current collector and then totally washed away by acetone. By this phenomenon, the necessity of pretreatment for increasing the adherence of the deposited carbon materials is thus confirmed.

IV.3   Activated Carbon – Influence of the thickness of the active film

Activated carbon (AC) is the most widely used carbon material for commercial supercapacitors, as it is cheap and able to offer an average performance at the same time.

Before preparing the interdigitated on-chip micro-supercapacitors described in Section III.1, AC was deposited on Au coated SiO_2/Si chip. Au coating was masked with photoresist and only a spot of 0.25 cm^2 Au was revealed for EPD. This way, with different deposition time, we could study the relationship between thickness of the carbon material and capacitance. Samples were tested electrochemically in a three-electrode configuration with Au coated Si chip as the counter electrode, Ag wire as the quasi-reference electrode and 1M NEt_4BF_4 as electrolyte (Figure II.6).
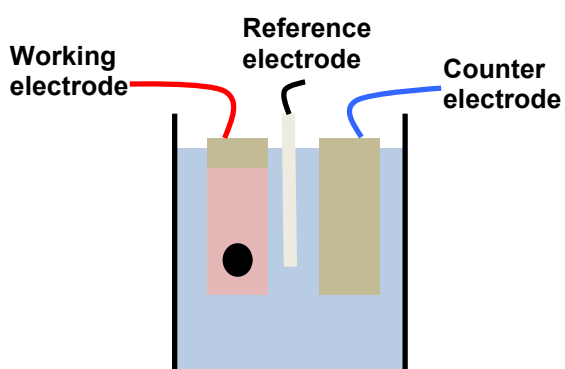
Figure II.6 A schematic illustration of the 3-electrode cell for thickness study.

The thicknesses of samples were measured by confocal microscope. Confocal microscopy is an optical imaging technique used to increase optical resolution and contrast of a micrograph by using point illumination and a spatial pinhole to eliminate out-of-focus light in specimens that are thicker than the focal plane [13]. It enables the reconstruction of three-dimensional structures from the obtained images, which allows the calculation of the average thickness of the 3-dimensional structure.

Eight samples were prepared with different deposition time, 5s, 10s, 15s, 20s, 30s, 40s, 50s and 60s. They were annealed at 250 °C for 2 hours before electrochemical characterization.

In order to test the combination of micro-scale on-chip device and carbon materials compared to macroscopic supercapacitors, the micro-supercapacitors were then characterized first in 1M NEt_4BF_4 in propylene carbonate (PC), which is a conventional organic electrolyte for macroscopic supercapacitors.

EIS measurement was performed with 10 mV as the potential amplitude and response were collected from 50 kHz to 10 mHz.

Figure II.7 shows the Nyquist plot measured by Electrochemical Impedance Spectroscopy (EIS) of sample with 5s of deposition in 1M NEt_4BF_4/PC electrolyte.

70
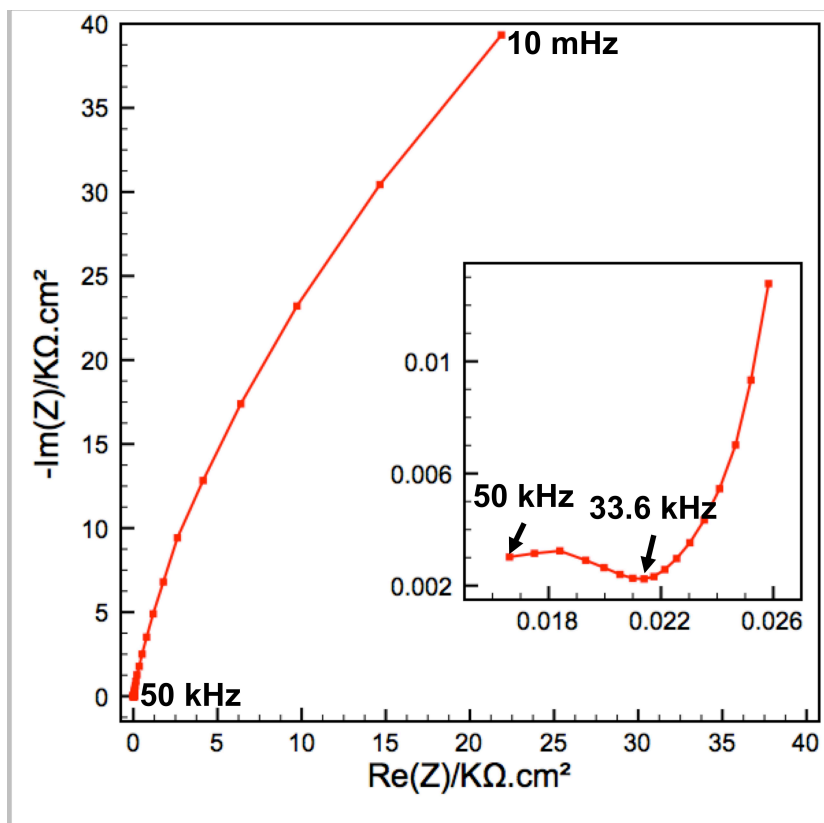
Figure II.7 The Nyquist plot of sample with 5s of deposition in 1M NEt₄BF₄/PC eletrolyte.

The plot shows deviation from the signature of the supercapacitors (vertical increase of the plot) as mentioned in Chapter I. This deviation from vertical increase indicates the undesired parasitic redox reactions taking place during the electrochemical characterization upon the application of a voltage. The leakage could be from redox decomposition of the organic residue or water content in the electrode materials at the gold current collectors. The inset of Figure II.7 shows the Equivalent Series Resistance (ESR) of the 3-electrode cell, around 16 $\Omega.cm^2$. The resistance seems high, but still reasonable, as the distance between the 2 electrodes is large compared to both macroscopic supercapacitors and micro-supercapacitors. The semi-circle loop at high frequency indicates a contact resistance due to the poor contact between current collector and electrode, probably owing to the short annealing time after EPD.

Figure II.8 a) and b) shows the CV results of the samples deposited 5s and 60s at 100 mV/s within 2.2 V in 1M NEt$_4$BF$_4$ in PC respectively.
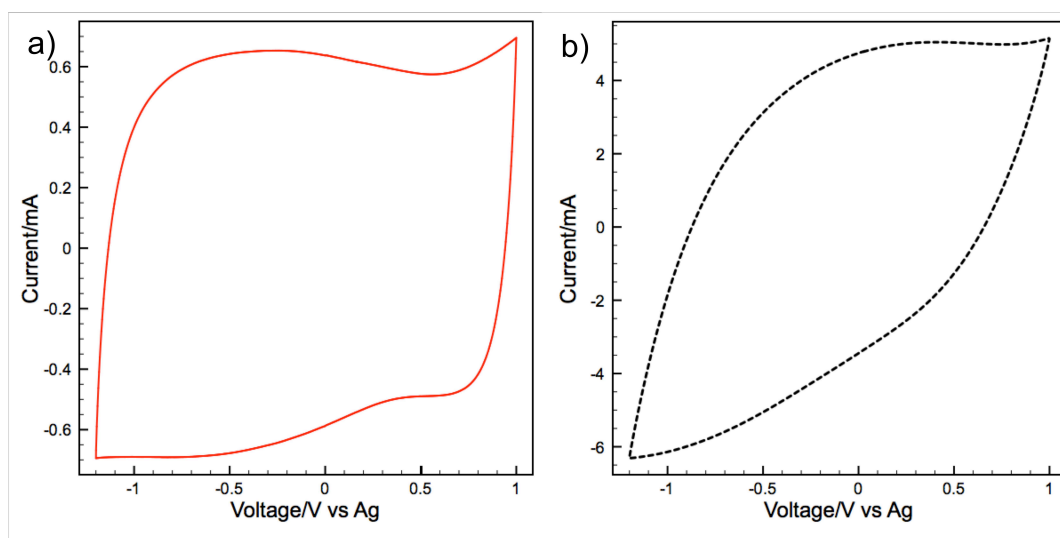
Figure II.8 The CV results of the samples with a) 5s and b) 60s of deposition at 100 mV/s within 2.2 V in 1M NEt$_4$BF$_4$ in PC.

The rectangular shape of 5s deposited sample indicates a typical capacitive behavior. The deviations from immediate increase of current at the beginning of both positive scan and reverse scan corresponds to the high ESR, also shown in Nyquist plot. Capacitive current was nevertheless reached in short time, meaning a short time constant for this 3-electrode cell, thanks to its thin layer, which allows fast electrolyte percolation compared to thick electrodes around 100 μm. In contrast, for 60s deposited sample, at the same scan rate, the CV plot is clearly distorted, indicating important ohmic drop in the carbon electrodes. Nevertheless, the capacitance of 60s deposited sample (53.43 mF) is much higher than that of 5s deposited (6.22 mF).

The relationships between deposition time and thickness of the carbon material and capacitance are shown below in Figure II.9 and in Figure II.10 respectively.

72
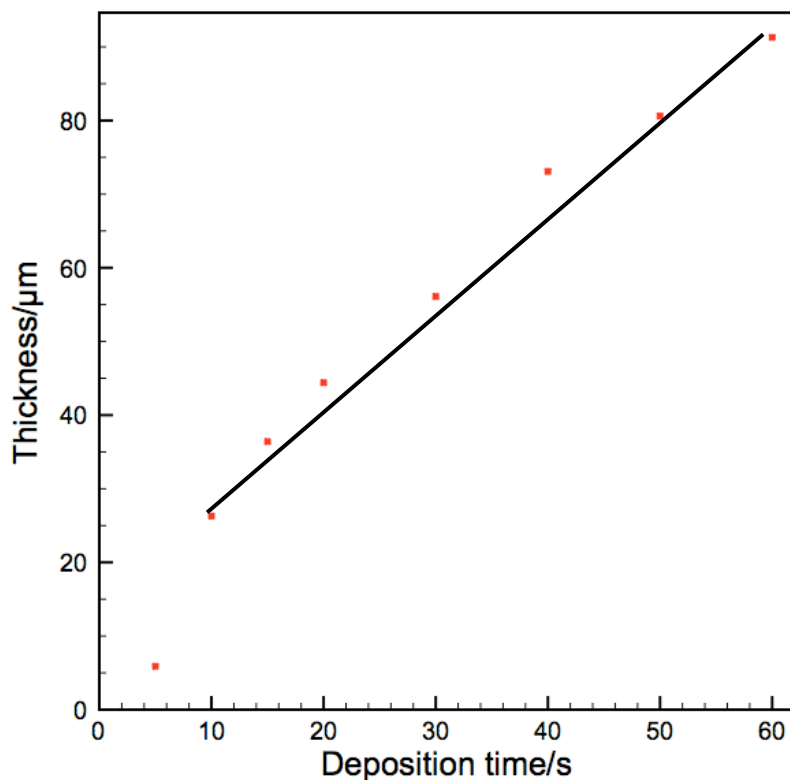
Figure II.9 The evolution of the thickness of carbon layer measured versus deposition time of EPD.

In Figure II.9, except the first point with only 5s of deposition time, thickness of the other six samples showed linear relationship with deposition time with little deviations. The 5s deposited sample has an exceptionally low thickness since the first second of deposition is not as efficient as it should because of the rising time of the machine. There are also some other factors affecting the thickness measured: the thickness was measured with confocal microscope of a small area, where the thickness was not necessarily the average thickness of the carbon film deposited; the deposition time was controlled manually but not the power source, which introduced the deviation; the washing step was also manual, which makes the amount of carbon grains washed away random; in addition, the electrolyte bath is not actually a suspension: it was constantly stirred by a magnetic stirrer. Thus, there was concentration

gradient in the quasi-suspension. Hereby the carbon thickness deposited was also proportional to the deepness where the patterned area was placed during EPD.

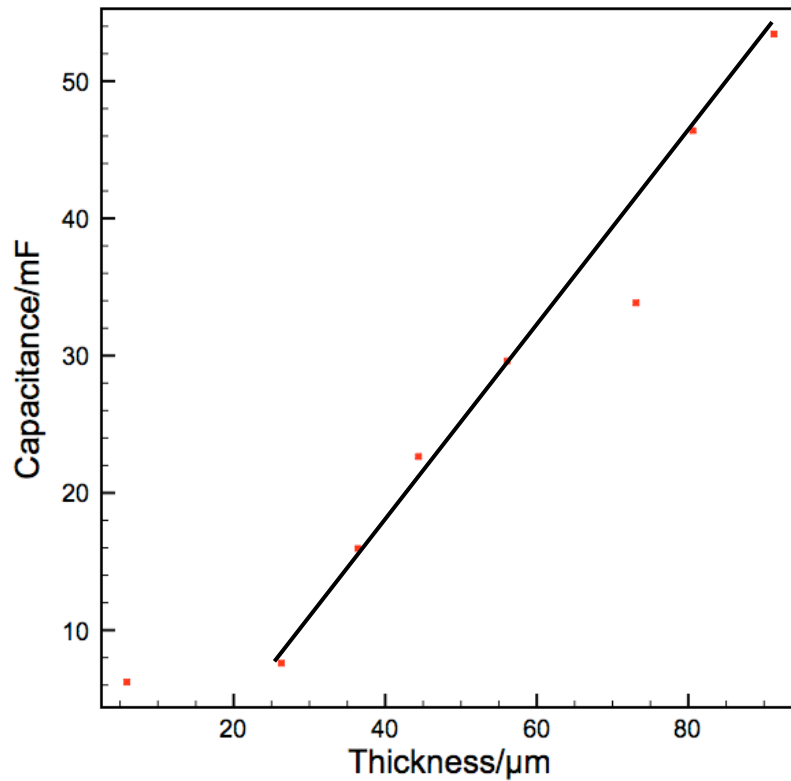The capacitance of the sample with different thickness is shown in Figure II.10.

Figure II.10 The evolution of capacitances of the single carbon electrode versus the thickness measured.

The capacitance increases as the thickness increases linearly, except for the sample deposited with only 5s, thanks to thin electrode that allows better electrolyte percolation and better electrolyte ion accessibility inside the carbon electrode: its volumetric capacitance (42.2 $F.cm^{-3}$) is about twice the one of thicker films ($\sim$ 20 $F.cm^{-3}$). The sample with 40s of deposition time, actually corresponding to the high thickness measured shown in Figure II.9, shows important deviation.

Therefore, the 5s of deposition, which offers exceptional better performance concerning volumetric capacitance, was chosen for deposition of carbon materials for fabrication of carbon-based interdigitated micro-supercapacitors.

IV.4   AC based on-chip micro-supercapacitors in PC based electrolyte

Activated Carbon (AC) was deposited onto the interdigitated patterned current collectors shown in Figure II.1b through EPD. As in Figure II.7, the Nyquist plot of the 3-electrode cell for thickness study indicated a leakage which is suspected to originate from the water content in the deposited carbon film, an annealing treatment of the samples at 250°C after EPD and drying process under vacuum at 120°C before electrochemical test were extended to overnight instead of 2h for each operation. Anhydrous PC solvent was also used to prevent the impurity.

Figure II.11 shows the Nyquist plot of this 5 μm thick AC based micro-supercapacitor in 1M NEt$_4$BF$_4$/PC electrolyte from 100 kHz to 10 mHz.
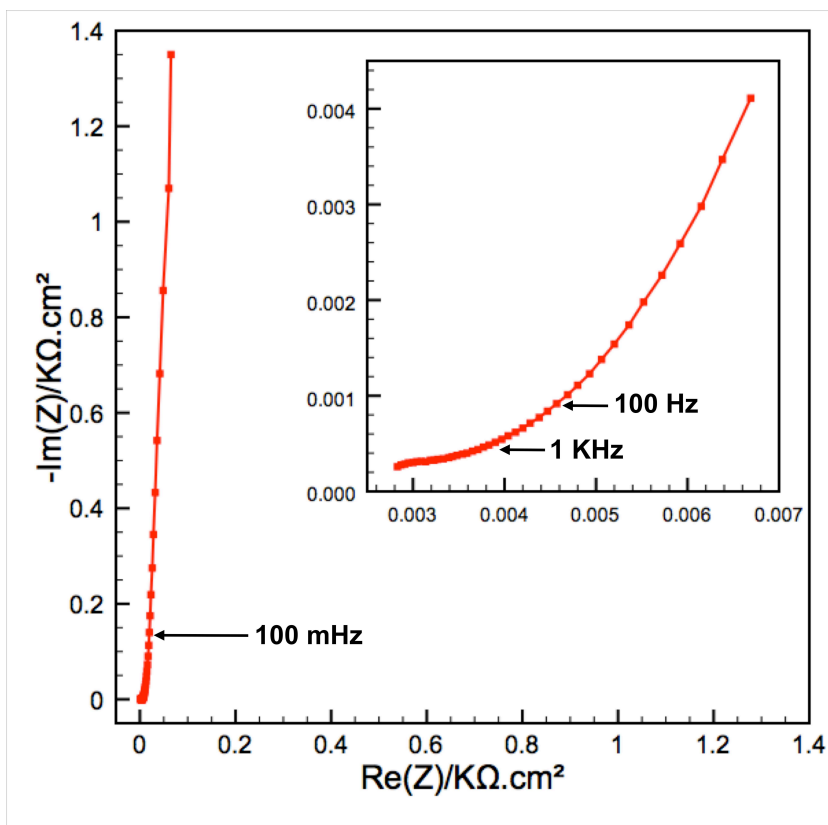
Figure II.11 Nyquist Plot of AC based on-chip micro-supercapacitor in 1M NEt₄BF₄/PC from 100 kHz to 10mHz with 10 mV as the voltage amplitude.

The value on the real axis of the beginning point of Nyquist plot at high frequency (inset of Figure II.11) defines the equivalent series resistance (ESR) of the cell, which is 2.8 $\Omega.cm^2$, comparable to carbon-based macroscopic supercapacitors in the same electrolyte [14]. At high frequency from 100 kHz to 1 kHz, the plot is almost horizontal, indicating difficulty in electronic transfer in the electrode. The carbon grains deposited with inorganic binders might not have good contact between each other and cause this difficulty. There is no semi-circle loop at high frequency in this micro-supercapacitors, meaning that the contact resistance between current collectors and active material is small. A good adherence between Ti/Au substrate and EPD deposited AC layer is thus confirmed thanks to longer annealing time after EPD. At 100 Hz, Nyquist plot is at the transition state between resistive behavior (an almost

horizontal line) and capacitive behavior (a nearly vertical line). This transition point is called "knee frequency". From 1 kHz to 100 Hz, there is still resistive behavior, linked with electrolyte ions accessibility inside the porous structure of AC. Finally, at low frequency below 100 mHz (Figure II.11), capacitive behavior of sharp increase of the imaginary part was observed similar to the dielectric capacitors, showing stable adsorption and desorption of electrolyte ions.

Complex capacitance was calculated from experimental Nyquist data according to Eq. 17.

Evolution of stack capacitance (C') with frequency is plotted in Figure II.12, showing an increase of capacitance with decrease of frequency, thus with evolution of time. However, the maximum capacitance (plateau) was not yet reached. The absence of plateau in the plot indicates a limitation during the electrochemical characterization, which is assumed to be linked with limited ion transport in the inner porous network of the activated carbon.
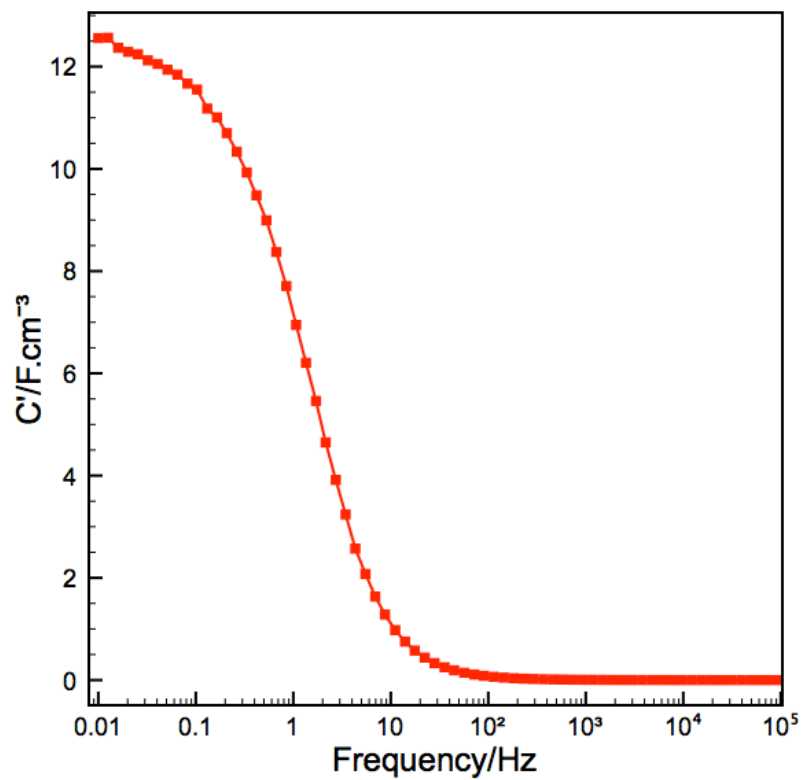
Figure II.12 Evolution of stack capacitance of AC based micro-supercapacitor in 1M NEt$_4$BF$_4$/PC versus frequency.

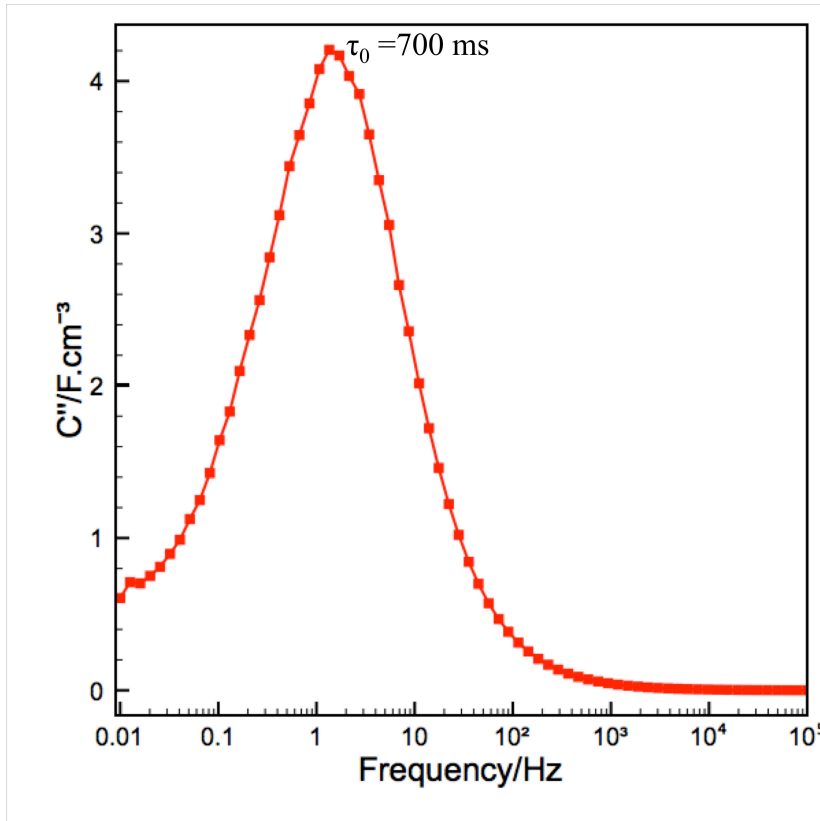Figure II.13 shows evolution of the imaginary part of the complex stack capacitance with frequency.

Figure II.13 Evolution of the imaginary part of the stack capacitance of the AC based micro-supercapacitor in 1M NEt₄BF₄/PC electrolyte.

The C'' peak is located at 1.43 Hz, corresponding to a time constant of 700 ms for AC based micro-supercapacitor in 1M NEt$_4$BF$_4$/PC electrolyte. This peak corresponds to a φ angle of -45°, i.e., to the minimum time needed to discharge the cell with the energy efficiency ≥ 50 %. This suggests a short time for electrolyte ions to reach stable adsorption rate. Compared to macroscopic supercapacitors with the same material (time constant $\tau_0 = 10$ s [14]), the relaxation time constant of the microdevice is much lower, thanks to the higher accessibility of electrolyte ions to carbon materials in this interdigitated configuration obviously due to the small thickness of the active film than in AC-based macroscopic supercapacitors. A higher rate capability could be expected and becomes an advantage for micro-supercapacitors compared to macroscopic supercapacitors.

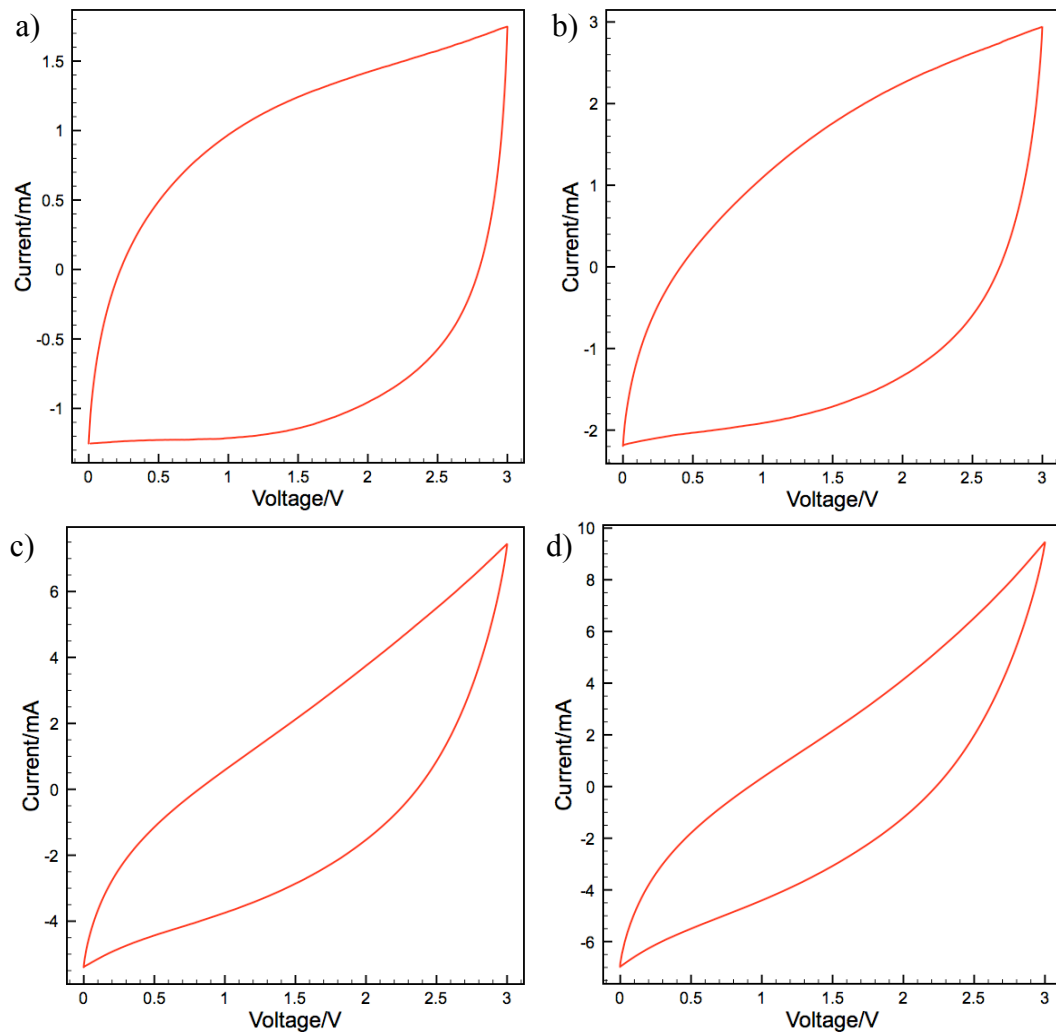CVs of AC based micro-supercapacitor from 500 mV/s to 10 V/s were collected within 3V shown in Figure II.14.

Figure II.14 CV plots of AC based micro-supercapacitor in 1M NEt$_4$BF$_4$/PC a) at 500 mV/s, b) at 1 V/s, c) at 5 V/s and d) at 10 V/s within 3V.

Although time constant is measured to be far shorter than that in macroscopic supercapacitors, at a scan rate as high as 500 mV/s, distortion was observed on the CV plot owing to the ionic resistivity, evidencing difficulties in migration of electrolyte ions transport in AC porous network at this scan rate. Although distorted, capacitive behavior was still kept up to 1 V/s as shown in Figure II.14b.

80

Two severely squeezed CV plots were shown in Figure II.14c and d, corresponding to the sample at 5 V/s and at 10 V/s. No capacitive behavior was observed and expected in these high scan rates even for micro-supercapacitors [1, 15], especially that based on porous carbon materials, owing to the high ionic resistance at these scan rates.

CV plots shown in Figure II.14 were distorted from a pure capacitive behavior marked by rectangular shape which could be observed in macroscopic supercapacitors using thick electrodes (~ 100 μm thick) at 20 mV/s [16]. Scan rate was increased from usually used 20 mV/s to 500 mV/s here in order to be able to test the micro-supercapacitors under a large voltage window. Because increasing scan rate increases the value of current measured, self-discharge and leakage current are hereby overcome. Moreover, this on-chip micro-supercapacitor survived scan rate up to 1 V/s which macroscopic supercapacitors could not achieve [17, 18]. In this sense, the advantage of micro-scale device on power performance is emphasized.

Evolution of capacitances of AC based micro-supercapacitor in 1M NEt_4BF_4/PC versus scan rates was plot in Figure II.15.
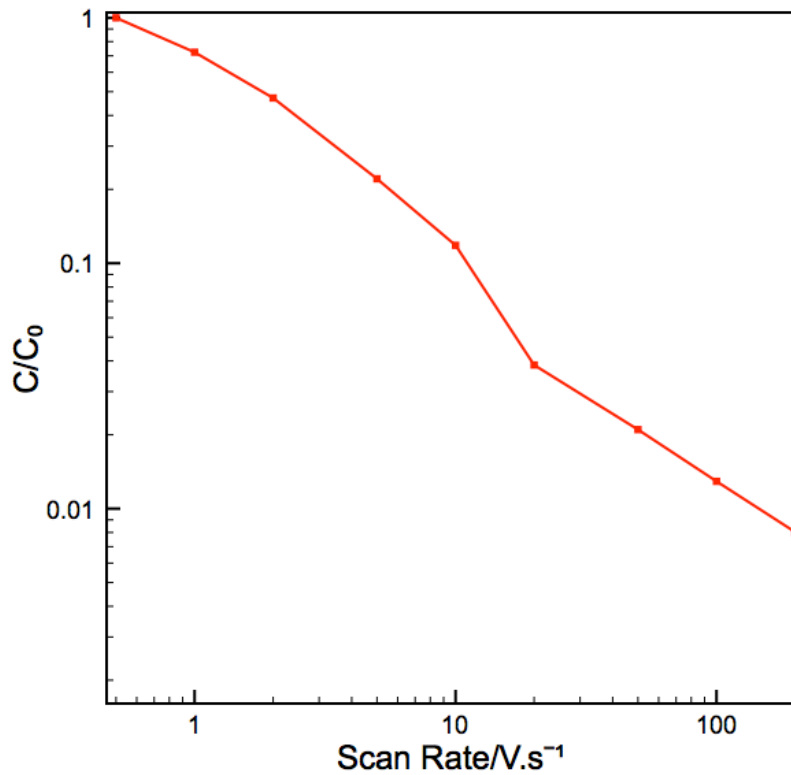
Figure II.15 Evolution of relative capacitance of AC based micro-supercapacitor in 1M NEt$_4$BF$_4$/PC versus scan rate.

The capacitance drops significantly and only 22% of initial capacitance at 5 V/s remains, indicating a limitation of ion transport in the inner porous network of AC.

A specific capacitance of 5.4 mF.cm^{-2} per footprint area was achieved at low rate from this AC based micro-supercapacitor in 1M NEt$_4$BF$_4$/PC, hence 24.3 mJ.cm^{-2} as specific energy and 0.500 W.cm^{-2} as specific power. For AC electrode material, 92.8 F.cm^{-3} was achieved as volumetric capacitance of AC, which is much higher than that in macroscopic supercapacitors with the same material [19]. In macroscopic cells, the thickness of electrode is much higher (~ 100 μm) and thus the accessibility of the electrolyte ions to the carbon materials is much worse than that in micro-supercapacitors. The advantage of micro-scale device was thus

proved not only with higher power capability, but also higher volumetric capacitance compared to macroscopic supercapacitors.

IV.5   OLC based micro-supercapacitor in PC based electrolyte – Ultra-high Power Performance

On-chip micro-supercapacitor showed a better power capability than macroscopic supercapacitors as mentioned in section IV.4, although limitation of ion transport inside the pore network in AC was observed. In order to further boost the high power competence, i.e. eliminating the limitation of ion transfer inside the pores of the activated carbon (with specific surface area of 2500 $m^2.g^{-1}$), onion like carbon (with specific surface area of 500 $m^2.g^{-1}$), which has no porous network inside the carbon grain, was used to prepare a 7 μm thick micro-supercapacitor with the same configuration by electrophoretic deposition (EPD). Electrochemical characterization was performed on it in the same electrolyte – 1 M NEt_4BF_4 in propylene carbonate (PC).

Nyquist plot of OLC based on-chip micro-supercapacitor in 1M NEt_4BF_4/PC electrolyte is shown in Figure II.16, indicating a typical capacitive behavior with a vertical increase even at high frequency, between 1kHz and 100 Hz shown in the inset, compared to that of AC which is shown in Figure II.11. This could be attributed to low thickness of the electrode and the high accessibility of the OLC surface without limitation of ion transport inside the porous network, which was the case for activated carbon. However, a small deviation was observed at frequency lower than 100 mHz, owing to leakage current in the system, probably from the electrolysis of impurities in the system.
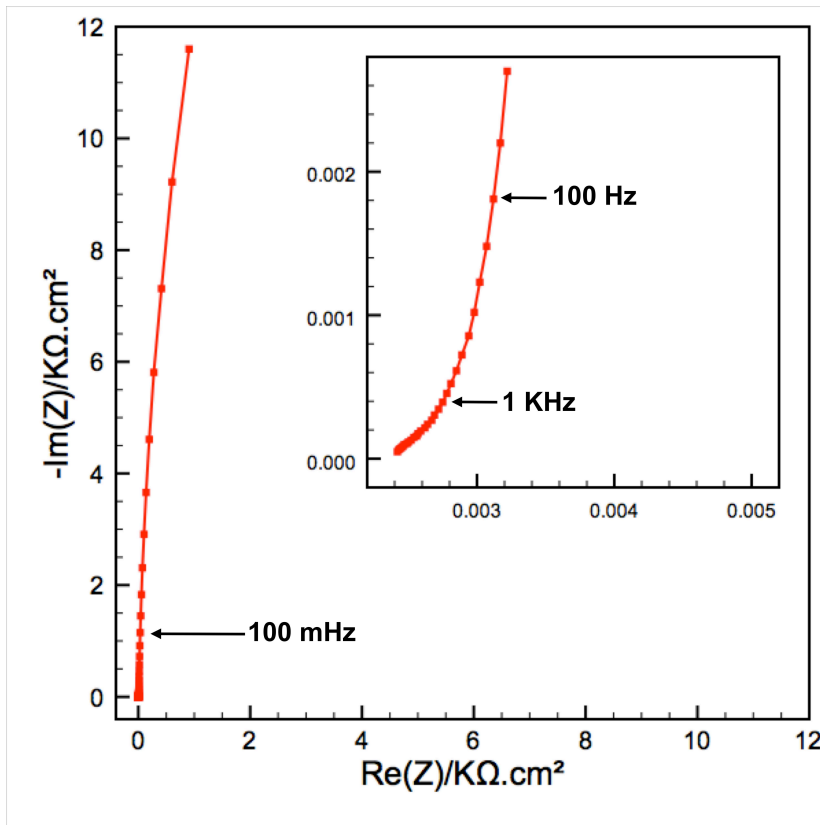
Figure II.16 Nyquist plot of OLC based on-chip microsupercapacitors in 1M NEt$_4$BF$_4$/PC from 100kHz to 10mHz with 10 mV as the voltage amplitude.

Figure II.17 shows the evolution of stack capacitance with frequency, indicating better capacitive behavior with a plateau at low frequency end, which was missing in the same plot of AC based micro-supercapacitor under the same condition in Figure II.12. The plateau is not totally flat, suggesting leakage in the system, in accordance with that observed in Nyquist plot. Despite of that, a micro-supercapacitor with little restriction of ion transfer in the electrode was achieved and high power capability was expected. The stack capacitance of OLC based micro-device (1.1 F.cm^{-3}) calculated from impedance is much lower than that of AC based micro-device (12.5 F.cm^{-3}) [20], since the lack of porous structure in OLC particle makes less surface area available for adsorption of electrolyte ions. To get high power capability, capacitance performance was compromised.
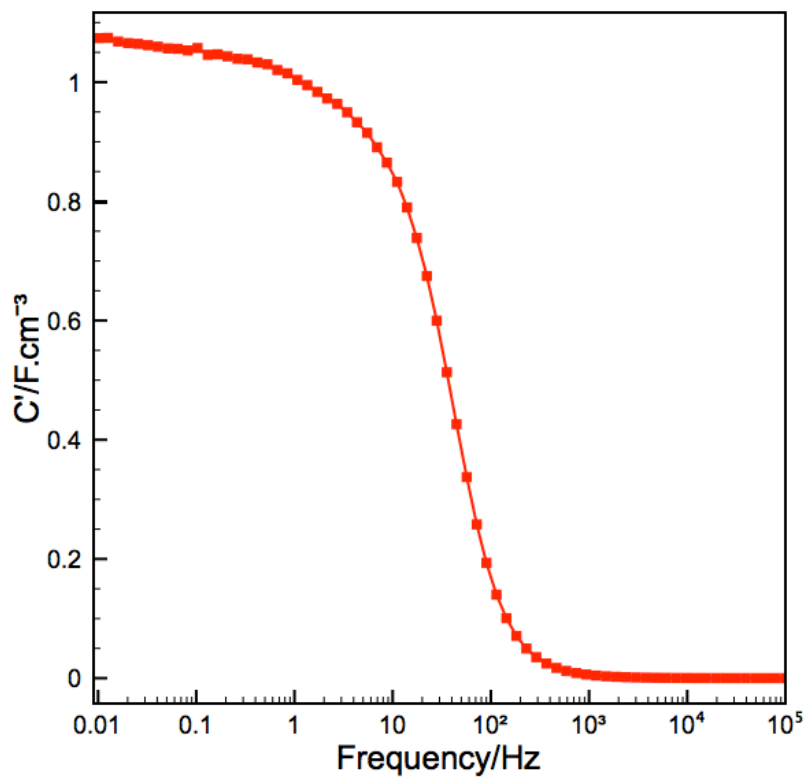
84

Figure II.17 Evolution of stack capacitance of OLC based micro-supercapacitor in 1M NEt4BF4/PC versus frequency.

Evolution of imaginary part of the stack capacitance of OLC based micro-supercapacitor in 1M NEt_4BF_4/PC electrolyte was shown in Figure II.18.
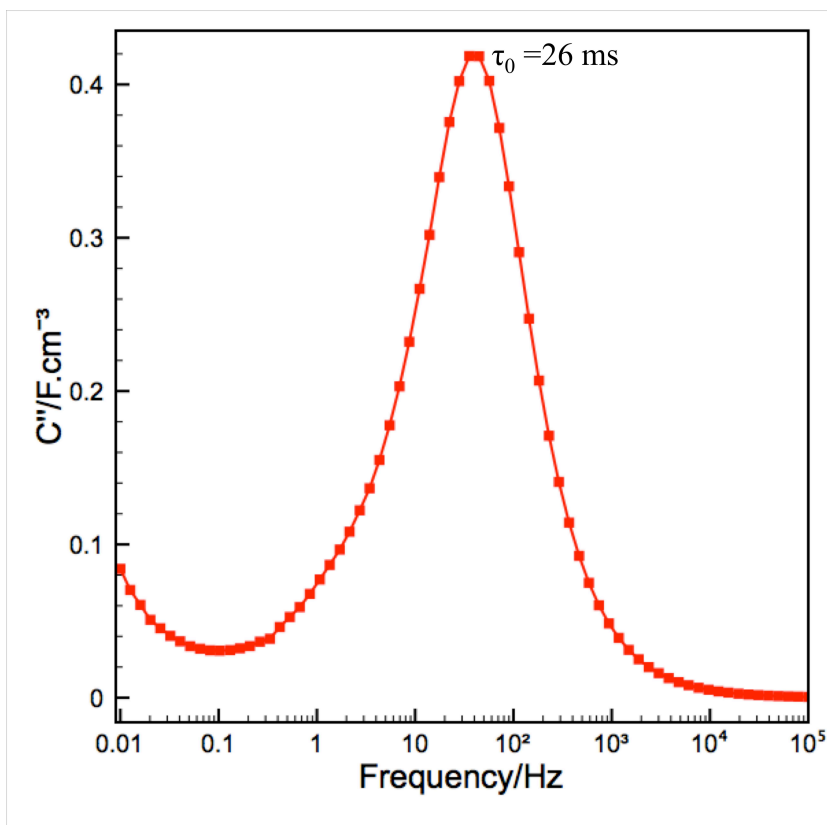
Figure II.18 Evolution of imaginary capacitance with frequency of OLC based micro-supercapacitor in 1M NEt$_4$BF$_4$/PC electrolyte.

The plot with OLC based micro-supercapacitor in 1M NEt$_4$BF$_4$/PC electrolyte shows a relaxation time constant of 26 ms, even shorter than AC based micro-supercapacitor in the same electrolyte, as OLC has the spherical structure to allow fully accessibility of electrolyte ions. The combination of OLC and microdevice configuration highly increased the rate capability, thus boost the power performance of the device.

The high power capability was also proved by CV measurements up to 100 V/s. CV plots at 1 V/s, 10 V/s, 100 V/s and 200 V/s are shown in Figure II.19 and Figure II.20.
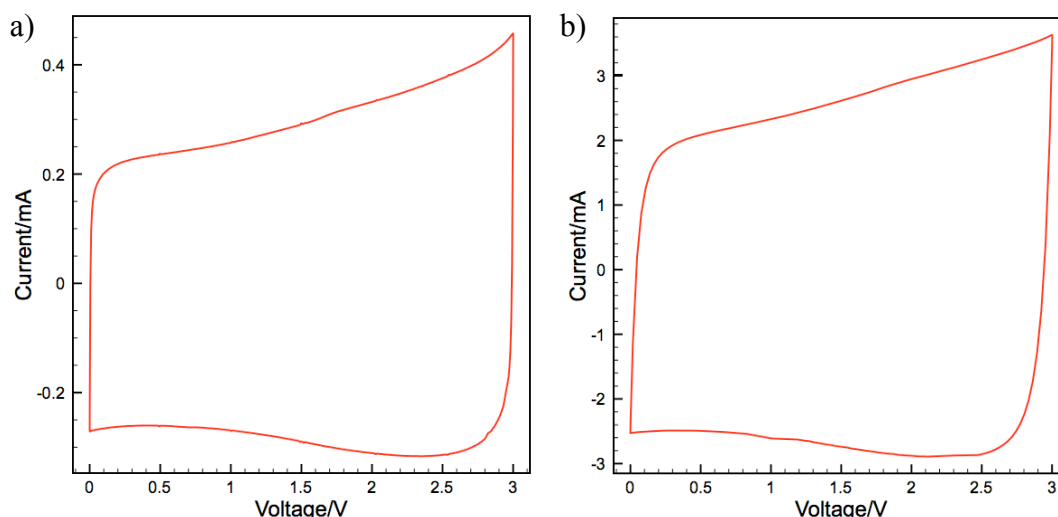
Figure II.19 CV plots OLC based micro-supercapacitor in 1M NEt₄BF₄/PC a) at 1 V/s and b) at 10 V/s.

Thanks to the fully accessible surface area of OLC particles to electrolyte ions and lack of inner porous structure, there is no restriction on ion transport here and capacitive behavior is still maintained at 10 V/s. At this scan rate, AC based micro-supercapacitor was not able to keep its capacitive behavior with a CV plot severely distorted as shown in Figure II.14c. Here it shows the synergy between the on-chip micro-supercapacitor and nanostructure carbon material with high rate capability.

Scan rate was further increased, in order to find out the limit of this micro-scale device. In Figure II.20, the CV plots at a scan rate of 100 V/s and 200 V/s are shown. The behavior is similar to that of AC electrode at 500 mV/s, i.e. it keeps a capacitive behavior even at 100 V/s This scan rate is more than two orders of magnitude higher than any results reported with alternative devices [17, 18], including microdevices [1, 15, 21] and micro-cavity electrodes [22, 23].
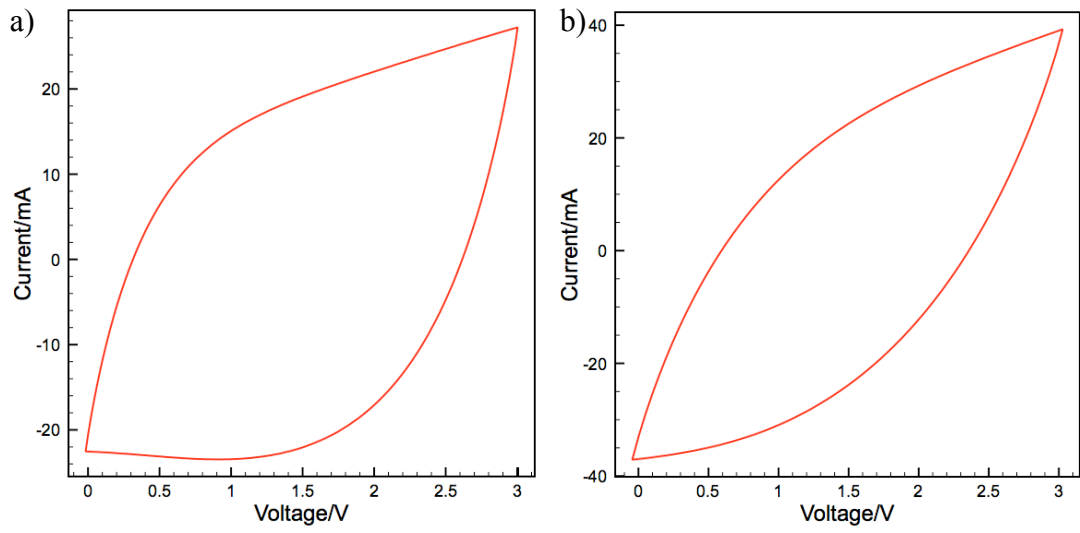
Figure II.20 CV plots of OLC based micro-supercapacitor in 1M NEt$_4$BF$_4$/PC electrolyte at 100V/s and 200V/s within 3 V.

Figure II.21 shows the evolution of stack capacitance of the micro-supercapacitor with scan rates in 1M NEt$_4$BF$_4$/PC electrolyte from 1 V/s to 200 V/s.

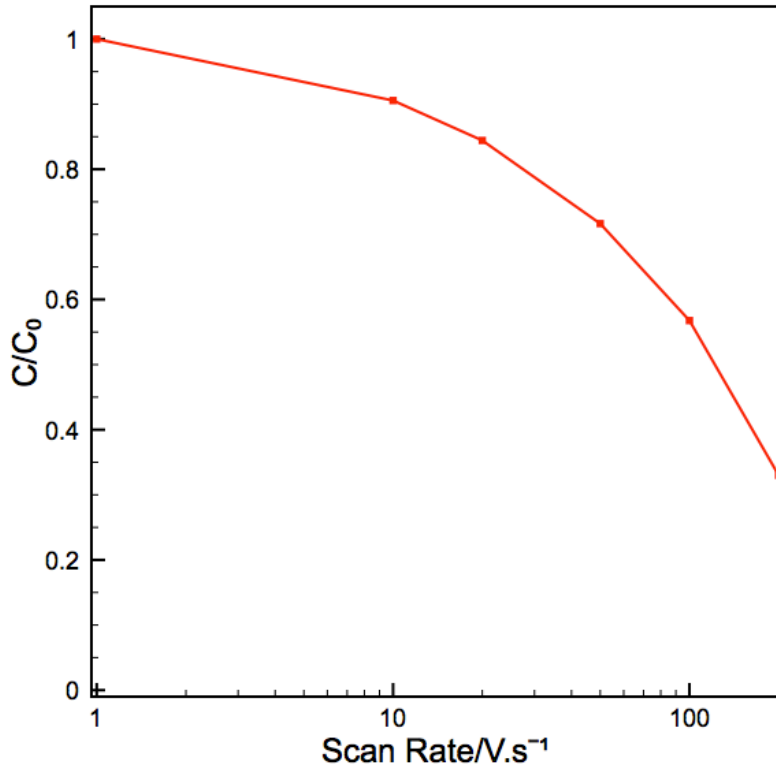**Figure II.21 Evolution of relative capacitance of OLC based on-chip micro-supercapacitor versus scan rate in 1M NEt$_4$BF$_4$/PC electrolyte .**

It shows that the capacitance decreases with scan rate slowly with 80% of capacitance kept around 30 V/s. Compared to the similar plot with AC electrode in Figure II.15, the power performance of OLC electrode is much better, thus proving that combination of on-chip micro-supercapacitor architecture and carbon nanomaterials boosts the power capability to an incredible level with capacitive behavior preserved up to 100 V/s.

Specific capacitance of 1.04 mF.cm^{-2} was achieved with OLC based on-chip micro-supercapacitor in 1M NEt$_4$BF$_4$/PC from CV test at 1V/s, hence 4.68 mJ.cm^{-2} as specific energy and 0.592 W.cm^{-2} as maximum specific power. Per electrode material, a volumetric capacitance of 9.7 F.cm^{-3} of OLC was achieved.

Cycling performance was tested at 10 V/s and shown in Figure II.22. Reproducible capacitance was remained almost unchanged up to 10000 cycles; hereby stability of this on-chip micro-supercapacitor in 1M NEt_4BF_4 in PC was confirmed.
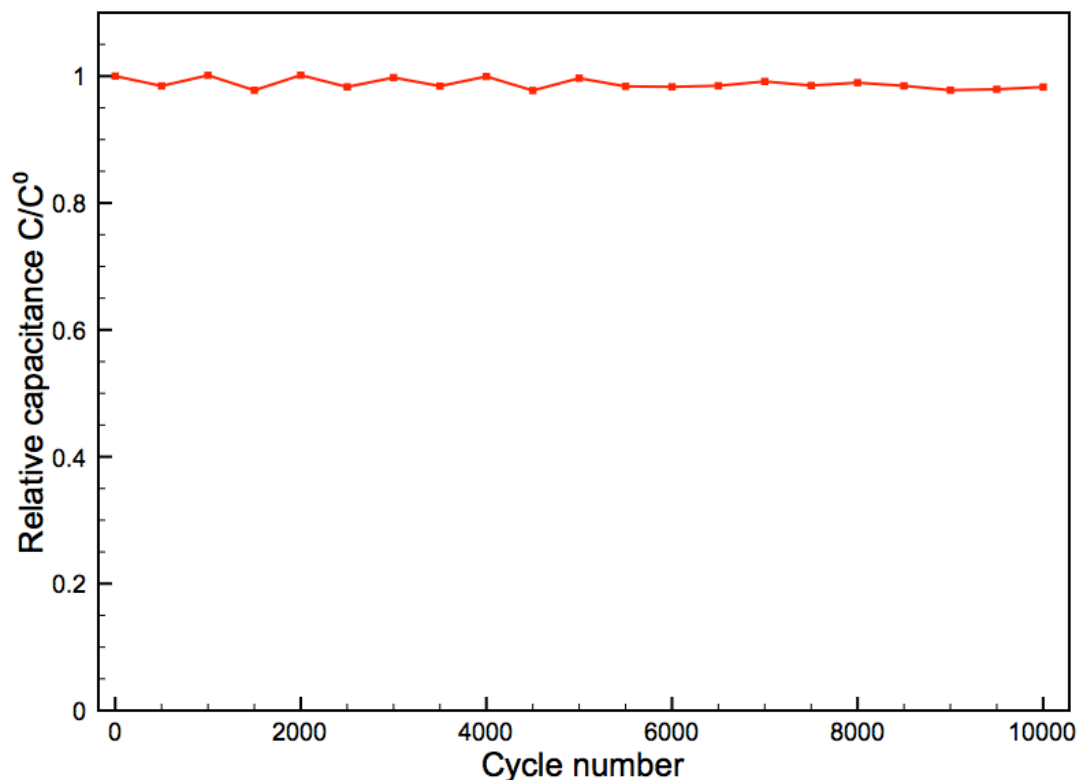

Figure II.22 Cycling results of OLC based micro-supercapacitor in 1M NEt_4BF_4/PC at 10V/s.

A stable OLC based on-chip micro-supercapacitor was successfully prepared by EPD technique. Ultra-high power capability was achieved in 1M NEt_4BF_4/PC by combination of highly accessible nano-scale carbon material and micro-scale power device configuration.

IV.6   Electrochemical Characterization of OLC in ILM under extreme temperatures

Micro-supercapacitor prepared through EPD showed outstanding performance as mentioned in sections above. To further improve the energy density, new type of electrolytes, which could tolerate large voltage window, should be considered. Ionic liquid could be one of

90

the solutions thanks to their large potential window. However, ionic liquids generally suffer from high viscosity, and low conductivity at room temperature and below. They are thus usually used at temperature higher than 60 °C [24, 25].

A eutectic ionic liquid mixture (ILM) of N-methyl-N-propylpiperidinium bis(fluorosulfonyl)imide (PIP$_{13}$FSI) and N-butyl-N-methylpyrrolidinium bis(fluorosulfonyl)imide (PYR$_{14}$FSI), as described in bibliographic part, is able to work under extreme temperatures down to -50°C, which is lower than PC (-30°C) and AN (-40°C) [26]. OLC based micro-supercapacitors with configuration shown in Figure II.1a were prepared with thickness of 7 μm in the same condition mentioned above and electrochemically characterized in ILM at -50°C, -40°C, 20°C and 80°C to explore the effect of the combination of this eutectic ILM with micro-scale device using a nanostructured carbon material.

IV.6.1 EIS Results

The EIS results of OLC based micro-supercapacitor in ILM from 500 kHz to 10 mHz with 300 mV as potential amplitude were shown Figure II.23 with an inset of the evolution of capacitance with frequency.
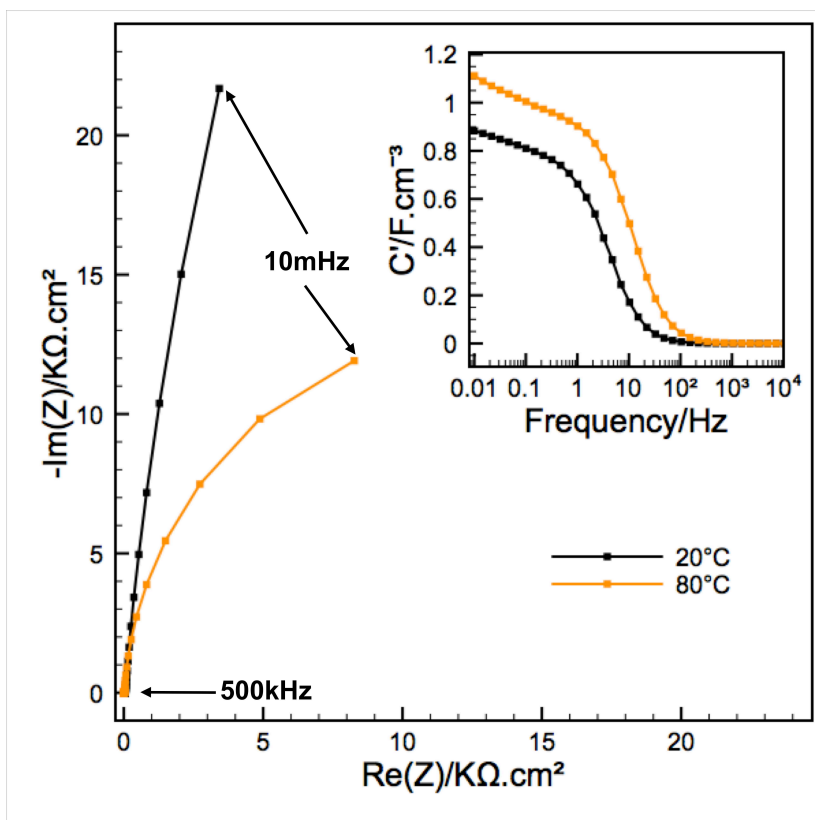
Figure II.23 Nyquist plot of OLC based micro-supercapacitor in eutectic ionic liquid mixture at 20°C and 80°C with volumetric capacitances versus frequency in the inset.

The high frequency part indicates a typical capacitance behavior for sample under both temperatures with a vertical increase without small loops at the high frequency ends, thanks to the high conductivity of the electrolytes at high temperature. However, the low frequency part of Nyquist plot of sample at 20°C shows a slight deviation from the ideal vertical increase, associated with the presence of a leakage current usually caused by undesired redox reaction such as decomposition of impurities presented in the system, with the help of gold current collectors which could be a catalyst. The sample at 80°C suggests significant deviation from the ideal capacitive behavior of vertical increase with the same reason enhanced by the high temperature. The higher temperature accelerated the redox decomposition of impurities.

The inset of Figure II.23 shows the evolution of capacitance versus frequency of the OLC based micro-supercapacitor in ILM at 20°C and 80°C. Both capacitances reach a plateau at low frequency end, however, sloping, indicating a leakage current involved in the process, in accordance with results drawn from the Nyquist plots.

The Nyquist Plots of the sample collected in the same condition as mentioned above at two lower temperatures are shown in Figure II.24 with an inset of evolution of capacitance versus frequency.
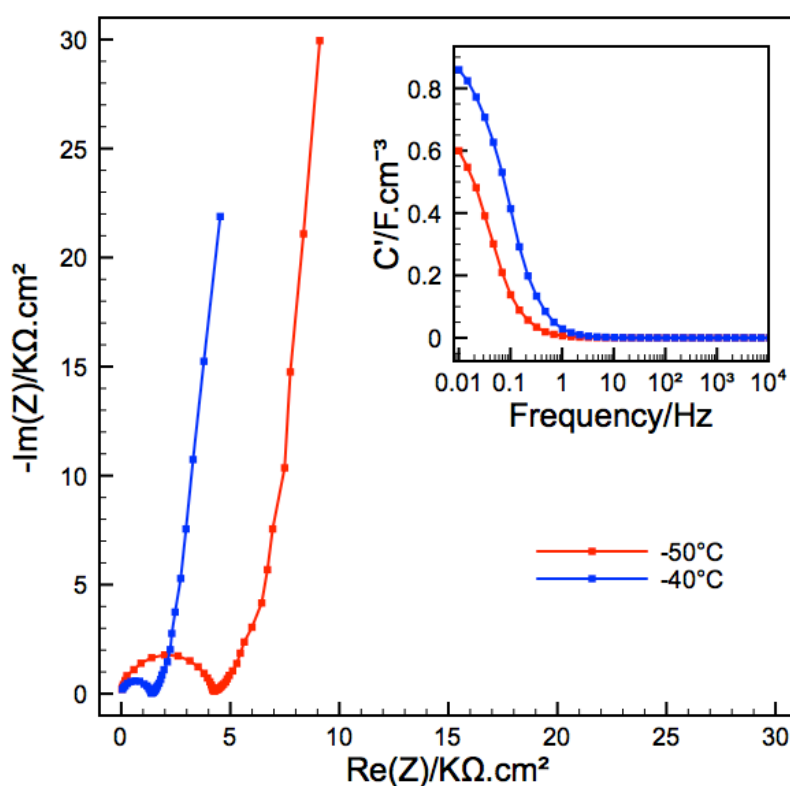

Figure II.24 Nyquist plot of OLC based micro-supercapacitor in eutectic ionic liquid mixture at -50°C and -40°C with volumetric capacitances versus frequency in the inset.

The two low-temperature Nyquist plots at -40°C and -50°C both show a semi-circle loop at high frequency end, as the resistance is high below 0 °C. At low temperature, the response of electrolyte ions slows down; a semi-circle loop due to the low conductivity of electrolyte is

thus shown at frequency at 500 kHz when temperature reaches -40°C. The right end of the loop intercepts the real axis at about 1.39 kΩ.cm^2 at -40°C and increases dramatically to 4.27 kΩ.cm^2 at -50°C, which is about 3 times the resistance at -40°C. The equivalent series resistance (ESR) of the cell depends mainly on the conductivity of the ILM at low temperature. The conductivity of the ILM is around 10^{-2} mS.cm^{-1} at -50 °C [6] compared to 4.9 mS.cm^{-1} at room temperature.

The low frequency sections both increase vertically as redox reaction from impurities is not favored kinetically at such low temperatures according to Arrhenius law. The inset shows the evolution of stack capacitance with frequency. Obviously, capacitance of this OLC based micro-supercapacitor in ILM at -40°C is much higher than that at -50°C. The capacitances increased as the frequency decreases, but failed to form a plateau at low frequency ends, corresponding to the restriction of ion mobilities in the gel-like ILM at these low temperatures.

IV.6.2 CV Results

Figure II.25 shows the comparison of the CV curves at 200 mV/s at two different temperatures, -40°C and 20°C up to 3.7V.
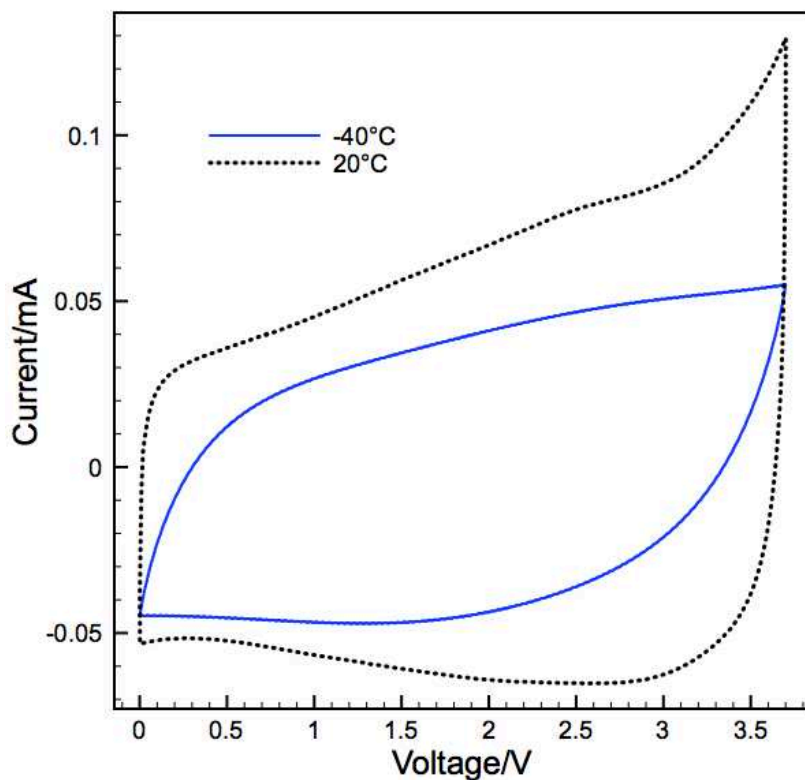
Figure II.25 CV plots of OLC based micro-supercapacitor in ILM at -40°C and 20°C at 200 mV/s within 3.7 V.

For this high scan rate as 200 mV/s, the CV curve at -40°C, which is a very low temperature, still showed capacitive behavior, although distorted. Since high temperature largely increases the conductivity of ILM, CV curve at 20°C demonstrates ideal capacitive behavior with deviation at the high voltage part which is due to the beginning of the decomposition of ILM electrolyte on Au current collectors. The immediate increase of current at initial scan and back scan indicates low resistance even at this relatively high scan rate 200 mV/s for ionic liquids [27], proving the synergetic benefit of combination between OLC and micro-supercapacitor configuration.

At high temperature 80°C, the voltage window could not reach 3.7 V but only 2.8 V. High temperature increases the kinetic (thus rate constant) of undesirable redox reactions at high

voltage, following Arrhenius law. Hereby, the voltage window of cyclic voltammogram is getting smaller with increase of the temperature.

Figure II.26 shows a comparison of the CV curves of OLC micro-supercapacitor in ILM at 1 V/s at 20°C and 80°C within 2.8 V.
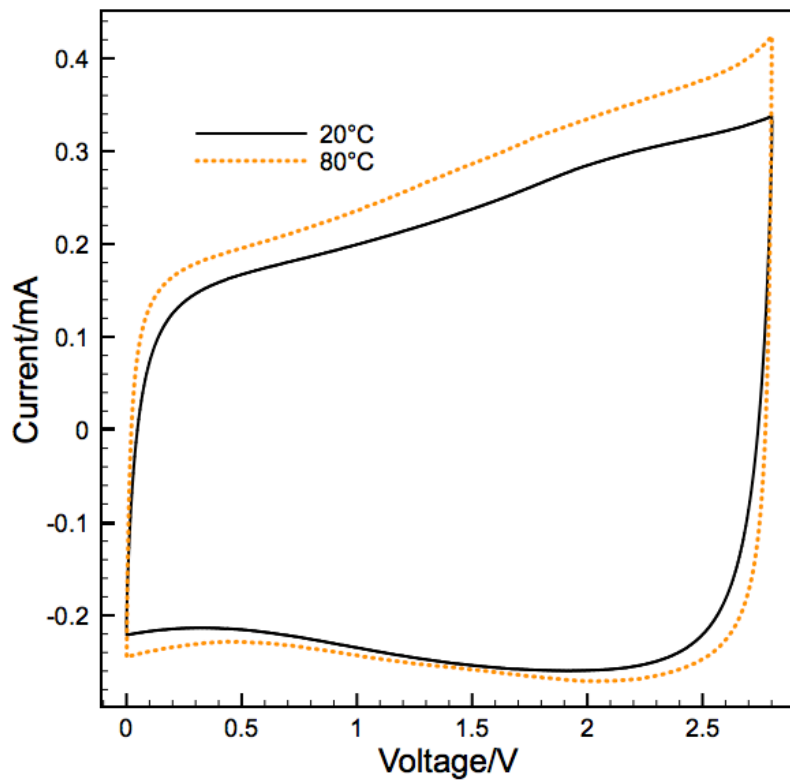

Figure II.26 CV plots of OLC based micro-supercapacitor in ILM at 20°C and 80°C at 1 V/s within 2.8V.

The charging current at 80°C is notably higher than that at 20°C, while the discharge currents were found to be similar, thus indicating a higher leakage current at 80°C, in accordance with the Nyquist plot at the same temperature shown in Figure II.23, decreasing the coulombic efficiency. Typical capacitive behavior without restriction was achieved with this micro-supercapacitor at 1 V/s at 20°C and 80°C, as the conductivity was ensured at these temperatures. CV tests at even higher scan rate have afterwards been performed.

96

Figure II.27 compares performance of the micro-supercapacitor at high scan rate 10 V/s (Figure II.27a) and 20 V/s (Figure II.27b) up to 2.8V.
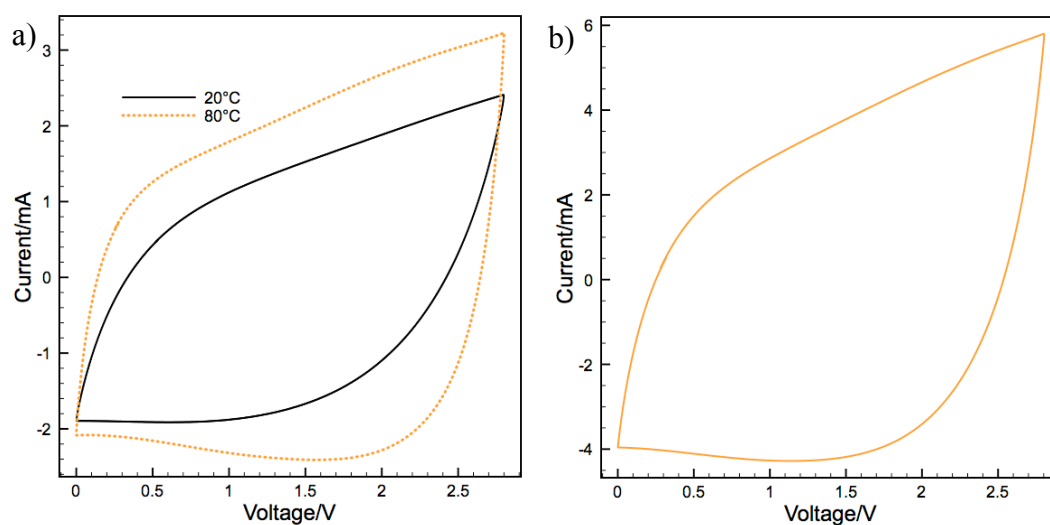

Figure II.27 CV plots of OLC based micro-supercapacitor in ILM a) at 10 V/s and b) at 20 V/s at 80°C up to 2.8V.

At 10V/s, sample under both 20°C and 80°C shows the advantage of temperature tolerance for this ILM. And even at 80°C, the micro-supercapacitor could exhibit a well-conserved rectangular shape at 20V/s, which is already a high scan rate even for micro-supercapacitors [1, 15]. Compared to OLC based micro-supercapacitor in 1M NEt_4BF_4/PC electrolyte, the rate capability has been compromised with ILM electrolyte. The shape of CV plot at 10 V/s within 2.8 V in ILM shown in Figure II.27a is more distorted than that at 10 V/s in PC based electrolyte shown in Figure II.19b, owing to the relatively higher viscosity of ILM.

Low temperature CVs (-50°C and -40°C) were also recorded with the OLC based micro-supercapacitor with ILM as electrolyte. At high scan rate such as 200 mV/s, sample at -50°C loses capacitive behavior with a severely squeezed CV plot, indicating important limitation by ohmic drops, i.e. low conductivity of ILM at low temperatures. However, the CV plot of sample at -40°C still exhibit a capacitive behavior with the quasi-rectangular CV plot shown in Figure II.28.
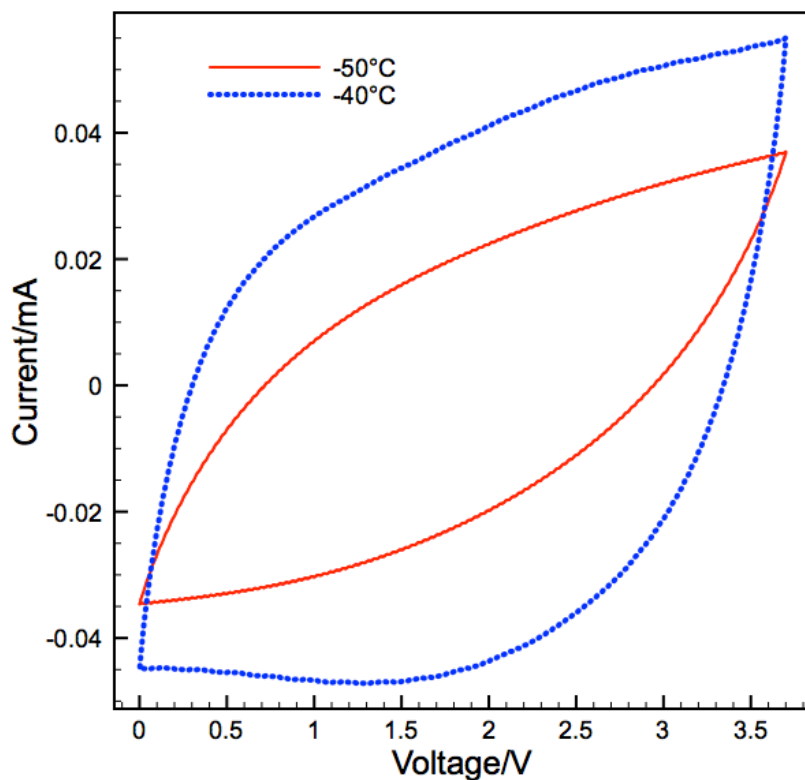
Figure II.28 CV plots of OLC based micro-supercapacitor in ILM at -50°C and -40°C at 200 mV/s up to 3.7V.

At low temperature, the conductivity of ILM electrolyte became very low and could not preserve capacitive behavior at high scan rate. To show the low temperature performance, cyclic voltammogram at relatively lower scan rates (from 10 mV/s) were collected.

Figure II.29 shows the CV results of the OLC based micro-supercapacitor in ILM at -50°C and -40°C at 10mV/s within 3.7 V.
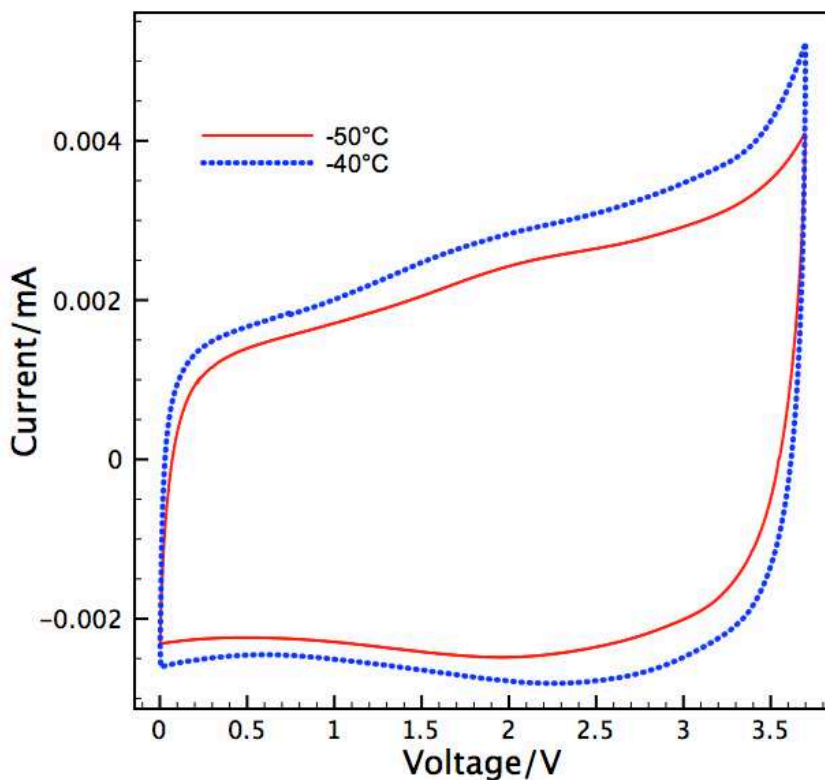
Figure II.29 CV plots of OLC based micro-supercapacitor in ILM at -50°C and -40°C at 10 mV/s up to 3.7V.

Capacitive behavior was preserved even at -50°C, where conventional electrolytes like AN-based electrolytes stop operating, within 3.7V, a larger voltage window (3 V for AN and PC-based electrolytes) [16]. At high voltage, the increase of current is due to the electrolyte degradation through redox reaction.

Volumetric capacitances of the micro-supercapacitor at different scan rates and different temperatures over 2.8 V were compared and shown at Figure II.30.
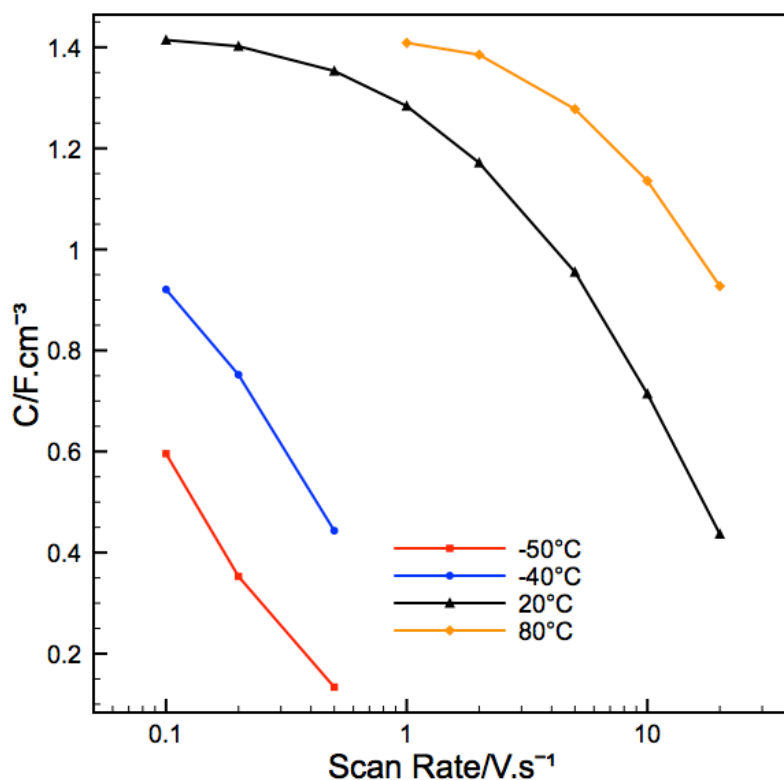
Figure II.30 Evolution of volumetric capacitance of micro-supercapacitor versus scan rate at different temperatures in ILM within 2.8 V voltage window.

The volumetric capacitance of micro-supercapacitor decreases with increasing potential scan rates, since the ohmic drop increases with increasing scan rate. Temperature plays an important role on capacitance. The lower the temperature the faster the capacitance decrease, since at low temperature the ionic conductivity of the electrolyte decreases, thus increasing the series resistance of the cell. The higher the temperature, the higher the capacitance at the same scan rate. This is also linked with the increase of the ionic conductivity at high temperature.

At 20°C, a maximum specific capacitance of 1.11 mF.cm^{-2} was achieved according to the footprint area of this OLC based micro-supercapacitor in ILM at 500 mV/s over 3.7 V. Hence a maximum volumetric capacitance of the device was calculated to be 7.36 F.cm^{-3}. The

capacitance at -50 °C and -40 °C kept 77% and 89% of that at 20 °C, respectively, although not at the same scan rate. Low temperature performance of this OLC based micro-supercapacitor in ILM is thus confirmed.

The change of the relative capacitance versus the cycle number at 1 V/s for the micro-supercapacitor is shown in Figure II.31. C_0 represents the capacitance achieved at the first cycle. Capacitance decreases with cycles, 90% of capacitance was remained after 1000 cycles.
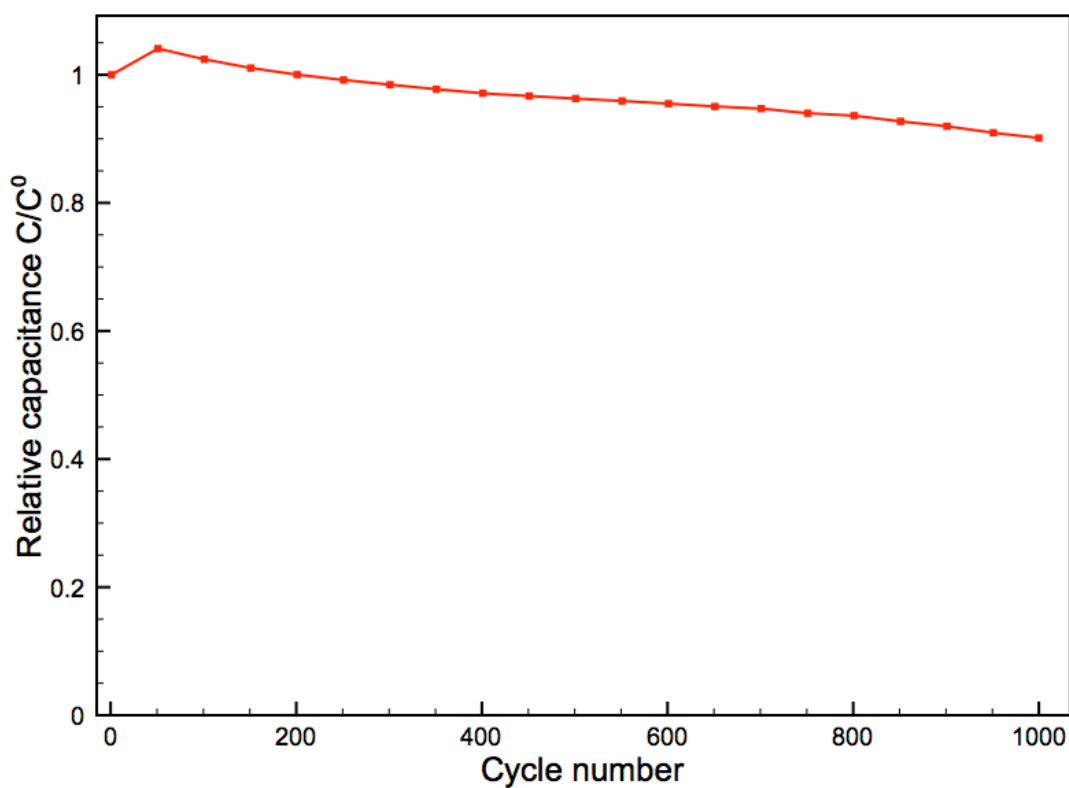

Figure II.31 Cycling test results of OLC based micro-supercapacitor in ILM at 1 V/s.

A stable OLC based micro-supercapacitor was achieved with 1.1 mF.cm^{-2} as the capacitance per footprint area of the device in ILM, hence a specific energy of 7.5 mJ.cm^{-2} and a specific power of 241 mW.cm^{-2}. Energy performance has been improved as expected with this ILM.

V   Conclusion & Perspectives

A series of micro-supercapacitors were prepared through electrophoretic deposition of different carbon materials, including activated carbon and onion like carbon. Activated carbon was deposited to study the relationship of the thickness and deposition time.

Performance of all the micro-supercapacitors demonstrated in this chapter is presented in Table II.2 below.

Table II.2 Performance of micro-supercapacitors with different carbon materials and electrolytes.

Carbon	Electrolyte	Configuration	C/mF. cm^{-2}	E/mJ. cm^{-2}	P$_{max}$/mW .cm^{-2}	Voltage window	Max. scan rate	Features
AC	1M NEt$_4$BF$_4$/PC	16 fingers	5.40	24.3	500	3 V	0.5 V/s	Higher C
OLC	1M NEt$_4$BF$_4$/PC	16 fingers	1.04	4.68	592	3 V	100 V/s	Ultra high Power
OLC	1M NEt$_4$BF$_4$/PC	4 fingers	1.04	4.68	203	3 V	10 V/s	-
OLC	ILM	4 fingers	1.11	7.50	241	3.7 V	20 V/s at 80 °C	-50 - 80 °C

Onion like carbon (OLC) was deposited and the micro-supercapacitors showed exceptionally high power in 1M NEt$_4$BF$_4$ in PC thanks to its ability of ultra fast charging and discharging. The OLC based micro-supercapacitor in 1M NEt$_4$BF$_4$/PC could conserve capacitive behavior at scan rate as high as 100 V/s, although the capacitance performance was compromised as OLC is not porous and doesn't have a large surface area. Besides, the configuration of micro-supercapacitors also played an important role in rate capability. The one with 16 fingers could tolerate 10 times higher scan rate than that with 4 fingers.

OLC-based micro-supercapacitors were also tested in an ionic liquid mixture, which is able to allow electrochemical characterization under extreme temperatures from -50 °C to 80 °C with a large voltage window: 3.7 V. The results show the ability of the micro-supercapacitor to work under the corresponding low temperature environment. The micro-supercapacitor

also kept the feature of OLC carbon of tolerating high scan rate until 20 V/s even in ILM. In addition, this ILM improved the capacitance of OLC material. With larger voltage window, a much higher energy density was reached as expected, although power density was compromised because of high resistance from the ionic liquid mixture electrolyte.

Theoretically, if thicker electrodes could be deposited onto the electrode, higher specific capacitance and energy would be achieved by micro-supercapacitors per cm^2. To achieve this goal, EPD conditions such as suspension solvent, charging agent, suspension composition, etc. should be further adjusted.

Other materials, especially new materials such as carbide derived carbon (CDC), could be deposited to produce new micro-supercapacitors and explore additional features when in small scale.

This chapter reported results on carbon-based on-chip micro-supercapacitors prepared by deposition – processing carbon powder into thin-films. The following chapter will introduce carbon film based micro-supercapacitors, to directly pattern carbon or carbon precursor thin films into interdigitated configuration.

Reference:

1. Pech, D., et al., *Elaboration of a microstructured inkjet-printed carbon electrochemical capacitor.* Journal of Power Sources, 2010. **195**(4): p. 1266-1269.

2. Boccaccini, A.R., et al., *Electrophoretic deposition of carbon nanotubes.* Carbon, 2006. **44**(15): p. 3149-3160.

3. Corni, I., M.P. Ryan, and A.R. Boccaccini, *Electrophoretic deposition: From traditional ceramics to nanotechnology.* Journal of the European Ceramic Society, 2008. **28**(7): p. 1353-1367.

4. Ogihara, H., J. Okagaki, and T. Saji, *A Facile Fabrication of Superhydrophobic Films by Electrophoretic Deposition of Hydrophobic Particles.* Chemistry Letters, 2009. **38**(2): p. 132-133.

5. Xiomara, C.n.-C.n., et al., *A carbon nanotube field emission cathode with high current density and long-term stability.* Nanotechnology, 2009. **20**(32): p. 325707.

6. Lin, R.Y., et al., *Capacitive Energy Storage from -50 to 100 degrees C Using an Ionic Liquid Electrolyte.* Journal of Physical Chemistry Letters, 2011. **2**(19): p. 2396-2401.

7. Maissel, L.I. and R. Glang, *Handbook of thin film technology*. 1970: McGraw-Hill.

8.   Sarkar, P. and P.S. Nicholson, *Electrophoretic Deposition (EPD): Mechanisms, Kinetics, and Application to Ceramics.* Journal of the American Ceramic Society, 1996. **79**(8): p. 1987-2002.

9.   Dickerson, J.H. and A.R. Boccaccini, *Electrophoretic Deposition of Nanomaterials*. 2011: Springer.

10.   Benjamin E. Russ and J.B. Talbot, *A Study of the Adhesion of Electrophoretically Deposited Phosphors.* J. Electrochem. Soc., 1998. **145**(4): p. 1245-1252.

11.   Mahapatro, A.K., et al., *Gold surface with sub-nm roughness realized by evaporation on a molecular adhesion monolayer.* Applied Physics Letters, 2006. **88**(15): p. 151917-151917-3.

12.   K. W. Bewig and W.A. Zisman, *The wetting of Gold and Platinum by Water.* The Journal of Physical Chemistry, 1965. **69**(12): p. 4238-4242.

13.   Pawley, J.B., *Handbook Of Biological Confocal Microscopy*. 2006: Springer.

14.   Taberna, P.L., P. Simon, and J.F. Fauvarque, *Electrochemical characteristics and impedance spectroscopy studies of carbon-carbon supercapacitors.* Journal of the Electrochemical Society, 2003. **150**(3): p. A292-A300.

15.   In, H.J., et al., *Origami fabrication of nanostructured, three-dimensional devices: Electrochemical capacitors with carbon electrodes.* Applied Physics Letters, 2006. **88**(8): p. 083104.

16.   Simon, P. and Y. Gogotsi, *Materials for electrochemical capacitors.* Nature Materials, 2008. **7**(11): p. 845-854.

17. Kajdos, A., et al., *Tailoring the Pore Alignment for Rapid Ion Transport in Microporous Carbons.* Journal of the American Chemical Society, 2010. **132**(10): p. 3252-3253.

18. Du, C.S. and N. Pan, *High power density supercapacitor electrodes of carbon nanotube films by electrophoretic deposition.* Nanotechnology, 2006. **17**(21): p. 5314-5318.

19. Chmiola, J., et al., *Anomalous increase in carbon capacitance at pore sizes less than 1 nanometer.* Science, 2006. **313**(5794): p. 1760-1763.

20. Portet, C., G. Yushin, and Y. Gogotsi, *Electrochemical performance of carbon onions, nanodiamonds, carbon black and multiwalled nanotubes in electrical double layer capacitors.* Carbon, 2007. **45**(13): p. 2511-2518.

21. Beidaghi, M. and C. Wang, *Micro-Supercapacitors Based on Interdigital Electrodes of Reduced Graphene Oxide and Carbon Nanotube Composites with Ultra high Power Handling Performance.* Advanced Functional Materials, 2012. **22**(21): p. 4501-4510.

22. Portet, C., et al., *Electrochemical characterizations of carbon nanomaterials by the cavity microelectrode technique.* Electrochimica Acta, 2008. **53**(26): p. 7675-7680.

23. Lin, R., et al., *Microelectrode Study of Pore Size, Ion Size, and Solvent Effects on the Charge/Discharge Behavior of Microporous Carbons for Electrical Double-Layer Capacitors.* Journal of the Electrochemical Society, 2009. **156**(1): p. A7-A12.

24.   Armand, M., et al., *Ionic-liquid materials for the electrochemical challenges of the future.* Nature Materials, 2009. **8**(8): p. 621-629.

25.   Arbizzani, C., et al., *Safe, high-energy supercapacitors based on solvent-free ionic liquid electrolytes.* Journal of Power Sources, 2008. **185**(2): p. 1575-1579.

26.   Ue, M., K. Ida, and S. Mori, *Electrochemical Properties of Organic Liquid Electrolytes Based on Quaternary Onium Salts for Electrical Double‚ÄêLayer Capacitors.* Journal of the Electrochemical Society, 1994. **141**(11): p. 2989-2996.

27.   Vatamanu, J., O. Borodin, and G.D. Smith, *Molecular Insights into the Potential and Temperature Dependences of the Differential Capacitance of a Room-Temperature Ionic Liquid at Graphite Electrodes.* Journal of the American Chemical Society, 2010. **132**(42): p. 14825-14833.

Chapter III   Micro-supercapacitors from Carbide Derived Carbon (CDC) Film

I   Introduction

Processing of carbon powder into a micro-size electrode has been the key issue for developing micro-supercapacitors. Usually, organic binder such as PVDF and PTFE are used for processing carbon powder into films. However, the carbon film processed from powder (Figure III.1a) has voids in the film that are filled with binders; the volume of carbon film increases with increasing the ratio of binders. Compared to the bulk carbon film (Figure III.1b), the carbon density of the film processed from powders is much lower, thus has lower capacitance, power density and energy density for the same material. In addition, binders are generally non-conductive and electrons are transferred via the contacts between carbon grains; a certain part of carbon grains is thus electrically isolated and conductivity of the whole film is reduced, compromising the total performance of micro-supercapacitors. Moreover, from material point of view, patterning thin-film is far more likely to be produced in quantity than processing powders into films; thus facilitate the mass production.
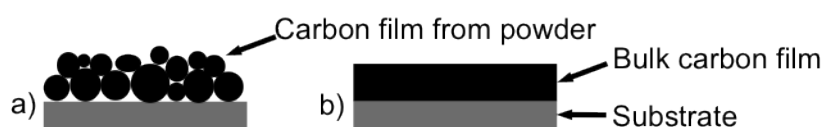

Figure III.1 Schematic diagram of a) carbon film processed from powder and b) bulk carbon film.

To increase the carbon density, hence the total performance of carbon-based micro-supercapacitors, binder-free bulk carbon films, such as carbide derived carbon (CDC) films could be used as electrode material for micro-supercapacitors.

As mentioned in Chapter I, thin-film supercapacitors with sandwich configuration based on CDC film [1] were reported. The sandwich was composed of a piece of CDC film on glass carbon as working electrode, a PTFE separator and a piece of processed activated carbon as counter electrode. A capacitance of 180 F.cm^{-3} was achieved, much higher than that of supercapacitors based on CDC powders (60 F.cm^{-3} of TiC-CDC in organic electrolyte) [2].

CDC film could be used to develop on-chip micro-supercapacitors, which is easier for integration into a system. Compared to sandwich configuration, planar interdigitated electrodes realized on-chip have the advantage of containing no separator in the device, facilitating the fabrication of this micro-scale devices. Electrochemical properties (power in particular) are expected to be enhanced at this scale.

In this chapter, we will present several on-chip micro-supercapacitors based on CDC films with different preparation processes, including reactive ion etching (RIE) of both CDC film and carbide film and focused ion beam (FIB) to etch away the undesired part of the film, thus patterning interdigitated electrodes. The current collectors were deposited afterwards on top of the electrodes. This configuration (current collectors on top of electrode material) was chosen because high temperatures are applied during chlorination of the carbide film: no metal placed underneath would sustain such a process (exposure to Cl$_2$ and high temperature) without being corroded. Materials characterization and electrochemical performance for each type of micro-device will be compared.

II   Materials and equipments

Titanium Carbide films were deposited by reactive DC magnetron sputtering with a Titanium target and acetylene (C$_2$H$_2$) gas as a carbon source [3] in Rowan University, New Jersey. The Ti target is run at 200 W at an overall pressure of 4 Pa. The gases were mixed in a manifold with an argon flow rate of 40 sccm (standard cubic centimeters per munites) and a

C$_2$H$_2$ flow rate of 2.5 sccm. The substrate is heated to approx 700°C to produce textured TiC in the (111) orientation. The resulting deposition rate was approximately 25 nm/min on Si wafer (resistivity 1~100 Ohm.cm with 200 nm wet thermal oxide). The SEM picture of TiC film is shown in Figure III.2.
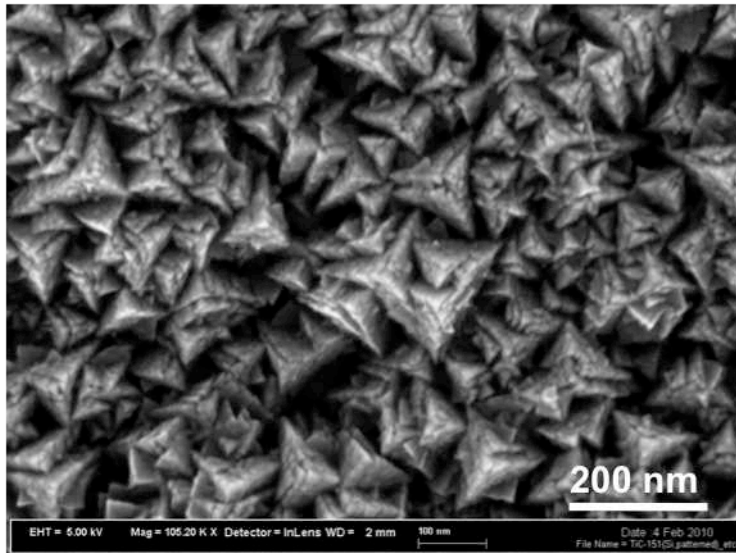

Figure III.2 SEM photo of top view of TiC film.

The silicon carbide film was deposited by sputtering in Ar atmosphere with a silicon carbide (SiC) target in LPN, France. The substrate was not heated during sputtering, and sputtering was conducted at a working voltage of 500 W with an overall pressure of 1 Pa.

Chlorination was performed in Drexel University, Pennsylvania. TiC-CDC and SiC-CDC films were obtained by chlorination of TiC or SiC films in a tube furnace at high temperature with Cl$_2$ inside as shown in Figure III.3.

Tube furnace
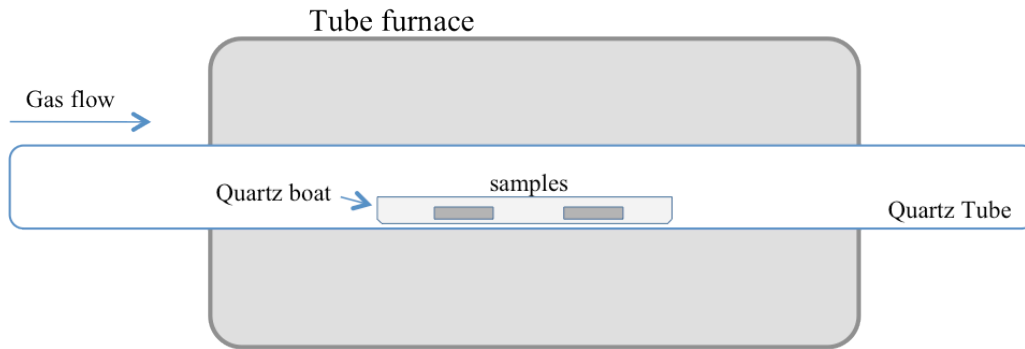
Gas flow →

Quartz boat → samples   Quartz Tube

Figure III.3 Experimental setup for chlorination process.

Reactive Ion Etching (RIE) was performed in Omega 201 equipment from SPTS, which is equipped with Inductively Coupled Plasma (ICP). The schematic diagram of the equipment is shown in Figure III.4.
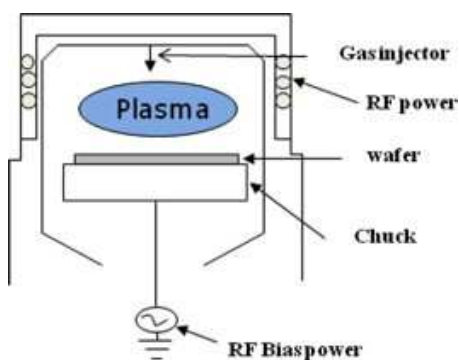
Plasma

Gas injector
RF power
wafer
Chuck
RF Bias power

Figure III.4 The schematic diagram of the equipment for RIE [4].

A spiral inductive coil was mounted on a dielectric window on the reactor. Plasma was generated inductively by coupling the oscillation radio frequency (RF) magnetic field (13.56 MHz). The CDC or carbide films to be etched were clamped on the chuck (bottom electrode) in the reactor. The chuck was powered by a separate RF source to control the ion bombardment energy (RF bias). [4]

II.1.1 Chlorination & Raman Results for SiC films

Chlorination was performed on SiC samples at 400 °C, 450 °C and 500 °C for 30 minutes. The corresponding Raman results of chlorinated samples recorded using the excitation wavelength of 514.5 nm are shown below in Figure III.5.
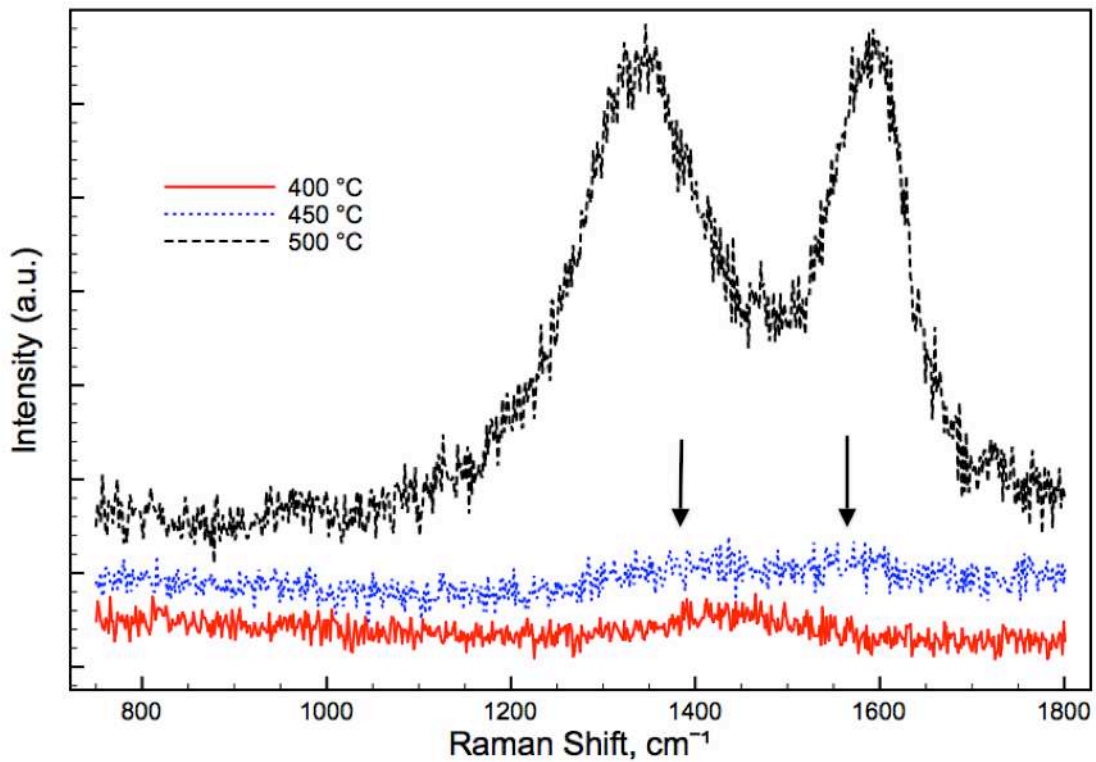

Figure III.5 Raman spectra of SiC film after chlorination at 400 °C, 450 °C and 500 °C.

For SiC sample chlorinated at 400 °C, there is a small broad bump at around 1450 cm^{-1}, between the D band position (1350 cm^{-1}) and the G band position (1600 cm^{-1}). However, without any trace of D band and G band, there is no CDC formed after chlorination at 400 °C.

For SiC sample chlorinated at 450 °C, there are small trace of peaks at around 1400 cm^{-1} and 1600 cm^{-1}. The peaks are almost hidden in the noise, indicating the formation of extremely small quantity of carbon. However, as there is no sign of D band peak or G band